Aalto University
School of Electrical
Engineering

Degree Programme in Electronics and Electrical Engineering

Jonas Nordfors

Designing a Wireless Sensor System for Elevator Condition Monitoring

Master's Thesis

Espoo, 17.5.2016
Supervisor: Professor Seppo Ovaska
Instructor: M.Sc. (Tech.) Jani Tertsonen

AALTO UNIVERSITY
SCHOOL OF ELECTRICAL
ENGINEERING

ABSTRACT OF THE MASTER'S THESIS

Author: Jonas Nordfors

Title: Designing a Wireless Sensor System for Elevator Condition Monitoring

Date: 17.5.2016 | Language: English | Number of pages: 8+79

Department: Department of Electrical Engineering and Automation

Professorship: Industrial Electronics | Code: S-81

Supervisor: Professor Seppo Ovaska

Instructor: M.Sc. (Tech.) Jani Tertsonen

The aim of this thesis is to design, implement and validate a prototype sensor system for wirelessly monitoring the condition of an elevator. One purpose of such system is long-term monitoring of the elevator, which could help detecting emerging issues in advance. The system could also be used by maintenance personnel as a real-time troubleshooting tool, assisting in device commissioning and maintenance situations, for example.

Due to requirements set by the use case and the elevator environment, a wireless, battery operated device is required. A significant part of this thesis focuses on aspects of selecting a suitable wireless technology, as the choice has a large impact on the performance of the system. Different wireless solutions are researched and compared, and a technology using the sub-GHz frequency bands is selected for the prototypes.

The prototype sensor is designed based on the choice of the wireless technology. The hardware and software of the sensor nodes, as well as a PC tool for collecting data, are presented. The performance of the sensor nodes and the functionality of the whole sensor system is tested using a batch of manufactured prototype devices. The prototypes and the selection of the wireless technology are considered successful. Minor improvements to the design of the prototypes are presented at the end of the thesis.

Keywords: Remote monitoring, Condition monitoring, Wireless technology, sub-GHz, Sensor network, Elevator

AALTO-YLIOPISTO
SÄHKÖTEKNIIKAN KORKEAKOULU

ABSTRACT (IN FINNISH)

Tekijä: Jonas Nordfors

Työn nimi: Langattoman anturijärjestelmän suunnittelu hissin kunnonvalvontaan

Päivämäärä: 17.5.2016	Kieli: Englanti	Sivumäärä: 8+79

Laitos: Sähkötekniikan ja automaation laitos

Professuuri: Teollisuuselektroniikka	Koodi: S-81

Työn valvoja: Professori Seppo Ovaska

Työn ohjaaja: DI Jani Tertsonen

Tässä työssä suunnitellaan, toteutetaan ja arvioidaan hissin kunnonvalvontaan tarkoitetun langattoman anturijärjestelmän prototyyppi. Järjestelmän käyttötarkoituksena on sekä hissin pitkäaikainen kunnonvalvonta, jonka avulla voidaan havaita orastavia vikoja etukäteen, että mahdollisuus käyttää laitetta reaaliaikaisena vianetsintätyökaluna, jota huoltohenkilöstö voisi käyttää apunaan esimerkiksi hissin käyttöönoton ja huoltotilanteiden yhteydessä.

Käyttökohteen asettamien vaatimusten takia on tarpeen suunnitella langaton, paristokäyttöinen anturi. Merkittävä osa tästä työstä käsittelee langattoman teknologian valintaan vaikuttavia tekijöitä, sillä valinnalla on suuri vaikutus järjestelmän suorituskykyyn. Työssä kartoitetaan ja vertaillaan erilaisia langattomia ratkaisuita, joista prototyyppilaitteeseen valitaan sub-GHz-taajuuksia käyttävä langaton teknologia.

Anturilaitteen prototyyppi suunnitellaan valitun langattoman teknologian pohjalta. Anturilaitteen elektroniikka, ohjelmisto, ja PC-tietokoneelle toteutettu datankeräystyökalu esitellään. Anturien suorituskyky sekä koko järjestelmän toiminta testataan valmistetuilla prototyyppikappaleilla. Prototyyppi arvioidaan toimivaksi ja langattoman teknologian valinta onnistuneeksi. Työn lopussa esitetään pieniä parannusehdotuksia prototyypin suunnitteluun.

Avainsanat: Etävalvonta, Kunnonvalvonta, Langaton teknologia, sub-GHz, Anturiverkko, Hissi

Preface

This thesis was done for KONE Oyj Finland Research and Development organization. The aim of the thesis was to map the possibilities of wireless technologies for the use in remote elevator condition monitoring, and to produce a proof-of-concept prototype. The expenses of this work, such as prototypes and equipment, were covered by the KONE PCBA Design Team, for which I am sincerely grateful.

I would like to thank my advisor Jani Tertsonen and my supervisor Seppo Ovaska for their advice on various subjects throughout the making of this thesis. Their expertise in the industry provided me valuable knowledge of real-world requirements for electronics and product design.

Equally important was the support and opinions I received from the members of the PCBA Design Team. Many interesting discussions took place as I aimed to justify my decisions, which were evaluated by the experts in the team.

Finally, I want to express greatest gratitude towards Giovanni Hawkins for providing the need and the starting point for this thesis in the first place.

Espoo 24.5.2016

Jonas Nordfors

Contents

Symbols and Abbreviations

η		Efficiency
φ		Phase
A		Amplitude
A_e		Aperture size
B		Bandwidth
C_{bat}		Battery capacity
d		Distance
G	[dB]	Gain
I_{ave}		Average current
I_{in}		Input current
I_{max}		Maximum current
I_{min}		Minimum current
I_o		Output current
I_Q		Quiescent current
P_{LDO}		Power dissipated in regulator
P_{noise}		Noise power
P_o		Output power
P_r		Received antenna power
P_{Tx}	[dBm]	Transmitter power
S		Power density
S_i	[dBm]	Receiver sensitivity
V_{in}		Input voltage
$V_{measured}$		Voltage measured with oscilloscope
V_o		Output voltage
x		Position
X_{ratio}		Active/Low-power mode ratio
ADC		Analog-to-Digital Converter
AES		Advanced Encryption Standard
AFA		Adaptive Frequency Agility
ASK		Amplitude Shift Keying
BLE		Bluetooth Low Energy
BPSK		Binary Phase Shift Keying
CMOS		Complementary Metal Oxide Semiconductor
CRC		Cyclic Redundancy Check
CSMA/CA		Carrier Sense Multiple Access with Collision Avoidance
CSV		Comma-Separated Values
DC		Direct Current
DECT		Digital Enhanced Cordless Telecommunications
DPRS		DECT Packet Radio Service
FEC		Forward Error Correction
FIFO		First In, First Out
FSPL		Free Space Path Loss
GUI		Graphical User Interface
I2C		Inter-Integrated Circuit
I2S		Inter-IC Sound
IC		Integrated Circuit
ID		Identifier
IoT		Internet of Things

ISM	Industrial, Scientific and Medical
LAN	Local Area Network
LBT	Listen Before Talk
LDO	Low-Dropout Linear Regulator
LED	Light Emitting Diode
Li-Fi	Light Fidelity
LNA	Low Noise Amplifier
LSD	Least Significant Digit
MAC	Media Access Control
MCU	Microcontroller Unit
MEMS	Microelectromechanical systems
ODR	Output Data Rate
PC	Personal Computer
PCB	Printed Circuit Board
PDA	Personal Digital Assistant
PSK	Phase Shift Keying
QAM	Quadrature Amplitude Modulation
QPSK	Quadrature Phase Shift Keying
RAM	Random Access Memory
RF	Radio Frequency
RMS	Root Mean Square
RSSI	Received Signal Strength Indicator
RTC	Real-Time Clock
RTOS	Real Time Operating System
RX	Receive
SNR	Signal-to-Noise Ratio
SPI	Serial Peripheral Interface
SRAM	Static Random Access Memory
TX	Transmit
UART	Universal Asynchronous Receiver/Transmitter
ULE	Ultra Low Energy
USB	Universal Serial Bus
VI	Virtual Instrument
VoIP	Voice over IP
Wi-Fi	Wireless Fidelity
WLAN	Wireless Local Area Network

1 Introduction

The evolution of mobility in the consumer market has led to an ever-increasing amount of wirelessly connected handheld devices, made possible by today's low-cost electronics and ease of connectivity. Industrial users are following in the same direction, albeit that the application for wireless devices in industry is commonly some form of a sensor system. Wireless sensing, remote monitoring and the Industrial Internet of Things are growing trends that are keenly explored in many commercial and industrial fields today [1].

The elevator and escalator industry, for example, could benefit from remote condition monitoring financially by improving the responsiveness of maintenance. Remotely monitoring the health of machinery allows detecting, even predicting, upcoming fault conditions. Not only can remote monitoring reduce the delay of dispatching maintenance, loss of service could be avoided entirely if worn equipment is detected in advance.

A condition-monitoring sensor could also function as a real-time troubleshooting tool. Such functionality would allow maintenance personnel to investigate possible issues during the installation and commissioning of machinery with no external tools required. In the case of an elevator, this would allow verifying that required ride comfort levels are met before the elevator is commissioned for public use, for example. With today's low-priced electronics, such sensors could be standard components of a larger device, preassembled already in the factory. After the commissioning, the sensor could be left in place to serve for the lifetime of the elevator, monitoring its health.

The aim of this thesis is to design, implement and validate a prototype system of sensors, capable of both real-time troubleshooting and a long lifetime of remotely collecting health data from the elevator. To achieve such different goals in one device, the system level design has to be carefully planned. The selection of wireless communication technology must be carefully evaluated, as it will have a great impact on the real-time performance of the sensor. Therefore, a significant part of the thesis focuses on investigating the technical properties of wireless technologies, researching different available wireless solutions, and selecting the most viable technology for the use case.

A prototype sensor device based on the selected wireless technology is developed. The prototype is designed to meet requirements which are described in detail in Section 1.1. The sensor system as a part of an elevator is further illustrated in that section. The functionality of the system, as well as the wireless range and power consumption of the prototypes is validated by several measurements described at the end of the thesis.

This thesis is divided into four main chapters. Chapter 2 introduces different criteria, such as the range and the data throughput rate of the connection, that should be evaluated when selecting the wireless technology. The methods and technical decisions that can be used to obtain certain functionality are explained. The relationship between different technical solutions and methods is also discussed, as tradeoffs often ensue if only certain aspects are focused on.

Chapter 3 focuses on choosing a suitable wireless technology for the elevator prototypes. The chapter presents different wireless technologies available today, and

possible upcoming solutions are also considered. These technologies include for example Bluetooth, different standards of WLAN, ZigBee, and proprietary solutions. The different solutions will be compared from the perspective of the technical properties presented in Chapter 2. A measurement for comparing the signal quality of different technologies was conducted in an elevator shaft, and the results are presented in this chapter. A certain technology is chosen based on the theoretical comparison and the preliminary measurement results.

Chapter 4 explains the design process of the condition monitoring sensor prototype. The planned functionality of the overall sensor system is described. Hardware decisions, based on the technology selected in Chapter 3 and the requirements specification in Section 1.1 will be justified. Considerations regarding power supply and antenna design are also discussed. The design of the sensor node software, as well as a PC software for collecting sensor data, will be described. The design documents of the prototypes are included in the Appendix.

In Chapter 5 the success of the sensor design, as well as the selection of a wireless technology will be evaluated. The range of the connection and the power consumption of the prototypes is tested thoroughly, as they are the most critical requirements for the sensor. The overall functionality of the system was verified in an actual elevator. Possibilities for improving the performance of the prototypes are presented. The next steps for future development are proposed in the conclusion part of the thesis.

1.1 Requirements for the sensor system

For monitoring the condition and ride comfort of a moving device, such as an elevator car, the physical quantities that need to be measured are acceleration, including vibration, and audio. The exact requirements for the quality of the measurements are presented in Table 1.

As stated before, there are two different use cases for the condition-monitoring sensor. First, the sensor is expected to be able to permanently monitor the condition of the elevator for a long period of time. Therefore, sufficient battery lifetime is required. Second, a possibility for real-time monitoring is needed for commissioning, troubleshooting and maintenance purposes.

In real-time troubleshooting situations it is beneficial to be able to monitor the elevator from outside of the shaft. Therefore, communication should be achievable through the elevator shaft structures. An example of such situation would be the maintenance person listening for structure-born vibrations in a specific location in the building, while simultaneously monitoring the vibrations of the elevator with the wireless sensor. Additionally, it is desirable that a sensor node could be placed inside the car without the need of going on the car roof, in an elevator where sensors are not preinstalled, and that communication could be achieved through the metal structures of the car.

Accurately monitoring the long-term health of the elevator demands high quality measurement data, as, for example, a subtle, high-frequency vibration could be the sign of an emerging breakdown of a component. The requirements for real-time troubleshooting are not as high, as it is sufficient to detect sudden noises, bangs and lower frequency vibrations. Therefore, lower quality measurements are sufficient for real-time purposes, while permanent condition monitoring requires high-quality data. The high quality measurement data can be stored onboard the sensor to be recovered

later, while real-time troubleshooting naturally demands low latency in acquiring the information from the sensor.

The major moving components in a traditional elevator shaft are the car and the counterweight, which are connected to an electric motor via hoisting ropes. The ropes meet at the top of the shaft in the machine room, where the electric motor is located. The most advanced elevators do not require a separate machine room; instead, the motor is located at the top of the shaft. Each of these parts will be monitored; therefore, a network of a minimum of three sensors is required. There will not be a power source available on the counterweight, which means that a battery operated device is needed. The lack of power and the distance between the components are the reasons for creating a wireless network.

The sensor system and its two use cases are illustrated in Figure 1. The red rectangles represent sensor nodes. A detailed list of requirements set for the sensor prototype is presented in Table 1.

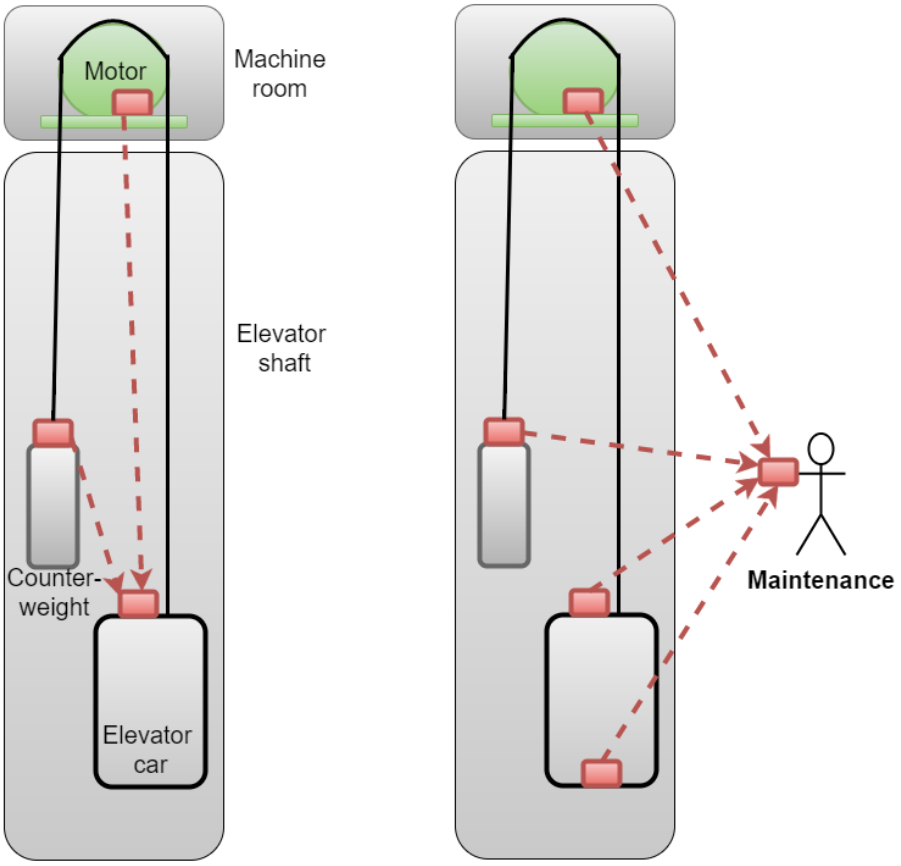

Figure 1: The sensor system. Permanent condition-monitoring situation on left, real-time troubleshooting on right

Table 1: Sensor requirements

Requirement	Specification
Audio sample rate, real-time troubleshooting	6 kHz
Audio sample rate, permanent monitoring	52 kHz
Acceleration (vibration) sample rate, real-time troubleshooting	3 dimensions, 0 – 2 kHz
Acceleration (vibration) sample rate, permanent monitoring	3 dimensions, 0 – 5.3 kHz
Acceleration range	± 2 G
Battery life	3 years
Wireless range	100 m
Nodes in a network	3
Other	Connection possible through car and shaft structures

Raw bit throughput rates for measurement data can be calculated from the sample rates presented in Table 1. The raw bit rate is needed for estimating the performance required from the wireless connection and the sensor itself. As mentioned before, high-quality data can be stored onboard the sensor, but the real-time data needs to be transferred without delay. Therefore, the data rate of the wireless connection has to be sufficient for the amount of data the sensor produces in real time. It shall be remembered that a slightly faster connection should be used in order to leave slight headroom for protocol and overall system overhead. The raw bit rate requirements for the measurements are presented in Table 2.

Table 2: Bit rate requirements for measurements

Measurement	Real-time bit rate	High-quality-data bit rate
Audio	16-bit * 6 kHz = 96 kb/s	16-bit * 52 kHz = 838 kb/s
Acceleration	3 * 10-bit * 2 kHz = 60 kb/s	3 * 10-bit * 5.3 kHz = 159 kb/s
Total	**156 kb/s**	**997 kb/s**

2 Criteria for selecting a wireless technology

Many wireless standards with different features have been developed for the growing number of wireless devices, gadgets and applications used in the modern world today. Ranging from Wi-Fi and other radio-wave standards to optical infrared communication in home entertainment remote controls, there is a technology for each different purpose. These technologies combine different technical solutions for achieving required functionality.

In the following sections, different criteria for selecting a wireless technology will be discussed. The most important criteria for the elevator sensor system are the range, data throughput rate and reliability of the connection. Additional criteria are the topology of the wireless network and security aspects. Because a connection is a combination of many different technical solutions, there is no single answer to which properties should be emphasized in order to gain certain functionality. Therefore, the following sections aim to give a general understanding of which properties should be considered when selecting a wireless technology, and how different technical solutions affect the connection and relate to each other. It will be seen that often there are both positive and negative effects in emphasizing certain properties.

2.1 Range

Multiple different aspects affect the range of a wireless connection. A wireless communication link consists of the transmitter, which defines the amount of power available for transmission, the signals path through air and obstructions, and the receiver and its ability to receive signal. The combined effect of these factors results in the maximum range that can be achieved in the particular wireless link. The term “link budget” is used for calculations of estimating the overall quality of the wireless link [2, p. 101]. Link budget will be described in detail in the next section.

The path of a radio-wave signal often contains obstructions, such as walls and even air, which attenuate the signal. Optical solutions, such as Li-Fi, are naturally restricted to the range visible to the link, or gained via a reflective path. Radio waves can propagate through many building materials, but some signal strength is lost due to absorption. The carrier wave frequency of the signal has an effect on the path losses of a radio-wave link. Higher data throughput rates lead to a lower range, due to reduced sensitivity of the receiver. These factors are discussed in sections 2.1.2 and 2.1.3.

2.1.1 Link budget

The term “link budget” is used for estimating the range and robustness of a wireless link. The equation for link budget can be expressed as

$$Link\ budget = P_{Tx} + |S_i|, \tag{1}$$

where P_{Tx} is the transmitter power and S_i is the sensitivity, or the minimum required signal strength of the receiver. The link budget equation gives the maximum amount of signal attenuation allowed from transmitter to the receiver, in order to establish a working connection [2, pp. 101-103]. Therefore, the best quality and longest range link will be achieved by maximizing the link budget i.e. maximizing transmitter power and receiver sensitivity.

The maximum transmission power of radio devices is regulated, and varies regionally and by different frequency ranges [3]. Different parts of the world have different regulations. Standards such as Bluetooth Low Energy (BLE) also define maximum allowed transmitter power, in order to meet the standard. Differences between standards are discussed in detail in Chapter 3. Because of regulations, standards and the physical capabilities of radio devices, increasing transmission power is possible only to a certain degree. Increasing transmission power is also detrimental for battery life, naturally.

Receiver sensitivity depends on the amount of noise in the receiver system. Minimizing electrical noise is thus a key factor in obtaining high receiver sensitivity [4]. The use of quality electronic components, as well as minimizing the amount of discontinuities, such as connectors, in the RF path of the device, will result in less noise and distortion in the electronics of the system. Additionally, receiver sensitivity directly depends on the data rate of the connection, thus, increasing the speed of the connection will always reduce receiver sensitivity. This relation is explained in detail in Section 2.1.3.

2.1.2 Carrier wave frequency

Using a higher carrier wave frequency leads to a lowered range of the wireless link. There are two reasons for this effect: first, the Free Space Path Loss (FSPL), which represents the loss of signal strength in ideal free-space conditions, increases with signal frequency. This is due to the fact that the ability of the receiving antenna to receive power depends on the wavelength of the received signal, as is explained next. Second, physical materials tend to attenuate higher frequency signals more, as is explained ahead.

The power that an antenna can capture from a signal with the power density of S depends on the aperture size A_e of the receiving antenna:

$$P_r = A_e * S. \tag{2}$$

The aperture of the receiving antenna is defined as

$$A_e = G * \frac{\lambda^2}{4\pi}, \tag{3}$$

where G is the gain of the antenna. [2, p. 71] Combining Eqs. (2) and (3), it is clear that an antenna receives more power when the wavelength of the signal increases:

$$P_r = G * \frac{\lambda^2}{4\pi} * S. \tag{4}$$

The results of this effect can be realized from the FSPL equation,

$$FSPL = \left(\frac{4 * \pi * d}{\lambda}\right)^2 = \left(\frac{4 * \pi * d * f}{c}\right)^2, \tag{5}$$

which shows that path loss in free space is proportional to the square of signal frequency f and the link distance d, and inversely proportional to the square of speed of light [2, p. 97]. Thus, it can be seen that the amount of path losses increases along with the frequency of the wireless signal.

Studies also show that as the signal frequency increases, so does signal attenuation of many building materials [5]. Multiple propagation models have been developed for estimating signal propagation inside buildings. COST231 Multi-Wall Model estimates that the attenuation of light walls at a frequency of 900 MHz is 1.9 dB, and 3.4 dB at 1800 MHz [2, p. 285], a 79% increased loss when the frequency is doubled. According to these results, using a lower carrier wave frequency will result in a longer range of the wireless link, especially inside buildings.

2.1.3 Receiver sensitivity

A signal level, which the receiver is capable of correctly receiving, is called the sensitivity of the receiver. A lower receiver sensitivity is therefore better, meaning that a −98 dBm receiver can detect signals that are half the power of those signals that can be detected by a −95 dBm receiver. Receiver sensitivity depends on the level of electrical noise compared to the signal level, known as the signal-to-noise ratio (SNR) [4].

Higher data rate requirements will result in reduced receiver sensitivity and thus a lower range of the wireless link. The two means for increasing the data rate of a connection are more complex modulation, and increased channel bandwidth. Both methods will decrease the sensitivity of the receiver. The effects of modulation are explained in more detail in Section 2.2.2.

Increasing channel bandwidth reduces the signal-to-noise ratio of the received signal due to added noise. A receiver contains narrow bandpass filters for selecting a certain frequency range that the receiver accepts. Widening the bandwidth of the wireless signal requires increasing the bandwidth of these bandpass filters. This will add thermal noise to the filtered signal, as the amount of noise that passes through a filter is proportional to the filters' bandwidth. Thermal noise is formulated in all electrical components, and it is nearly uniform across any frequency range, meaning that doubling filter bandwidth doubles the amount of noise. [4, pp. 26-28]

The power of thermal noise can be expressed as

$$P_{noise} = kTB, \tag{6}$$

where k is the Boltzmann's constant, T is the absolute temperature and B is the bandwidth of the noise [4, p. 27]. Eq. (6) can be used for estimating the theoretical sensitivity of the receiver in relation to channel bandwidth. For a channel bandwidth of 100 kHz, a filter bandwidth of 311 kHz could be selected. The thermal noise power in room temperature that passes such filter is

$$P_{noise} = 1.38 * 10^{-23} \frac{\mathrm{J}}{\mathrm{K}} * 290\ \mathrm{K} * 311\ \mathrm{kHz} = 1.244 \ldots * 10^{-15}\ \mathrm{W}. \tag{7}$$

Converted to decibel-milliwatts, the thermal noise is

$$\begin{aligned} P_{noise}[dBm] &= 10 * \log_{10}(1000\ * 1.244 \ldots * 10^{-15}\ \mathrm{W}) \\ &\approx -119\ \mathrm{dBm}. \end{aligned} \tag{8}$$

In an ideal situation, the receiver would therefore be able to receive data from a signal with the bandwidth of 100 kHz, whose power is just above the −119 dBm noise level.

However, real world filters do not provide an immediate cutoff at the filter frequency, which results in more noise passing through the filter. Additional noise is formulated after the filter in the electrical components of the receiver, mainly depending on the quality of the low noise amplifier. For example, in the TV industry, an additional 11 dB reduction is typically assumed when estimating receiver sensitivity [6]. The use of modulation increases the required signal-to-noise ratio even further, as will be explained in Section 2.2.2.

2.2 Data throughput rate

Data throughput rate can be a defining attribute when selecting a wireless technology. Depending on the application, a minimum data rate may be mandatory in order to achieve certain functionality, which eliminates slower options entirely. The data throughput rate of a wireless connection can be adjusted by the means of increased channel bandwidth, and modulation, which are described in the sections ahead. However, as mentioned before, high data rates result in adverse effects on other properties, such the range of the connection, due to decreased SNR. Additionally, overhead decreases the data rate that can be realized by the user application, as will be shown in Section 2.2.3.

Radio devices transfer information in the form of symbols. A symbol is a distinguishable value of a certain variable, such as the amplitude or frequency of the signal. For example, signal amplitudes of 1 V and 2 V are separate symbols.

The number of symbol changes per second is known as the symbol rate of the connection. The symbol rate is also known as baud rate, expressed in Bd. The symbol rate depends on the used channel bandwidth. The rate of actual data transferred in bits per second is called the data rate of the connection. The data rate can be lower, equal or higher than the symbol rate of the connection, by the use of different modulations.

2.2.1 Channel bandwidth

Channel bandwidth indicates the amount of frequency spectrum the wireless signal occupies. Channel bandwidth directly correlates with the symbol rate of a wireless connection. According to the Nyquist theorem, a maximum of two pieces of information can be sent every second per every Hertz of bandwidth. Therefore, a number of $2B$ symbols can be sent every second over a channel with the bandwidth of B. [7, p. 262]

The aforementioned is an ideal situation, in which no distortion or noise is present in the path of the signal. In practice, the symbol rate of $2B$ can never be achieved due to unavoidable noise in the received signal. It can, however, be concluded that increasing channel bandwidth will increase the possible symbol rate of the connection.

Channel bandwidth is regulated, as is the case with many other properties of wireless technologies. Regulation is needed in order to avoid channel congestion and to keep frequency spectrum available for other devices operating in close vicinity. More information of channel congestion is included in sections 2.3 and 3.1. Thus, channel bandwidth cannot always be adjusted in the hope of increasing the performance of the connection. As explained before, widening channel bandwidth will also decrease the sensitivity of the receiver due to increased noise.

2.2.2 Modulation

Modulation can be used for increasing the data rate of the connection without the need for increasing the bandwidth of the signal. Modulation specifies the way of how information is represented in the carrier wave signal. Two examples of digital modulation schemes are Amplitude Shift Keying (ASK) and Phase Shift Keying (PSK).

In the simplest form of ASK, the bits 0 and 1 could be represented by the signal amplitudes of 1 V and 2 V, for example. In PSK, the modulating variable is the phase of the signal, representing bits 0 and 1 by the phases of 0 and π respectively. Since there are only two different symbols which represent a total of two bits, these modulations are called binary modulations.

Increased data rates can be achieved by combining different types of modulations, and adding more possible symbols to a single modulating variable. Increasing the number of symbols results in higher order modulations. Today's digital communication utilizes a multitude of different modulations, such as the Quadrature Amplitude Modulation (QAM), which is a combination of ASK and PSK [8, p. 223].

The effect of modulation on the data rate of a connection is easily observed by comparing binary PSK to quadrature PSK. The difference of quadrature modulation over binary modulation is simply that four different phase symbols are used instead of two. In QPSK, bit sequences 10, 00, 01 and 11 are represented by the carrier phase of π/4, 3π/4, 5π/4 and 7π/4 respectively. 16-QAM allows 16 different symbols by using different combinations of signal amplitude and phase, increasing the amount of bits transferred by each symbol to 4 [8, pp. 222-223].

A common way of visualizing the modulation of a signal is a constellation diagram. Essentially, a constellation diagram displays all possible symbols of a modulation scheme, plotted in a complex plane, called the IQ-plane. In Figure 2, the constellation diagrams of BPSK, QPSK and 16-QAM are presented. The blue points represent the different symbols. In 16-QAM, a signal amplitude of A_1 and phase of φ_1 denotes the binary sequence 0011, for example.

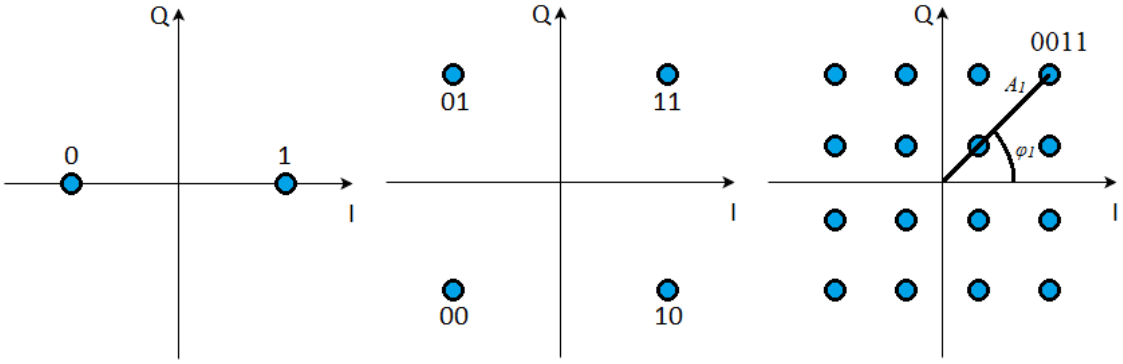

Figure 2: Ideal constellation diagrams of BPSK on left, QPSK at center and 16-QAM on right

With the help of the constellation diagram, the adverse effect of noise in real systems on modulation is easily observed. In a noiseless system, the angle and phase of the received symbols are always exact. In theory, this would allow for an infinite amount of separate symbols and thus, an infinite data rate [7, p. 10], as the receiver would always be able to distinguish different symbols. However, as real-world noise and distortion are introduced to the signal, uncertainty is added to the position of the symbols on the

diagram. This effect is illustrated in Figure 3. If the signal is very noisy, a received symbol could be interpreted as a different symbol entirely, leading to a detection error and corruption of data.

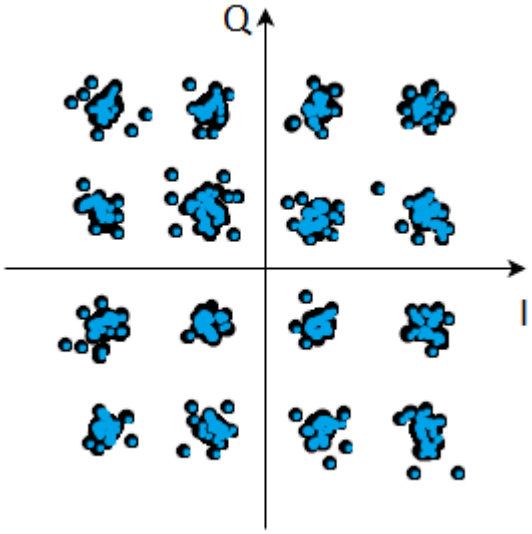

Figure 3: Constellation diagram of a real 16-QAM modulated signal

Minimizing the amount of detection errors requires a certain signal-to-noise ratio in the receiver. Intuitively, the required SNR depends on the complexity of the modulation i.e. the combination of different types of modulating variables, and the amount of symbol states of those variables. Table 3 presents the SNR required to obtain a certain detection error probability for different common modulation schemes. The simple BPSK and QPSK modulations require a low SNR to function correctly, whereas the complex QAM modulations, which are capable of transferring more data, require a higher SNR.

Table 3: Signal-to-Noise ratio required to achieve Detection Error Probability of 10^{-6} [7, p. 705]

Modulation	Required SNR [dB]
BPSK	10.6
QPSK	10.6
16-QAM	14.5
32-QAM	17.4

A complex high-order modulation scheme is clearly more sensitive to noise and other disturbance the signal experiences during transmission. These disturbances include fading- and Doppler-effects caused by a moving signal source or receiver, making higher state modulations more suitable for stationary radio links. The large amplitude changes of QAM require high linearity of the amplifiers in the transmitter and receiver, a feature which leads to low energy-efficiency. [8, p. 224] Because of these reasons, complex modulations such as QAM are not ideal for mobile, battery-powered devices.

2.2.3 Overhead

In wireless communication, overhead means the excess data that is not usable information, which needs to be transferred in order for the communication protocol to function correctly. This overhead includes several factors such as handshaking and collision avoidance before actual data transmission, packet headers and error detection and error correction. Packet headers include synchronization structures such as a preamble, a sync word, packet length and address information, and error detection

methods such as Cyclic Redundancy Check (CRC) bytes. Overhead caused by error detection is explained in detail in Section 2.3.2.

The amount of overhead compared to actual usable data could be described as the efficiency of the transfer protocol. The usable information in a packet is called the payload. If there is excessive overhead, the size of the payload will be a fraction of the total data that is transferred. Minimizing overhead will thus increase the data throughput rate that the users' application can utilize.

Overhead depends largely on the wireless protocol used and type of transferred data. For example, 802.11 protocols are designed for large payload data packets, and applications that transfer smaller packets more frequently, such as Voice over IP (VoIP), suffer from low throughput rate as the ratio of overhead to payload data is high. On the other hand, data blocks significantly larger than the payload size will increase overhead due to fragmentation as multiple packets, each including overhead, are needed. Figure 1 in [9] shows clearly the effects of payload size and data fragmentation in 802.11 protocols: the throughput of the connection increases as payload size is increased, up to the payload size of 1472 bytes, where fragmentation occurs. [9]

If a standard wireless technology is used, the amount of overhead cannot be controlled by any other means than adjusting the amount of data transferred in packets to the preferred payload, and selecting the most appropriate technology for the application. If a proprietary solution is used, good design of the protocol can decrease the amount of overhead considerably. However, some headroom for overhead needs to be reserved, since packet headers cannot be completely eliminated in digital communication.

In a battery operated device, overhead also decreases battery lifetime. A simple model for radio energy consumption assumes that each bit transferred requires a fixed amount of electrical energy, such as 50 nJ/bit at a certain distance [10]. If the amount of overhead is significant compared to the payload data, excess energy will be wasted in transferring bits that are not actual usable data.

2.3 Connection reliability

A wireless connection should provide a means for transferring data between remote devices with solid throughput and without loss of information. Maximizing the strength of the received signal and minimizing noise results in the best quality wireless link, due to decreased probability of errors in data. The previous sections discussed some factors that have an impact on signal strength, and should be considered in order to obtain a reliable connection.

However, even a good quality wireless connection will suffer from some transmission errors especially in changing conditions such as during movement, and due to external interference. Congestion of available frequency bands is a growing issue with the increasing number of devices operating in the same bands. Wireless protocols include multiple methods for minimizing loss of information and performance in unideal situations. These methods include frequency agility and collision avoidance, and error detection, error correction and retransmission of corrupted data. The following sections describe various means that are used for improving the functionality and reliability of a connection in sub-par conditions.

2.3.1 Channel congestion and compliance methods

Channel congestion occurs when multiple wireless systems are operating in the same frequency bands and in close proximity to each other. Compliance methods such as Listen Before Talk (LBT) and Adaptive Frequency Agility (AFA) are used for allowing devices using the same frequencies to avoid overlapping each other, and to dynamically change channels in order not to fully reserve a single frequency. In order to meet European radio standards, this kind of compliancy is mandatory in certain frequency ranges, such as the sub-GHz bands above 800 MHz frequencies [11, pp. 54-57]. If LBT and AFA are not used, regulations may limit the active duty cycle of a radio device to a short period such as 0.1 % per hour [11, p. 28]. In the 915 MHz bands used in the United States, no regulation on duty cycle or frequency agility is imposed [12], which may lead to high amount of interference since compliance is not mandatory.

A collision avoidance protocol, such as CSMA/CA, allows different technologies that support the protocol to co-operate in the same carrier frequency band in the same area. It involves a device requesting a turn for transmission before transmitting its data, avoiding multiple devices transmitting at the same time. This has the negative effect of adding delay and decreasing the data throughput rate of the coexisting systems. For example, a decrease of 4.6 % to 52 % in throughput can be observed when a pair of 2.4 GHz 802.11 devices operate alongside a pair of 2.4 GHz ZigBee or Bluetooth devices in the same area [13]. Such decrease in real-time data throughput may not be acceptable, and congested frequencies should be avoided altogether.

2.3.2 Error correction methods

Adding redundancy is a means for detecting and correcting the transfer errors that remain after taking all precautions for avoiding them. Transmitting data that includes absolutely no redundancy, i.e. data in which every bit is crucial for correct information, results in communication that cannot be totally error-free [7, pp. 734-745]. Thus, many digital communication systems add intentional redundancy to the transmissions, which also increases the amount of overhead.

Forward Error Correction (FEC) codes are used for achieving redundancy. Depending on the type of FEC, the added redundancy allows the detection, and in some cases, correction of errors. Error correction is achieved by appending redundant check bits to transmitted data bits, which increases the possibility of correctly interpreting the original data bits. Clearly the size of transferred code increases quickly, leading to inefficiency as shown in Table 4. Furthermore, the codes are not capable of correcting multiple consequent erroneous bits. Additionally, decoding such correction codes requires large memory storage and high complexity decoder in the receiver end. [7, pp. 802-805]

Table 4: Code efficiency of some Error Correcting Codes [7, p. 805]

Amount of correctable errors	Total bits / data bits	Code efficiency
1	3, 1	33 %
1	7, 4	57 %
2	15, 8	53.3 %
3	23, 12	52 %

Another way of achieving error correction is to implement error detection and Automatic Repeat Request (ARQ) functionality. Error detection requires less check bits

than error correction, leading to higher code efficiency [7, p. 805]. Upon detecting errors, it is up to the application to implement data re-transmission functionality. In some applications, it might be enough only to detect loss of information integrity, and re-transmitting data may not be necessary.

Error detection is achieved by calculating a check value for each sequence of data that will be transmitted, and adding the check value to the transfer. Upon receiving the data and the check value, the receiver can compare if the data still matches the check value. This relatively simple and efficient method can be implemented even in hardware, and is thus included in many of today's communication technologies. An example of a widely used error detection code is Cyclic Redundancy Check code. [7, pp. 805-822]

2.4 Network topology

Different network topologies can be used in wireless systems consisting of multiple devices. In a *star* type network, wireless devices communicate directly with only a single base station, which manages data routing between all the end nodes. In a *mesh* network, all devices may communicate directly with each other, and data can be routed to physically far away nodes using multiple hops through the nodes in between. A *hybrid* network is a combination of the two previous network types, where the network consists of several base stations relaying the communication between multiple clusters of end nodes.

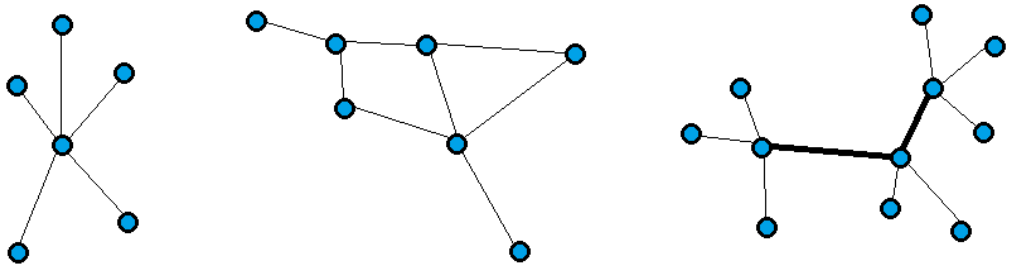

Figure 4: Structures of a star network on left, mesh network at center and hybrid network on right

Different network structures have advantages and disadvantages that should be examined considering the requirements of the application. First, a mesh network is generally better suited for low data rate applications where delay in information is not critical, whereas a point-to-point star connection is faster. This is due to the fact that in a multi-hop path, each hop involves a node first listening for data incoming from a source, and then switching to transmit mode and forwarding the data towards its destination, adding delay. Additional decrease in throughput comes from added overhead of routing information appended to the data. A decrease of up to 50 % in data throughput rate can be observed with each hop in a mesh network such as ZigBee [14].

Second, network topology affects the power consumption of the nodes in the network. Clearly in a multi-hop network, the nodes responsible for relaying the data of other nodes are active longer than the nodes actually producing or receiving the data. In the case of battery operated devices, this leads to the battery of the middle nodes draining faster than the battery of the far away nodes. On the other hand, in a star network, the power consumption is high for devices far from the base station, as high transmission power is required in order to achieve long range connection.

Third, the maximum coverage of the network can be extended by the choice of network topology. The range of a star-network is limited to the physical propagation capability of the wireless signal. However, in a mesh network, very large network coverage can be achieved due to the middle nodes functioning as repeaters for other nodes. Only the maximum number of nodes limits the range of a mesh network.

A dynamic hybrid network is capable of providing maximum battery lifetime for all nodes in a network. By monitoring the amount of energy stored on each node, and constantly changing which nodes operate as base stations, power consumption can be evenly distributed among all nodes, independent to their location in the network [10]. Naturally, a hybrid network will achieve similar coverage as a regular mesh network. However, the decreased data rate of a multi-hop network cannot be eliminated, and if a fast data rate is required, a star type network topology should be chosen over a mesh or a hybrid network.

2.5 Security of a wireless system

The security of wireless systems becomes an increasingly important subject as the number of wirelessly connected personal devices, as well as industrial machinery increases. However, the application, the nature of the information in the system, and the consequences of a security breach should also be kept in mind, before designing security for a system. As is the case with all design procedures, it is sufficient to design a system that is only good enough.

The elevator condition monitoring system is only used for collecting information of the health of the elevator. The system is not capable of controlling or affecting the operation of the elevator in any way, so unwanted, possibly dangerous behavior cannot be initiated by an attacker. Thus, a breach in security cannot lead to harm to people or to the monitored device, and absolutely impenetrable security is not necessary.

However, financial losses could be caused by feeding malicious data into the system, which would indicate a falsified breakdown of a component of the elevator. This could be used for triggering extra maintenance visits, unnecessary part replacements and downtime for the elevator. Furthermore, the real measurement data from the elevator could become unusable, as it would be disrupted by the fabricated data. If health data leaks outside of the system, it could potentially be used by competitors to locate weaknesses in the design of the elevator. Due to these reasons, security that prevents adding false data, as well as preventing others from acquiring the real data transferred inside the system, should be included.

Perhaps the simplest method of adding a layer of security to a system is to add encryption. Encryption is used for encoding messages in the system in such way, that the original information can be decoded only by knowing a predefined encryption key. It is generally thought that modern encryption methods, such as the Advanced Encryption Standard (AES) are so strong that they cannot be forcefully decoded by today's computing power, and thus offer an effective way of hiding information.

Additionally, an authentication method should be included for preventing unauthorized users from accessing the system. Authentication is achieved by storing information such as unique identifier numbers of allowed users, and using a suitable procedure for validating the user before accepting connection. Such method prevents unauthorized connection and feeding fabricated information into the system.

3 Choosing a wireless solution for the sensor system

An elevator is considered a difficult environment for electronics equipment. The most significant obstacle for a wireless network is the relatively long distance between the elevator car, the machine room and other components system. The moderately high data rates of the system require high SNR, which is especially challenging to obtain through the car structure and outside the shaft. Equally important is the long-term availability of the technology, and capability for reliably functioning in areas densely populated with other wireless networks, such as office buildings.

The elevator shaft is traditionally made of concrete as a part of the building structure, with the height of tens of meters to hundreds of meters, depending on the height of the building. In modern elevators the shaft may be steel, glass or even open (for example in ship elevators) for visual and space-saving reasons. A solid shaft could potentially benefit wireless communication by reducing the amount of outside interference. In open shafts, this will not be the case.

The car travels in the shaft and is suspended from ropes, with the traveling cable providing power and wired communication to the car. In most elevators there is also the counterweight, moving in the direction opposite to the car direction. As the elevator moves, the position of the elevator components in the shaft varies drastically. At some point the counterweight moves past the elevator car, which obscures line-of-sight from the motor on the top of the shaft to the counterweight, for example.

The distances in the shaft, as well as the positioning of the different components, set requirements for the range and penetration capability of the wireless technology used in an elevator shaft. Additionally, the counterweight has no electrical power available, adding a constraint to the power consumption of the wireless sensors. The bit rates presented in Table 2 define the minimum data rate capability for the connection.

In Sections 3.1 and 3.2, different possible methods of wireless communication are researched and reviewed from the perspective of requirements for elevator use. These wireless solutions include common ISM-band radio technologies, and a light based solution, Li-Fi.

Section 3.3 describes an initial signal quality measurement conducted in a true operating environment of the sensors: an elevator shaft. The test was done for comparing the signal quality between different wireless technologies in the ISM frequency bands.

In Section 3.4, the different wireless technologies are compared based on their technical properties, as well as taking into account the results from the measurements. A technology best suited for use in the elevator environment is selected. The selection serves as a starting point for designing the sensor prototype in Chapter 4.

3.1 ISM-band radio-wave technologies

Radio waves are the standard means of wireless communication in today's electronic products. The use of different frequency bands is heavily regulated, but some ranges have been reserved for free, unlicensed use as long as some compliance requirements, such as interference tolerance and maximum duty cycle, are met. These unlicensed bands are called the Industrial, Scientific and Medical (ISM) bands, which include

frequencies from a few megahertz up to the 246 GHz range, depending on the application and regional restrictions. [3] [15]

Two common ISM frequency ranges are the 2.4 GHz band and the 315-920 MHz sub-GHz bands, of which the former is used by most of today's short-range devices. The high frequency band was made available for unlicensed use when the microwave oven started becoming a common household item [16]. This frequency range has since become the most commonly used range for all sorts of consumer applications, such as Wi-Fi and Bluetooth. The 2.4 GHz band is also the only ISM range commonly available worldwide. For these reasons, the number of devices operating in the 2.4 GHz today is very large, and the band suffers from high level of congestion [17].

The sub-GHz bands on the other hand are a relatively new solution for wireless communication. In 2010, the European Parliament released frequency bands around the 800 MHz frequency available for unlicensed use in Europe [18]. This decision was done after the shutdown of analogue television broadcasting. In other parts of the world, the frequencies around 433 MHz and 915 MHz are common. The interest in using low frequency bands for digital communication has been growing, since the frequencies can effectively be utilized for long-range wireless communication. As stated in the Section 2.1.2, lowering the carrier frequency will benefit the maximum connection range.

Using Eq. 5, the free air range benefit of using an 868 MHz wireless link instead of a 2.4 GHz link can be calculated. By making the free space path loss for the two frequencies equal, the range benefit can be obtained as follows:

$$FSPL_{868\ MHz} = FSPL_{2.4\ GHz} \tag{9}$$

$$\left(\frac{4 * \pi * d_1 * 868\ MHz}{c}\right)^2 = \left(\frac{4 * \pi * d_2 * 2.4\ GHz}{c}\right)^2 \tag{10}$$

$$d_1 * 868\ MHz = d_2 * 2.4\ GHz \tag{11}$$

$$\frac{d_1}{d_2} = \frac{2.4\ GHz}{868\ MHz} \approx 2.76. \tag{12}$$

Therefore, by reducing the carrier frequency from 2.4 GHz to 868 MHz, the range of the link could be almost tripled if the same transmit power is used. Calculated differently, an 8.9 dB higher signal strength can be expected if the two different frequency links operate at the same distance [19, p. 7]. As suggested by propagation models through building materials, an even greater benefit will be observed if the wireless link operates through the elevator shaft, due to reduced losses in building structures.

3.1.1 ZigBee

ZigBee is a network standard aimed for very long lifetime, battery operated wireless sensors, operating at both the 2.4 GHz and the sub-GHz frequency bands. It follows the 802.15.4 physical layer standard for low-rate networks, which limits the maximum data rate of the technology to 250 kb/s. The protocol defines a maximum packet size of 127 bytes, of which 89-93 bytes are available for the user application due to overhead [14], which lowers applicable data rate. Additionally, the 250 kb/s data rate is only available

when the 2.4 GHz carrier frequency is used, and the sub-GHz bands are limited to 20 and 40 kb/s data rates. The topology of ZigBee is a hybrid network consisting of end nodes, router nodes and a single coordinator node. The long lifetime is achieved with low duty-cycle ratio of the sensor nodes. [20]

ZigBee and other 802.15.4 based technologies have been successfully used in applications such as agricultural monitoring [21], and monitoring structural health [22]. Often the applications for these type of low-rate networks only require intermittent, or non-real-time data, which allows a very low duty cycle for the sensors. Thus, sensor nodes can be powered down for most of the time, and transmit a single value, such as a temperature measurement, infrequently. A battery lifetime of several years can be achieved by such duty cycle scheme. There are not many real-time applications for low-rate networks, mainly due to the limited data rate. In an experiment evaluating the performance of ZigBee for voice streaming applications in the 2.4 GHz bands, a steady throughput of 30 kb/s was achieved. [14]

Due to the low applicable data rates of ZigBee, it is not a suitable solution for the monitoring sensor because of the higher real-time data rate requirements. However, the low duty cycle operation of ZigBee could be adopted for decreasing average power consumption in permanent condition monitoring purposes.

3.1.2 Bluetooth and BLE

Bluetooth is a standard designed for medium throughput applications such as multimedia transfer in mobile phone accessories. Standard Bluetooth offers a 1 Mb/s data rate using frequency shift keying modulation, and an enhanced data rate of 2 Mb/s using higher order phase shift keying [23]. The Bluetooth standard is solely restricted to the higher 2.4 GHz frequency bands, thus suffering from frequency band congestion and relatively low range. The range lost due to the high frequency can be compensated by the maximum allowed transmission power of +20 dBm for Bluetooth class 1 devices. [20]

BLE is the latest addition to the Bluetooth standards. As implied by its name, the standard aims to minimize power consumption, and it offers a solution for low power IoT devices. However, in order to obtain low power consumption, the transmission power of BLE standard devices is limited to +5 dBm, naturally leading to lower range than when using regular Bluetooth. Thus, the standard in fact trades off link range in order to decrease power consumption.

Additionally, BLE is aimed for transferring only a limited amount of data in certain time span. Similarly as in ZigBee, BLE nodes can remain powered down most of the time, and when data is ready to be transmitted, the nodes wake up to advertise the data. This advertising method is unidirectional, as data flow direction is restricted from the data producer nodes to a receiver node. Unlike regular Bluetooth, no continuous connection is therefore required for simple data transfers. Due to the intervals in data transfers, an experiment evaluating the real performance of BLE obtained the applicable data rate of only 58.5 kb/s. [24]

The greatest advantage of Bluetooth is that it is widely accepted as a standard means of communication today. Using a widely spread standard allows fast and easy application development, and gives the possibility to connect to the system with different vendor devices. Nearly every laptop and mobile phone on the market supports Bluetooth, which

would allow a sensor network to be easily accessed by service personnel without the need for any additional equipment. On the other hand, the vast amount of Bluetooth and Wi-Fi devices operating in the same frequency bands results in interference, lowering the quality of the signal and thus limiting the range and throughput rate that can be achieved.

An example of a device monitoring application using Bluetooth is the Steelman Pro Bluetooth ChassisEAR, a wireless tool aimed for diagnosing fault locations in the chassis of a car. The system consists of four separate nodes that can be attached to various parts on the car, and headphones which are used for listening audio from one of the end nodes at a time, in real-time. This allows the car to be driven while the maintenance person sits inside the car listening for noises which could indicate faulty parts. [25]

3.1.3 802.11 standards

802.11, more commonly known as the Wireless LAN, is a set of protocols used for linking personal computers and other devices to a wireless network. The different standards are designed for a high throughput, continuous and reliable connection, often requiring the devices either to have constant supply of power or a large power storage. The data rates vary from 1 Mb/s to 600 Mb/s, with channel bandwidths of 20 MHz to 160 MHz. The widest channel bandwidths and thus increased data rates are achieved using multiple separate antennas. Various complex modulation schemes, such as 16- or 64-QAM, are used to obtain the highest data rates. The different protocols operate at the 2.4 GHz and 5 GHz frequency bands. [26]

The WLAN standards are widely used and accepted as a means of wireless communication. Additionally, an 802.11 standard technology would clearly feature high enough throughput for the data requirements of the elevator monitoring sensor. However, as described in Section 2.1.3, using unnecessarily complicated modulation and wide channel bandwidths will increase noise in the communication link, which leads to lowered receiver sensitivity and thus a shorter wireless range than what could be achieved with a more optimized technology. The combination of the high carrier frequencies of 2.4 and 5 GHz, as well as the high data rates, result in a relatively low range for WLAN connections.

Additionally, as shown in Section 2.2.3, 802.11 protocols are designed for large payload data. In a sensor system producing a low amount of data, the large ratio of overhead compared to payload will lead to lowered throughput rate even if the physical connection is capable of fast bit rates. Due to these reasons, 802.11 is not the optimal choice for a system with moderate data rate requirements, such as the elevator sensor system.

3.1.4 802.11ah

802.11.ah is an upcoming WLAN standard operating at the sub-GHz frequency bands. The aim of the standard is to create a low power, long range version of currently used 802.11 standards, more suitable for large scale sensor networks [27]. This is made possible by the naturally better propagation characteristics of the lower carrier frequency, while still maintaining the easy connectivity of traditional WLAN protocols. Another advantage is the lower external interference, due to the lower amount of devices and compliance requirements that are mandatory in the sub-GHz frequencies.

In 802.11ah, numerous design choices have been made with low-power networking in mind. Channel bandwidth can be varied from 1 MHz to 16 MHz and multiple modulation schemes, such as QPSK and 16- to 256-QAM, are available. Adjustable data rates from 100 kb/s to 11 Mb/s can be achieved, making the standard scalable for different data throughput and range needs. More compact frame formats are implemented in order to reduce protocol overhead, allowing for better efficiency in data transfer. For example, MAC overhead is reduced by 60 % compared to legacy 802.11, from 30 bytes to 12 bytes. In addition, power saving mechanisms such as alternating between an awake and a sleep state, which are already implemented in 802.11 protocols, have been revised for the new standard. Shorter awake periods can be used while still being able to detect incoming signals, resulting in reduced energy use. [27]

The standardization of 802.11ah should be completed in early 2016 [27], meaning that it will probably take a few years until the technology starts gaining more interest. If accepted as a new standard for machine-to-machine communication, the technology would offer a simple and functional means of communication in an elevator environment. Due to improvements targeted towards sensor networking, as well as maintaining the connectivity of traditional 802.11 protocols, 802.11ah could be a viable solution for developing wirelessly connected devices in the future.

3.1.5 DECT

Digital Enhanced Cordless Telecommunications (DECT) is a wireless standard commonly used in cordless telephones and baby monitors. It operates in the 1.8-1.9 GHz frequency ranges, enabling slightly longer wireless range than 2.4 GHz technologies, but shorter range than sub-GHz technologies. The standard is mainly aimed for transferring digital audio, but it also includes a DECT Packet Radio Service (DPRS) for transferring Internet Protocol packet data with speeds from 840 kb/s up to 5 Mb/s using a variety of modulation techniques. [28]

New power saving features have resulted in a new ultra-low energy standard, DECT ULE, which is aimed for home security and home automation applications. Similarly as other very low-power solutions, DECT ULE achieves low average power consumption by specifying a low duty cycle for the devices. The ULE protocol is achieved entirely by software extensions, meaning that devices could support both ULE for low-power applications, while maintaining support for standard DECT functionality.

DECT could be a technically suitable solution for the use in the elevator monitoring sensor. The advantage of the technology is the use of the uncommon 1.8-1.9 GHz frequency band, lowering the amount of interference from other devices in close proximity. The technology is aimed towards transferring digital audio as well as including capability for data transfer, which are features that fulfill the requirements of the elevator sensor entirely.

However, as DECT is used in cordless telephones, certain locations such as office buildings could suffer from excessive amount of congestion if the same technology is used in office equipment. The relatively high carrier frequencies do not offer similar range as the sub-GHz technologies. In addition, DECT was launched already in 1987, and has not since gained mentionable interest in the wireless communication market. Especially high performance applications are largely dominated by other technologies. As it could potentially be substituted by other technologies, DECT might not be the most long-lasting solution for the elevator monitoring system.

3.1.6 Proprietary solutions

In addition to the available standardized technologies, one possibility to achieve communication is to create a new type of wireless solution, suitable for a specific application. This type of application-specific approach can yield good results with minimal amount of downsides. Most of the aforementioned wireless technologies offer both advantages and disadvantages, fulfilling some requirements but lacking performance in other areas.

When defining a new type of solution, the properties of the wireless technology can be selected so that specified requirements are fulfilled as well as possible. For example, a carrier frequency from the sub-GHz bands should be selected for the longest wireless range, and certain channel bandwidth and modulation schemes can be used for obtaining the minimum required data rate, while minimizing unnecessary noise. The transmission power of the devices can be freely adjusted, as long as regulations for the specific frequency bands are fulfilled.

Another benefit of a proprietary connection is the possibility for minimizing protocol overhead, leaving more of the connection bandwidth free for the user application. As mentioned before, for example both BLE and ZigBee offer far less throughput for the user application than the maximum data rate of the physical connection would allow. Minimizing overhead includes adjusting the frame format of transferred packets to include the most payload and the least amount of header overhead. Additionally, unnecessary verification of connection integrity, including retransmission of data, can be minimized if the application can tolerate some errors in the communication. The real-time operating mode of the elevator sensors can function with some amount of errors, as will be explained in Section 4.3.3.

However, an entirely new protocol has to be designed from the ground up, meaning that there is no protocol for device discovery and authentication, easy connectivity, and ensuring connection integrity, for example. All additional functionality, other than transferring raw data from a source to a predefined end node, has to be created by the designer himself. Care has to be taken that RF standards are met. Thus, using a proprietary technology requires by far the most amount of work in order to achieve functional communication.

An example of a 2.4 GHz proprietary technology application is a CMOS Short-Range Wireless-Sensor-Network interface developed for replacing sensor cables in a vehicle with a wireless connection [29]. The technical features such as the range and data-rate of the system resemble those of ZigBee; however, a proprietary solution was created to achieve good real-time performance. The communication protocol was designed to allow plug-and-play of new sensor nodes to the network, as well as allowing maintenance to access the system remotely via a handheld PDA tool. A different application for collecting real-time vibration data from a network of 40 different sensors on a highway bridge was designed using a proprietary technology [30], a feat which would be difficult to achieve with any of the standardized solutions presented before.

3.2 Li-Fi

In addition to new sub-GHz frequencies in the ISM bands, the visible part of the electromagnetic spectrum is also gaining interest as a data transmission medium. Fiber optics are already used for obtaining data transfer rates of several gigabits per second.

Li-Fi is an upcoming technology, which moves the light-based communication from optic cables into free air, functioning much like traditional Wi-Fi, as the name implies.

The motivation for using light for communication comes from the increasing congestion in traditional radio wave frequency ranges, and the abundance of light sources already available in modern environments. By altering the intensity of the light sources very rapidly, information can be modulated into the light without affecting its visual appearance. In addition, the high frequency ranges of visible light allow very high connection speeds. Simple, single wavelength systems have reached data rates up to 3.5 Gb/s [31], while some more complex systems have promised data rates up to hundreds of Gb/s.

Another benefit of using visible light for communication is that the range of the system is limited to the area visible to the wireless devices. The range of light in fact results in a new concept of wireless cell size, the optical attocell, which limits communication even into a single room. In a confined space, such as the elevator shaft, this results in communication which is completely free of interference from outside systems. [31] An elevator shaft, with the exception of glass shafts, is also protected from elements which are highly disadvantageous for optical communication: weather and sunlight. As long as line of sight is maintained, the range of a light-based system is not an issue, as functional ranges of several kilometers have already been achieved [32]. Additionally, the system could not be accessed from outside of the shaft, increasing its security.

However, the limited range is also the greatest disadvantage of light-based communication. Naturally such system is not best suited for connecting mobile devices that may lose line of sight during movement. For a permanent installation in an elevator this is not a defining issue, as the positioning of the devices can be oriented so that visibility is always maintained. Connectivity through car and building structures still require the use of an additional wired or wireless connection, increasing the overall cost and complexity of the system. Thus, for fulfilling all the requirements set for the condition-monitoring sensor, traditional radio-wave based communication methods offer a more applicable solution.

Additionally, Li-Fi is still a very fresh and developing technology. Unlike for fiber-optic communication, off-shelf transceivers for free-air optical communication cannot be easily found. It is difficult to say whether Li-Fi will become a widely accepted means for communication in the future. Once the technology is more matured, the feasibility of using light for elevator communication should be re-evaluated.

3.3 Preliminary measurements with different technologies

A measurement for comparing wireless technologies was conducted in a test elevator in the office building of KONE Hyvinkää. The aim of the test was mainly to compare the signal quality between 2.4 GHz and 868 MHz carrier frequencies in a real environment, and to see the penetration capability of both frequencies through the metal chassis of the car. In addition, the test showed how ZigBee and BLE protocols affect the amount of errors in communication, and how a different data rate affects the quality of the received signal.

3.3.1 Test setup

The tests were carried out in an elevator shaft with the car run distance of 21.4 meters. For each different test case, three runs were made in order to avoid sporadic issues in

the connection and to get an average result. Each run consisted of the elevator car traveling from the top to the bottom of the shaft, the doors opening to the landing and then closing, and the car traveling back to the top of the shaft. The counterweight traveled to the direction opposite to the direction of the car. The receiver was inside the car along with a PC logging the received packets, and the transmitter was placed onboard the counterweight using magnets. The test setup is illustrated in Figure 5, and the installation of the devices can be seen in Figure 6.

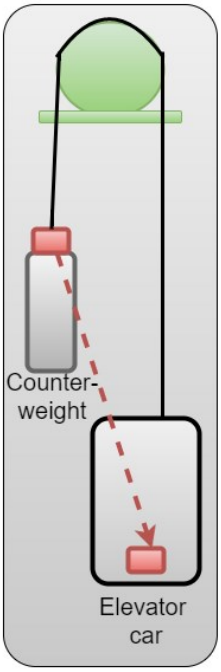

Figure 5: Test setup for preliminary measurements

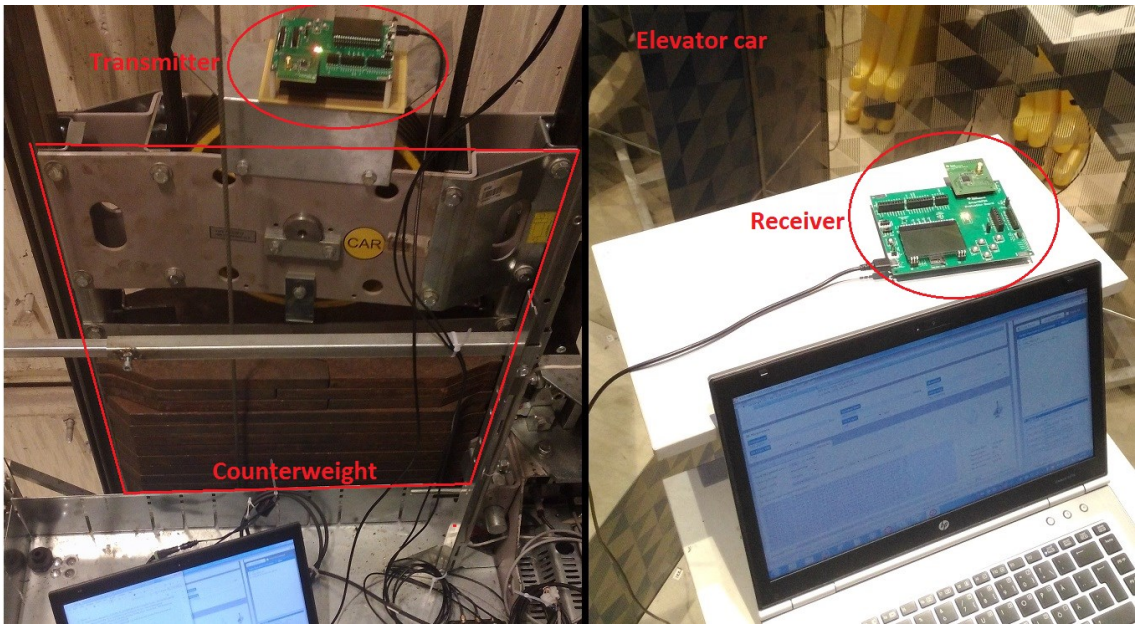

Figure 6: Installation of the transmitter on the counterweight on left, and the receiver inside the car on right

The tests were done using SmartRF06 Evaluation Boards from Texas Instruments, fitted with different types of radio modules for the different wireless technologies. These modules are the Texas Instruments CC1310 sub-GHz module, and the CC2650 2.4 GHz

ZigBee/BLE module. For obtaining as comparable results as possible for the different technologies, a constant transmission power of +5 dBm was used. Additionally, a single run with the transmission power of −10 dBm was tested. The software used for logging the received packets was Texas Instruments SmartRF Studio 7. The different test cases are summarized in Table 13.

Table 5: Test cases for comparing wireless technologies

Test case	Technology	Settings	Graph
1	868 MHz proprietary	200 kb/s, +5 dBm	Figure A1
2	868 MHz proprietary	400 kb/s, +5 dBm	Figure A2
3	868 MHz proprietary	400 kb/s, −10 dBm	Figure A3
4	2.4 GHz ZigBee	250 kb/s, +5 dBm	Figure A4
5	2.4 GHz BLE	1 Mb/s, +5 dBm	Figure A5

Three important parameters for each run were recorded: the received signal strength indicator (RSSI) of received packets, the amount of CRC errors, and the amount of packets lost entirely. The CRC calculation is an automatic feature of the radio modules. Calculating the number of lost packets was simple: as each transmitted packet included an incrementing identifier number (ID), by subtracting the ID of two consequently received packets from each other, the number of packets missing in between can be obtained. These three parameters were plotted on a graph along with a 20 period moving average of the RSSI value.

3.3.2 Test results

Figures A1-A5 in appendix A show the results of test runs for different wireless technologies. Each plot follows the same general form: first the counterweight and the car move towards each other and the measured signal strength increases. At the middle of the shaft the car and the counterweight move past each other, and from that point the signal strength starts decreasing. This forms the first spike in the RSSI plot.

After the first spike, the car stops at the bottom of the shaft and the landing doors open. This caused a drop in the signal strength and often resulted in a number of packet errors, if the signal strength dropped below the sensitivity of the receiver. This effect was present in nearly all of the 21 runs made during the testing, which indicates a possible decrease in signal quality every time the landing doors are opened. The reason for the effect could be that the elevator shaft in fact might act as a waveguide, and the doors opening to the side of the shaft change the impedance of the waveguide at the landing locations. However, this should be further studied in a controlled environment, before making assumptions on the mechanism or generalizations to other shafts.

The decreased signal strength is compensated by the LNA of the receiver, which adjusts its gain to bring the signal strength back to an adequate level. This effect is most clearly seen in Figure A3 at x-axis position 500, where the signal level is quickly increased from −90 dBm to −80 dBm, and then stays exactly at the −80 dBm level. This functionality of the LNA forms slight bumps in the RSSI plots in around the middle of the graphs.

After the landing doors are closed, the car travels back to the top of the shaft. This forms the second spike in the RSSI plot, as the car and the counterweight once again pass each other.

From Figures A2, A4 and A5, the improved range and penetration capability of the lower signal frequency can be clearly observed. As suggested in Section 3.1, the strength of the 868 MHz technology is around 10 dB higher (Figure A2) compared to the 2.4 GHz technologies (Figures A4 and A5). Table A1 shows the percentage of corrupted and lost packets for each tested setting. Due to the increased signal strength, the proprietary sub-GHz technology is clearly superior in receiving packets reliably, having approximately 8 times lower error rate than the higher frequency technologies.

Additional runs with a lower bit rate of 200 kb/s and a lower transmit power of −10 dBm were tested with the sub-GHz radio. Comparing Figures A1 and A2 it can be seen that halving the data rate slightly increases the received signal strength, which leads to almost zero packet errors. The reduced data rate allows narrower channel bandwidth, a narrower bandwidth of the receiver filter and thus, a better SNR, as was implied in Section 2.1.3. When testing the sub-GHz technology with the lower transmit power of −10 dBm, the amount of packet errors reached the same rate as the 2.4 GHz technologies at +5 dBm power. This run is plotted in Figure A3.

As suggested by theory, the test confirms that a better quality connection can be achieved using a lower carrier frequency technology. In addition, the maximum transmit power of CC1310 is +14 dBm, which leaves a 9 dB headroom to the tested +5 dBm level. As the run distance in the test was only 21.4 meters, the ability to increase transmission power will most likely be necessary when the link distance is increased to the specified 100 meters.

3.4 Selecting a technology

Selecting a technology from the vast amount of possibilities is not a straightforward task since all technologies have strengths and weaknesses in different areas. Some properties, such as the range of the connection, are naturally more important than others, but they might be difficult to compare since they are affected by multiple different factors. In some cases, certain properties might be difficult to evaluate as information may be sparse or in such format that it is difficult to compare to other technologies. For example, the range of a light-based system cannot be evaluated by comparing the frequency of the system, as can be done with radio-wave technologies.

For aiding the comparison of different technologies, a selection matrix with multiple weighted indicators was created. The matrix includes indicators which are both numerically comparable, but also factors that need to be evaluated in a more general manner, such as predicted ease of implementing the technology. The different factors are weighted according to their importance from the perspective of requirements for sensors in elevator environment. The indicators and their importance are summarized in Table 6.

Each technology will be given a score between 0 and 1 for every indicator in Table 6. The score will be weighted with the weight of the indicator. For each technology, an average of the weighted scores will be calculated, which results in an overall score between 0 and 1 for each technology. The total score can be used for roughly organizing the technologies from the best to the worst.

Table 6: Indicators used for selecting a wireless technology

Indicator	Weight	Explanation
Carrier wave frequency	0.9	A lower carrier wave frequency increases the range and penetration capability of the signal. Li-Fi is limited by visible sight and transmission power.
Data rate	0.9	Measurements produce data at rate of 156 kb/s, but headroom needs to be reserved. Excess data rate is useless and has other adverse effects on the connection. Adjustable data rate is desirable.
Modulation scheme	0.7	Simpler modulation schemes result in a more reliable connection. Availability of different modulation schemes for different situations is beneficial.
Channel congestion	0.7	Less congestion allows more available frequency spectrum and a better quality connection.
Ease of implementation	0.5	A widely accepted, mature technology is proven and offers features, such as security. A proprietary technology needs to be designed and implemented by the designer himself.

As suggested before, it is difficult to determine the importance of all properties of a wireless technology exactly. Also, as mentioned before, the properties of different technologies might be challenging to compare to each other. Therefore, a selection matrix should never be the only indicator used for making an important decision, and some freedom of choice should be left for the designer as well. A selection matrix will guide this decision, but the greatest aid comes from the planning of the matrix, which forces the designer to carefully think which properties are the most crucial for the application.

The technical properties of the different technologies are summarized in Table 7. The weighted results for each technology are presented in Table 8.

Table 7: Summary of properties of wireless technologies

Indicator	Proprietary sub-GHz	WLAN	802.11ah	Bluetooth / BLE	DECT	Li-Fi
Carrier wave frequency	868 MHz	2.4 – 5 GHz	868 MHz	2.4 GHz	1.9 GHz	-
Data rate	Up to few Mb/s	1 – 600 Mb/s	0.1 – 11 Mb/s	1 - 2 Mb/s	0.84 – 5 Mb/s	Several Gb/s
Modulation scheme	Simple	Complex	Variable	Variable	Variable	-
Channel congestion	Low	High	Low	High	Moderate	None
Ease of implementation	Low	High	High	High	Moderate	Low

Table 8: Wireless technology selection matrix

Indicator	Proprietary sub-GHz	Wi-Fi	802.11ah	Bluetooth / BLE	DECT	Li-Fi
Carrier wave frequency	1	0.6	1	0.6	0.7	0.5
Data rate	0.8	0.9	1	0.9	0.9	0.8
Modulation scheme	1	0.7	0.9	0.8	0.9	0.5
Channel congestion	0.9	0.4	0.9	0.4	0.8	1
Ease of implementation	0.5	1	1	1	0.8	0.4
Overall score	0.64	0.52	0.71	0.54	0.61	0.48

According to the selection matrix, sub-GHz 802.11ah is the technically the best technology for the elevator sensor, followed by a proprietary sub-GHz technology. 802.11ah achieves the long range of the low carrier frequency and features a suitable data rate, while preserving the benefits of standardized, widespread WLAN protocols. Unfortunately the standardization of 802.11ah is not yet ready, and there are no devices available for implementing the technology.

The second option is to create a proprietary connection using the sub-GHz frequency bands. Using a proprietary technology involves the most amount of design work, but allows obtaining the best features required by the application. All additional functionality such as device handshaking has to be implemented in the application software. On the other hand, at the same time this allows minimizing protocol overhead, and realizing the most available throughput for the user application.

The other technologies fall short mainly due to the higher carrier frequencies leading to lowered wireless range. It should be noted that Li-Fi is given an average result in the carrier wave frequency and modulation categories, as Li-Fi cannot be directly compared to other technologies. As the range requirements for the sensor are demanding, the sub-GHz technologies immediately become a very feasible choice. Due to the lack of a ready-made standard, a proprietary sub-GHz technology is selected. The option for 802.11ah, or similar upcoming technology, should be reserved as a possibility for future improvement.

4 Designing the sensor system prototype

The following sections explain the design procedure of the wireless sensor system prototype. As a proprietary sub-GHz technology was selected for communication, the design of the sensor nodes started from selecting a device suitable for such wireless connection. An MCU with an integrated processor, memory and RF section is selected, since it provides fast and easy implementation for the core of the sensor. An overview and the general functionality of the whole sensor system is described in Section 4.1, followed by the hardware design of the sensor nodes in Section 4.2.

Section 4.3 describes the structure of the sensor node software. A simple LabVIEW software for gathering data and controlling the sensors is presented in Section 4.4. A small batch of prototypes was produced for evaluating the performance of the design. The manufacturing of the sensor prototypes is briefly described in Section 4.5.

4.1 System overview

The overall sensor system consists of three units: a transmitter, a receiver and a data processor device. The transmitter is responsible for producing measurement data, which is combined into radio packets and transferred wirelessly to the receiver. The system may contain multiple transmitters.

The receiver deconstructs the packets from the transmitter, and writes the measurement data to a UART port, which is then read by the data processor. The receiver is also capable of producing measurement data itself, since it features the same measurement devices as the transmitter. However, data from only a single transmitter or the receiver can be transferred or examined at a time. This limitation is the result of the relatively slow proprietary connection, which does not include any additional features other than transmitting raw data, thus making it difficult to obtain data simultaneously from multiple sources. The processor device is responsible for storing, processing and visualizing the collected data. During the prototyping phase the processor is a standard PC, but it could be replaced by a data router device that would send the data to a cloud service for remote condition monitoring.

Figure 7 visualizes the different units in the system, their tasks and the data flow between the units. The tasks are visualized as the grey rectangles inside each actor. It should be noted that the tasks are presented as general functionality of the unit, and do not represent the actual software tasks running onboard the units.

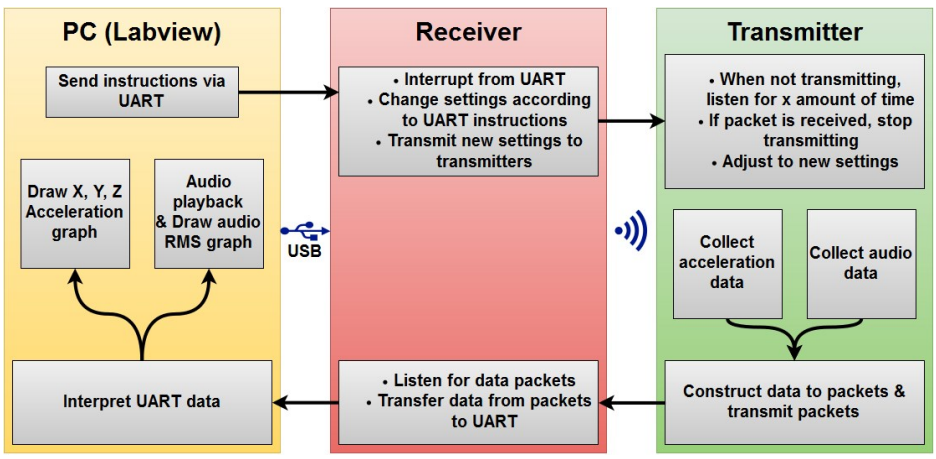

Figure 7: Overview of sensor system

The receiver node is always powered and is constantly listening for wireless data from the transmitters. The receiver may also receive control instructions from the processor device through the wired UART connection. The processor controls which measurements are needed, what resolution and sample rate should be used by the sensors and which transmitter is selected for real-time listening. The control instructions are mainly used for altering the functionality of the system in real-time troubleshooting situations. The receiver transmits new settings to the transmitter nodes wirelessly.

It should be noted that it is necessary for each unit in the system to always know the state of the system and the selected measurement settings. In Section 4.3.2, it will be seen that for example the way how the transmitter structures measurement data in packets may vary depending on the resolution of the measurements, and the amount of information that is transferred in the system. Thus, it is required that the receiver and the data processor devices also know the format of received packets in advance.

The transmitter nodes produce the measurement data. As the system is aimed for both real-time use and permanent monitoring, the functionality of the transmitter varies slightly depending on the operating mode. In real-time monitoring mode, measurement data is sampled, constructed into a packet and transferred to the receiver constantly. As stated in previous chapters, overhead can quickly decrease the data rate of a connection. Thus, in real-time operating mode, no handshaking or other means of synchronizing are used, and the transmitter functions much like a walkie-talkie, constantly transmitting data. Since a sub-GHz frequency is used, RF compliance regulations described in Section 2.3.1 must still be followed.

The transmitter also switches momentarily to receive mode in order to listen for possible control instructions from the receiver node. If the transmitter receives a packet containing control information, it will adjust the measurement settings according to the instructions received in the packet.

In permanent monitoring mode, measurement data is produced at a rate which is too high to be transferred directly using the wireless connection. Therefore, data is temporarily stored in a Flash-memory onboard the sensor, and transferred when no measurements are ongoing or the memory becomes filled with data. A method of authenticating the devices should be implemented, in order to increase the security of the system, and to prevent unauthorized access, as described in Section 2.5.

In permanent condition monitoring mode, the transmitters wake up on detecting movement of the elevator, and return to a power-down mode after the movement cycle of the elevator is finished. One movement cycle of an elevator consists of a positive and a negative acceleration, which can be used to detect when the elevator has moved and stopped, and when a measurement cycle is completed.

The processor device connects to the receiver node and acts as the host for the whole sensor system. In real-time operating mode the processor visualizes collected data and receives input from the user. The user input is translated into control instructions which control the entire system. In permanent operating mode, the processor collects data from the sensors, which can be stored onboard or transferred to a remote service.

4.2 Sensor node hardware

A single sensor node consists of 6 hardware sections: the main MCU and RF section, a power supply section, a microphone section, an accelerometer, a Flash-memory storage and USB. A block diagram illustrating the hardware, peripheral buses and data flow indicators of a sensor node is presented in Figure 8. Dashed lines indicate the data flow in real-time operating mode. Dotted lines indicate the data flow in permanent condition monitoring mode. Figure 8 also includes the specific components that were chosen for the sensor – the selection of the components will be justified in the sections ahead. Power supply and power consumption estimates are presented in Section 4.2.5, and antenna considerations are discussed in Section 4.2.6.

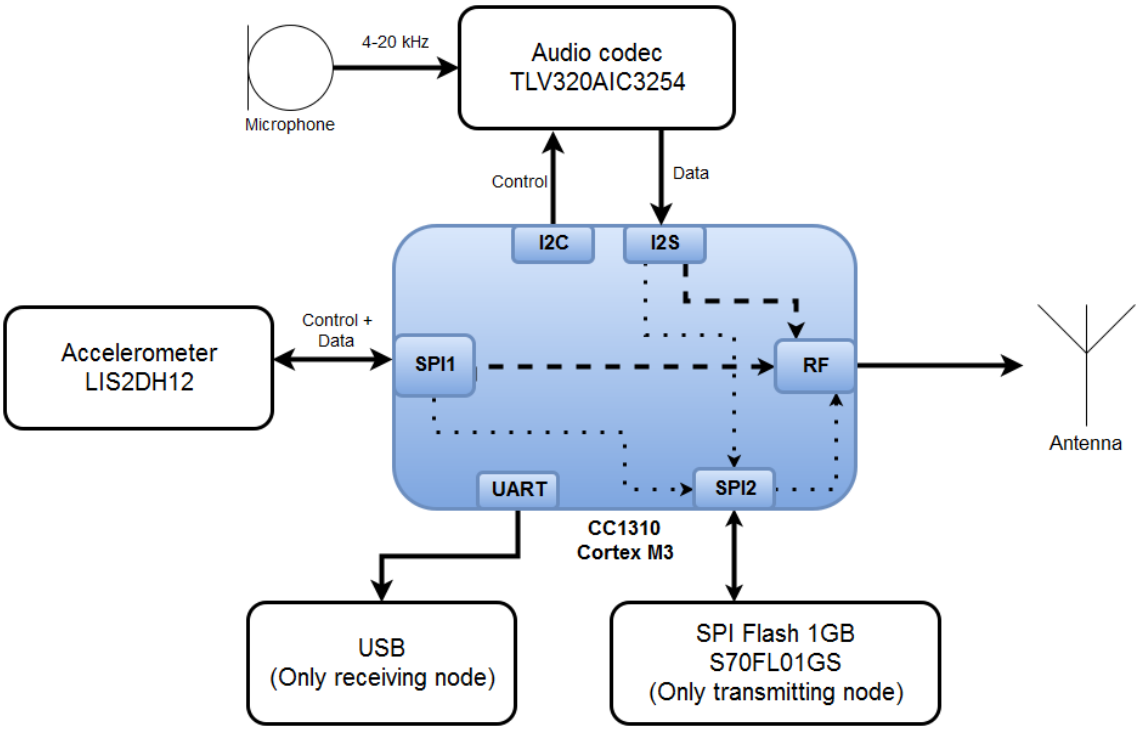

Figure 8: Block diagram and data flow of a sensor node

Two types of sensor nodes were designed: a transmitting node and a receiving node. The receiver collects data from the transmitters or its own sensors, and transfers the data to a host device via USB. Therefore, the receiver has access to wired power, and does not require a battery. The transmitters are entirely wireless, and require battery power but no USB section.

The transmitter nodes feature a Flash-memory, which is used for storing high quality measurement data during permanent condition monitoring. Transmitting such high amounts of data in real-time is not yet possible using the sub-GHz proprietary connection. This might not be the case in the future, when, for example, 802.11ah is more widely available, which could potentially eliminate the need for the temporary storage. The receiving node does not require a temporary storage, since it transfers all data directly to the processor device.

4.2.1 MCU selection

The MCU is the core of any embedded system, providing the general functionality of the device and connecting together the different circuits of the system. For easier and faster development of the sensor prototype, an MCU with an integrated RF section was

desirable for the prototypes. As mentioned in Section 2.1.1, the RF performance could be slightly improved by using discrete components, but for the first prototype optimizing RF performance is not the most important design factor. Three candidates for the MCU selection were taken into closer comparison. The comparison is presented in Table 9. Similar weighted scoring system was used for selecting the MCU as was used for selecting the wireless technology in Section 3.4.

An MCU with a modern 32-bit processor core is desirable for making a future-proof design. Using a reasonably powerful and advanced processor provides more capacity for demanding tasks, such as Fast Fourier Transform, which could be calculated onboard the sensor device in the future. The same hardware design could even be used in an entirely different, more demanding application. Generally, the MCU's aimed for sub-GHz networking seem to often feature a 32-bit ARM processor, rather than an 8-bit processor. In some situations, however, an 8-bit processor could be a better choice.

The advantages of an 8-bit processor over a 32-bit counterpart are lower power consumption, lower cost, and efficiency and speed in hardware-near operations [33]. In the design of the wireless sensor, these advantages are diminished by the other components on the sensor. The power consumption of the radio front-end, audio measuring circuit and the Flash-memory will outweigh the power consumption of the processor, as will be seen in Section 4.2.5. These components, with the added cost of the battery, will also dominate the price of the sensor device. Thus, the only area where an 8-bit processor would be advantageous is the efficiency of hardware-near operations, such as hardware interrupt detection. For example, an interrupt routine that stores a single bit from an SPI peripheral to SRAM takes 12 clock cycles on an 8-bit AVR processor, whereas a 32-bit Cortex M0+ takes 33 cycles to complete the same action [33].

32-bit processors on the other hand tend to have generally higher clock speeds and larger amount of RAM, features which surpass the efficiency of the 8-bit processor. Especially a large RAM is beneficial when processing the large amount of high-quality data that the sensor produces in real-time.

Using the most compatible and universal buses simplifies the implementation of peripheral drivers, which reduces the time of software development. Standard buses such as SPI and I2C are available in virtually every MCU on the market, but some buses such as I2S, aimed for audio applications, may be rare. As the amount of the sensor data will be high, care has to be taken in selecting a device with buses capable of such data rates. The achievable data rate depends also on the peripheral devices themselves, which is especially true for external memory.

One defining attribute of the MCU selection is the capability for the audio measurement. In order to achieve high quality audio, a measurement resolution of 16 bits is desirable. If the ADC of the MCU is used, it needs to be capable of 16-bit resolution. Not many MCUs feature such accurate ADCs, and furthermore, the lowest bits of resolution are often lost to noise, decreasing the true accuracy of the measurement. The sampling rate is usually not an issue, since most ADCs are capable of hundreds of thousands of samples per second. If the ADC is not used for the audio measurement, a suitable bus for an audio codec, such as I2S, is mandatory.

The power consumption of the MCU is an important factor, since the transmitting nodes are battery powered. Power consumption during active data transmission will always be relatively high, but some devices stand out with sub-par levels. More important are the power saving capabilities of the MCU, since the sensors will be in low-power mode for most of their lifetime. All of the compared devices offer similar current consumption in low-power operating modes.

Table 9 summarizes the important factors of MCU selection and presents three sub-GHz MCUs from different manufacturers for comparison. In Table 10 the different factors are weighted, and each MCU is given an overall score based on their properties. The price of the devices, although not critical in the scope of this thesis, is included in the comparison. The prices were collected from Mouser electronics in April 2016.

Table 9: Summary of MCU properties [34] [35] [36]

Attribute	Texas Instruments CC1310	NXP MKW01Z	Silicon Labs EZR32LG
Processor	48 MHz Cortex M3	48 MHz Cortex M0+	48 MHz Cortex M3
RAM	20 KB	16 KB	32 KB
ADC	12-bit	16-bit	12-bit
I2S	Yes	No	No
Current consumption, TX +10 dBm	12.9 mA	33 mA	18 mA
Current consumption, RX	5.5 mA	16 mA	10 mA
Processor current consumption @ 48 MHz	2.5 mA	6.9 mA	10.1 mA
Current consumption (low-power), RTC on	0.6 µA	0.457 µA	0.65 µA
Bit rate	500 kb/s (4 Mb/s in the future)	600 kb/s	1 Mb/s
Maximum TX power	+14 dBm	+17 dBm	+20 dBm
Receiver sensitivity	-124 dBm @ 0.625 kBd	-120 dBm @ 1.2 kBd	-133 dBm @ 0.1 kBd
Price / 10k pcs	4.20 €	2.62 €	4.76 €

Table 10: MCU selection matrix

Attribute	Weight	CC1310	MKW01Z	EZR32LG
Processor	0.7	1	0.8	1
RAM	0.8	0.8	0.6	1
ADC	0.9	0	1	0
I2S	0.9	1	0	0
Current consumption, TX +10 dBm	0.6	0.9	0.5	0.7
Current consumption, RX	0.4	1	0.5	0.7
Processor current consumption @ 48 MHz	0.6	0.9	0.6	0.4
Current consumption (low-power), RTC on	0.8	0.8	1	0.7
Bit rate	0.9	0.8	0.8	0.9
Maximum TX power	0.7	0.6	0.8	1
Receiver sensitivity	0.8	1	1	1
Price / 10k pcs	0.6	0.7	1	0.6
Overall score		0.56	0.53	0.47

Table 10 shows that Texas Instruments CC1310 receives the highest score while the lowest score is given to Silicon Labs EZR32LG. CC1310 lacks the greatest transmit power and highest wireless bit rate, but on the other hand features the lowest active power consumption of the three. It also provides an I2S bus for an audio codec, and a decent amount of RAM. EZR32LG features the largest RAM of 32 KB, but lacks I2S and energy efficiency. The NXP MKW01Z has the lowest power consumption in low-power mode. However, active power consumption is very high, and the amount of RAM is the lowest of the three. All candidates support the different sub-GHz carrier frequencies ranging from 315 MHz to 955 MHz, meaning that the same device could be used globally. From the three candidates, Texas Instruments CC1310 was selected for the sensor prototype. The final choice between the MKW01Z and the CC1310 was the considerably lower power consumption of CC1310 in active transmit mode.

In addition to the Cortex M3 main processor, the CC1310 includes a secondary Cortex M0 processor for controlling the radio front-end hardware and implementing low-level functionality in order to minimize input required from the application software. The processor implements functionality such as LBT and clear channel assist, for meeting European RF standards. AES-encryption is included for enabling simple security in the communication. The radio processor also includes automatic CRC functionality. [34]

Transmit and receive operations can be queued in the memory of the radio processor to be executed sequentially. This allows the user application to return to executing other tasks, without blocking on tasks involving the radio. Currently the radio front-end supports only Frequency Shift Keying and On Off Keying modulations, and data rates up to 500 kb/s. The datasheet promises a data rate of 4 Mb/s in the future. [34]

Additionally, a third, very low power sensor processor is included, which can be used for low duty-cycle measurements and maximizing battery lifetime. However, as the elevator monitoring sensors involve measuring continuous data, the sensor processor cannot be utilized in the elevator application. An internal 128 KB Flash-memory is included for program code, and the memory can also be used for storing non-volatile variables during software operation. [34]

4.2.2 Accelerometer

The requirements presented in Table 1 stated that a 3-dimension accelerometer with the frequency bandwidth from 0 Hz to 2 kHz is required. These requirements guided the search towards MEMS accelerometers, since most of them are capable of measuring accelerations down to the 0 Hz level. Digital MEMS accelerometers also include an I2C or SPI bus for simple interfacing to the accelerometer for collecting the data. Another beneficial feature of most MEMS accelerometers is the capability for self-testing. This feature can be used to determine if the delicate sensor inside the accelerometer has sustained any damage during storage or handling.

The upper bandwidth limit of many MEMS accelerometers is 400 Hz or 1 kHz. For very high measurement bandwidths, a piezoelectric accelerometer should be selected due to their high upper limit of tens of kHz. However, piezoelectric accelerometers are AC coupled, which results in the loss of 0 Hz measurement capability [37], a critical requirement for the condition monitoring sensor. Additionally, piezoelectric accelerometers require additional components for amplifying the analog signal from the sensor. Higher-end MEMS accelerometers have the measurement capability up to 5.3 kHz, which is adequate for the sensor. In digital accelerometers the sampling bandwidth of the accelerometer is also called the Output Data Rate (ODR), and the usable bandwidth of the sensor is ODR/2, as stated by the Nyquist theorem. However, in high-resolution operating modes, the usable bandwidth may be lower than ODR/2 due to oversampling techniques used for gaining resolution.

The accelerometer is the component which wakes up the rest of the sensor each time motion is detected. The current consumption of the accelerometer contributes greatly to the average consumption of the sensor device in power-down mode, as it is the single device on the sensor that is constantly powered on. A low-power, automatic wake-on-motion operating mode with interrupt generation is desirable. Such operating mode is available in many digital MEMS sensors.

Table 11 presents a closer comparison of four digital MEMS accelerometers and one piezoelectric accelerometer. The selected accelerometers represent reasonable candidates for the sensor prototype. Although the piezoelectric accelerometer alone is not suitable due to the lack of DC measurement capability, it could be added in the future to increase the bandwidth capability of the measurements.

Table 11: Comparison of accelerometers [38] [39] [40] [41] [42]

Attribute	LIS2DH12TR	IIS2DHTR	BMA250	ADXL362	ACH-01
Type	"Femto series" MEMS	MEMS	MEMS	MEMS	Piezoelectric
Sample rate	0 - 5.3 kHz	0 - 5.3 kHz	0 - 1 kHz	0 - 400 Hz	2 Hz – 20 kHz
Resolution	8-12 bits	8-12 bits	10 bits	12 bits	-
Current consumption	3 - 185 µA	3 – 185 µA	8 – 139 µA	270 nA – 3 µA	30 – 90 µA
Interface	I2C, SPI	I2C, SPI	I2C, SPI	SPI	Analog, amplifier required
Physical size	2 x 2 mm	2 x 2 mm	2 x 2 mm	3.5 x 3.5 mm	18 x 13 mm
Axes	3	3	3	3	1
Self-test	Yes	Yes	Yes	Yes	-
Wake-on-motion, Return-to-sleep	Yes	Yes	No	Yes	-
Price / 10k pcs	0.545 €	1.34 €	0.887 €	4.6 €	19.21 €

The digital MEMS accelerometer LIS2DH12 from ST Microelectronics was selected, as it fulfills all set requirements and is the lowest priced one of the compared accelerometers. It features selectable acceleration range from ±2g up to ±16g, selectable ODR from 1 to 5.3 kHz, and selectable resolution from 8 to 12 bits. In 8- and 10-bit operating modes the usable bandwidth of the device is ODR/2. If the higher resolution of 12 bits is used, the usable bandwidth is ODR/9. In addition, ODR is limited to 1.3 kHz in 10- and 12-bit operating modes. Increasing measurement resolution therefore limits the frequency range of the device. In low power mode, the accelerometer draws only 3 µA current at the ODR of 10 Hz, and 6 µA at 50 Hz ODR. Maximum current consumption is 185 µA in high resolution and high bandwidth operating modes. The accelerometer features a FIFO buffer capable of storing 32 measurements. [38]

4.2.3 Audio codec

Table 1 stated that a 6 kHz sample rate for audio measurement is required for the real-time operating mode. For permanent monitoring, a sample rate of up to 52 kHz is expected. In order to achieve high quality audio, a resolution of 16 bits is desirable. As the selected MCU only features a 12-bit ADC, a separate audio codec IC is required. Using an audio codec also provides other useful features, such as anti-aliasing filtering, noise and echo cancellation and other digital signal processing. The signal processing and control of the measurements is entirely offloaded to the external audio codec, simplifying the software development of the main MCU.

As the MCU features an I2S bus designed for transferring audio data at selectable sampling rates, an audio codec supporting the I2S bus was selected. TLV320AIC3254 from Texas Instruments suits the technical requirements very well. It features adjustable sampling rate from 8 kHz up to 192 kHz, selectable resolution from 16 bits to 32 bits, and the possibility to adjust to different power consumption needs by shutting off each

unused block and channel of the device. Only a single voltage supply is required, which simplifies the sensor power supply design as many audio codecs require two supply voltages. The IC features microphone biasing, eliminating the need for external power supply or amplifier components for the microphone. Control of the audio codec is achieved using an I2C bus. [43] [44]

The high measurement bandwidth sets requirements to the audio sensing element itself. All researched digital MEMS microphones have a frequency response only up to 10 kHz, and in rare cases up to 15 kHz. Therefore, a simple electret microphone became a reasonable candidate. An electret condenser microphone from CUI INC was selected, since it provides a relatively flat frequency response from 100 Hz up to 20 kHz. The CUI part number for the microphone is CMC-5044PF-A. [45] As mentioned before, biasing for the microphone is available directly from the audio codec IC, eliminating the need for external components.

4.2.4 Flash-memory and UART-USB converter

As calculated in Table 2, the rate of measurement data can be as high as 1 Mbit/s. As the wireless connection is not capable of such data rates, a temporary storage is required in the transmitting nodes. A 1-Gbit memory can store roughly 1000 seconds of measurement data, which is enough for storing multiple elevator movements, depending on building height.

A 1-Gbit SPI Flash-memory from Spansion was selected. The selection of memory is not crucial for the prototype, as long as the programming speed of the memory meets the required rate of measurement data. The selected NOR-type S70FL01GS features a 1.5 MB/s (12 Mb/s) programming speed, which is more than adequate [46]. Typically a NAND-type Flash-memory would be selected for faster programming speeds [47], but such memories were not found with SPI interfacing.

The receiver node transfers all measurement data to the host device via USB. As the UART of the selected MCU is capable of a baud rate up to 3 MBd [48, p. 22], it is sufficient for transferring the amount of data the sensors are producing. Thus a basic UART-USB converter from FTDI was selected. The selected converter is FT230X, which features baud rate up to 3 MBd, a fully integrated USB protocol on the chip and easily available Windows drivers, which minimize the need for USB driver development in both the host PC and the sensor MCU sides [49].

4.2.5 Power supply considerations

Minimizing the power consumption of the sensor node is mandatory for obtaining reasonable battery lifetime. As the elevator is stationary, the sensors are powered down unless a data transfer is ongoing. Thus, for the majority of their lifetime, the sensors will remain in a power-down mode, and minimizing power consumption during these periods has a great impact on the total battery lifetime. Smart use of low power modes of each device on the sensor is crucial. Reducing the power consumption in active operation is difficult, since some power is always required during measurements and radio transmissions.

The Flash-memory contributes significantly to the total power consumption of the prototype, both in active operation and in low-power mode. This is due to the general structure of Flash-memories, in which a charge-pump circuit is used for increasing the internal voltage used for cell erase and write operations. Read operations require

considerably less current (<18 mA) than write operations (100 mA) [46]. For minimizing current consumption of the Flash-memory, a separate load switch was added for disabling power input to the Flash-memory completely. The switch also disables the power to the audio codec IC.

As the minimum input voltage for the Flash-memory is relatively high 2.7 volts [46], a high voltage power source is required. 3.0 V lithium-manganese-dioxide batteries quickly reach a voltage level of 2.5 V under high pulse loads [50], which makes them unsuitable for the sensor. Lithium-ion batteries in general have an initial voltage of over 3.7 V in open-circuit or very low-load situations, which could damage many of the sensors components since their maximum input voltage is 3.6 V. A rechargeable Lithium-polymer battery will reach a voltage of over 4.2 V in full charge. In addition, the receiver node will be powered with 5 volts from the USB port. Due to these reasons, a voltage regulator is required.

A low-dropout linear regulator (LDO) was chosen for the input voltage regulation. A linear regulator has the advantage of very low output noise compared to switching mode regulators. As stated in Section 2.1.1, minimizing noise is a key factor in increasing the range of the radio link. The selected regulator is LP5907 from Texas Instruments, which is especially designed for RF applications as it provides a <10 µV output noise [51].

For most of its lifetime, the sensor consumes a minimal amount of current, as will be explained ahead. Due to the low load current and small voltage drop across the LDO, efficiency similar to switching mode regulators can be achieved. When comparing datasheets, it is clearly seen that at below 1 mA loads the efficiency of a conventional buck converter drops drastically due to high quiescent current. The efficiency of Texas Instruments TPS62125 switcher is 45% at 20 µA load and 4 V input voltage [52], for example. The quiescent current for the selected linear regulator is 12 µA. For an output current of 20 µA, the power dissipated in the regulator, P_{LDO}, is

$$P_{LDO} = I_o * (V_{in} - V_o) + I_Q * V_{in} \tag{13}$$

$$= 20\ \mu\text{A} * (4\ \text{V} - 3.3\ \text{V}) + 12\ \mu\text{A} * 4\ \text{V} = 62\ \mu\text{W}, \tag{14}$$

where I_o is the output current, V_{in} is the input voltage, V_o is output voltage and I_Q is the quiescent current of the regulator. The power dissipated in the load is

$$P_o = I_o * V_o = 20\ \mu\text{A} * 3.3\ \text{V} = 66\ \mu\text{W}. \tag{15}$$

This results in an efficiency of

$$\eta = \frac{66\ \mu\text{W}}{62\mu\text{W} + 66\ \mu\text{W}} * 100\ \% \approx 52\ \%, \tag{16}$$

which is better than the efficiency of a switching mode regulator at very low loads.

The current consumption of all devices on the sensor is summarized in Table 12. Due to the general operation of the sensor system, the Flash-memory will never be written to simultaneously with the radio transmitting data. Therefore, when calculating the total current consumption in active mode, only the higher current of the two was taken into account. As explained before, the Flash-memory is only present in the transmitting

node, and USB is present only in the receiving node. Due to the lack of Flash-memory, the high side switch is not needed in the receiver, and it is bypassed with a jumper.

Table 12: Power consumption of devices on the sensor [34] [38] [43] [46] [49] [51] [53]

Device	Low-power mode	Active mode
CC1310 (Radio)	-	TX +10 dBm: 12.9 mA RX: 5.5 mA
CC1310 (Cortex M3)	0.6 µA	2.5 mA
Accelerometer	3 µA	185 µA
Audio codec + mic.	2.7 µA	4.84 mA
Flash-memory	8 µA	100 mA
USB	125 µA	8.3 mA
Regulator	12 µA	250 µA
High-side switch	150 nA	200 nA
Total, receiver	**143.3 µA**	**21.79 mA**
Total, transmitter	**15.75 µA**	**108.6 mA**

Table 12 shows that the current consumption of the transmitter node in low-power mode is decent, but the active mode consumption is large. This is mainly due to Flash storage which uses a considerable amount of power. Eliminating the temporary storage is not currently possible, therefore the only method for decreasing average power consumption is to operate the sensors so that they are active for the least amount of time, and in the low-power mode for the most of their lifetime. The average current consumption of the transmitter is

$$I_{ave} = X_{ratio} * I_{max} + (1 - X_{ratio}) * I_{min}, \quad (17)$$

where X_{ratio} is the duty cycle of the device, or ratio of the time spent in active and low-power modes. I_{min} and I_{max} are the minimum and maximum, or the low-power and active mode current consumptions of the sensor node.

As previously stated, not every run of the elevator needs to be captured. Furthermore, an elevator is typically stationary for long periods of time, and is only running for a certain amount of time in a day. This leaves room for creating an operating scheme with a very low duty cycle. The required duty cycle can be calculated by first selecting a battery, which is reasonable for the sensor both in physical size and cost-wise, and determining the average current that can be sourced from such battery. An AA sized, 3.6 V lithium-thionyl-chloride battery from Saft with the capacity of 2.6 Ah [54] was selected for the sensor prototype. Similar batteries cost approximately 5 € at Mouser Electronics.

The average current that can be sourced from a battery over a time period is

$$I_{ave} = \frac{C_{bat}}{T}, \quad (18)$$

where I_{ave} is the average current in Amperes, C_{bat} is the battery capacity in Ah, and T is the expected device lifetime in hours. Combining Eqs. (17) and (18), the required ratio of low-power and active modes for such battery capacity can be derived as follows:

$$\frac{C_{bat}}{T} = X_{ratio} * I_{max} + (1 - \mathrm{X_{ratio}}) * I_{min} \quad (19)$$

$$X_{ratio} = \frac{\frac{C_{bat}}{T} - I_{min}}{I_{max} - I_{min}} \tag{20}$$

$$= \frac{\frac{2.6\ \text{Ah}}{3\ \text{years} * 365\ \text{days} * 24\ \text{h}} - 15.75 * 10^{-6}\ \text{A}}{0.1086\ \text{A} - 15.75 * 10^{-6}\ \text{A}} = 0.000766 \ldots \approx 0.077\ \% \tag{21}$$

Thus, such operation scheme shall be created that the sensors are active only 0.077 % of their lifetime, and in low-power mode for the rest of the time. This will be achieved by approximately 66 seconds of active operation each day for a 3-year period. Such low duty cycle will still result in an adequate amount of measurement data for long-term condition monitoring.

For comparison, in order to achieve a duty cycle of 1% for 3 years, a 28.4 Ah battery would be required. Such a large and costly battery would be impractical in a moderately sized wireless device such as the sensor.

It should be noted that the active operation of the device includes also transmitting the data. Data transmission consumes approximately 80% less power than the active measurement, so most of the time budget can still be reserved for data acquisition. Furthermore, the cell voltage of the battery will decrease when the battery is discharged, and due to aging. However, the datasheet of the selected battery does not specify an aging or a discharge curve for the battery voltage, so these effects cannot be estimated. As long as the supply voltage of the battery remains over the minimum of 2.7 V, the sensor nodes remain operational.

4.2.6 Antenna considerations

The design of the antenna contributes largely to the performance of any wireless system. The antenna is responsible for both converting electrical signals into electromagnetic waves in the transmitter, as well as converting radio waves back to electrical signals in the receiver. Thus, any issues in the performance of the antenna will have a two-fold effect on signal strength in the overall wireless link.

One purpose of the antenna is to direct radio waves in a certain direction. In fact, all antennas are directional to some extent, as it is not possible to create an ideal, isotropic antenna that would radiate power equally in all directions. A more realistic definition of an antenna with a low directivity is an omnidirectional antenna. Such antenna radiates power equally in a plane, such as horizontally, but the amount of vertically radiated power varies. [2, p. 67]

Some antennas are designed to radiate most power specifically to a certain direction. Such directional antennas are advantageous when the positioning of the receiver and the transmitter is known beforehand, and the devices remain stationary. Directional antennas result in the largest possible range, as most power is radiated to the direction of the other end of the wireless link. For the elevator monitoring system, directional antennas are not a valid option for two reasons. First, for troubleshooting situations it is required that connection can be achieved outside the shaft. In such situations, the location of the maintenance person outside of the shaft may vary greatly, and the

antennas in the shaft would require constant realignment as the person moves, which would be highly unpractical.

Second, high directivity would be disadvantageous even inside the shaft in permanent condition monitoring mode, as the directivity of such antennas is high in only one direction of an axis. An example of the radiation pattern of a directional YAGI PCB antenna is presented in Figure 9, which shows that the radiated power is around 7 dBi in the positive x-axis direction, and around −3 dBi in the negative x-axis direction, a difference of 10 dB. It should be noted that the decibel values are expressed in relation to the radiation pattern of an isotropic antenna, and do not relate to the absolute amount of radiated power. This difference would result in a scenario where the link quality is high when the elevator car is above the counterweight, for example, but once the location of the car and the counterweight is reversed, the link quality would decrease considerably. As explained before, both the receiving and the transmitting antenna contribute to the total link, thus in the case of the YAGI antenna, a loss of around 20 dB could be expected when the location of the elevator components changes.

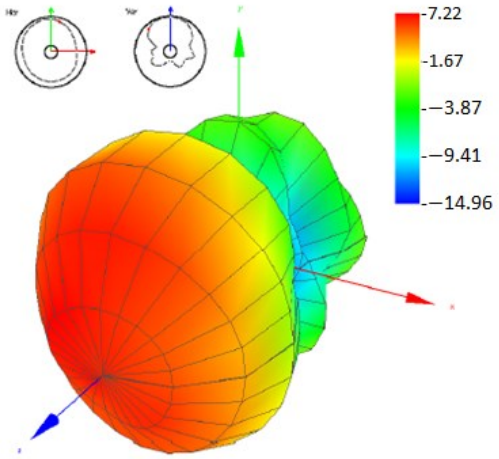

Figure 9: 3D Radiation pattern of a YAGI Directional Antenna [55, p. 13]

It would be possible to design the monitoring system so that transfer of collected data would occur only when the elevator is at a known position, and best signal quality is achieved. Thus, in a very high elevator shaft where all of the available signal strength is required, and the possibility real-time maintenance outside of the shaft is not crucial, directional antennas could be a viable solution.

For all of the intended use cases of the sensor prototype, an omnidirectional antenna is a better suited candidate. An omnidirectional antenna can achieve directivity in two directions, such as up and down in an elevator shaft. Additionally, some power is radiated in the direction perpendicular to the plane of highest directivity. An example of the radiation pattern of an omnidirectional PCB antenna is presented in Figure 10. It can be seen that greatest power is radiated in both directions along the x-axis, while some power is also radiated to the directions perpendicular to the x-axis.

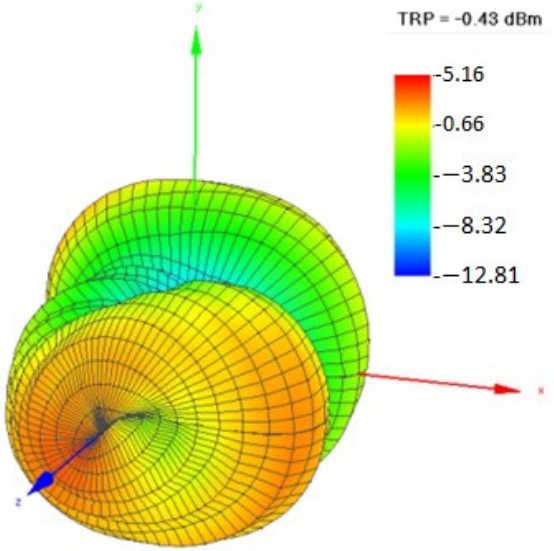

Figure 10: Radiation pattern of TI board 6 reference antenna [55, p. 15]

Other aspects of selecting a suitable antenna are the price of the antenna and the physical space available. Multiple different types of antennas are available: whip antennas, PCB antennas and chip antennas, to name a few. As the monitored devices in an elevator are relatively large, the size of the sensor device in total is not critical. However, certain types of antennas, such as a whip antenna, are not ideal as they could be easily installed in such a way that they could become damaged by moving components. The added price of the discrete antenna and required connectors may be in the range of tens of dollars [19, p. 56]. A PCB antenna is often the cheapest type of antenna, as it is etched directly on the circuit board, and the only added cost is the board material. Additionally, a PCB antenna can still offer very good performance, even when compared to a discrete whip antenna [19, pp. 61-73].

For the sensor prototypes, a reference PCB monopole antenna design from TI was selected. It features an excellent efficiency of over 97 % [56], which is the highest efficiency of all PCB antennas offered by TI [57]. The radiation pattern presented in Figure 10 is the radiation pattern of the selected antenna type.

4.3 Sensor node software

The MCU on the sensor nodes features a 48 MHz Cortex M3 processor that runs Texas Instruments Real-Time Operating System (TI RTOS). As the MCU integrates much functionality such as the radio front-end, RTC, peripherals and different power saving features, it is beneficial to use a TI specific RTOS that is capable of handling all the different functionality with minimal user input required. In fact, TI only provides support for using the selected MCU if TI RTOS is used.

In addition to hardware-level management, the RTOS includes standard kernel features such as task threading, pre-empting and task synchronization using structures such as semaphores and mailboxes.

The software structure for both the transmitting and receiving nodes is presented in the next section. Due to lack of time and I2S audio driver missing from the RTOS, the audio functionality, as well as functionality related to the permanent condition monitoring mode, are not yet implemented in the software. However, the software was

fully designed, and the basic task structure and synchronizations were completed and verified. The real-time operating mode for one transmitter and receiver, excluding the audio measurement, was implemented. Details of wireless optimization and functionality regarding software are discussed in sections 4.3.2 and 4.3.3.

4.3.1 Software structure

The task structure of the transmitter node is presented in Figure 11. There are 5 separate tasks visualized by different colors: `RX task`, `Radio control task`, `TX task`, and tasks for collecting accelerometer and audio data. There are two semaphores for controlling the use of the radio, and two mailboxes for transferring measurement data between tasks. In addition, there is one hardware interrupt from the accelerometer. The interrupt is used to wake up the system in the permanent condition monitoring mode. The transmitter software operates as follows:

- The semaphore `tx_is_done` is initialized to 1 on wakeup, in order to allow the radio to enter listening mode in the beginning of the software operation. Otherwise the semaphore is posted by the `TX task`, indicating that all transmissions are over and the radio is free for use.
- The `RX task` is responsible for switching the radio to listening mode. The `RX task` pends the `do_rx` semaphore, which is posted by the `Radio control task`. The `RX task` commands the radio processor to enter listening mode, indicated by the `start rx` command in Figure 11. If a packet is received, other tasks shall be suspended and the operating mode of the sensor is adjusted according to the instructions in the packet. The operating mode and peripheral settings are stored in the Flash-memory of the MCU. The `start rx` command is non-returning and does not include a timeout, therefore blocking the `RX task` and reserving the radio until canceled. Thus the `Radio control task` is required for canceling the listening command.
- The `Radio control task` pends for the `tx_is_done` semaphore, which is posted by the `TX task`. The semaphore indicates that the radio has transmitted all measurement data, and the radio is free for use. The task then posts the `do_rx` semaphore, and after a specified timeout cancels the listening command and powers down the radio. The time the radio spends in listening mode is defined by the wait command in the `Radio control task`. The listening time is adjusted according to the packet transmit interval, and the baud rate of the transmission. This timing scheme is further explained in Section 4.3.2.
- The `TX task` is collects measurement data from mailboxes 1 and 2. Depending on the operating mode, the data is then either stored in the Flash-memory, or appended into a radio packet and transmitted immediately. The structure of the radio packet depends on the settings of the sensor. If such settings are selected that audio data is not needed, for example, the `TX task` shall only pend for `mailbox_1` and collect data from the accelerometer. After transmitting the data, the task posts the `tx_is_done` semaphore, allowing the radio to enter listening mode. If the node is operating in permanent monitoring mode, the node powers down after transmitting the data that was stored in the Flash memory during the measurement. It is not yet defined if data transmission occurs after each elevator movement, or after the Flash memory is filled with data from multiple measurement cycles.

- The accelerometer and audio data collecting tasks read data from the appropriate peripherals. Either task can be suspended if such settings are selected that data from either peripheral is not required. The tasks append the measured data into mailboxes, which are read by the `TX task`.

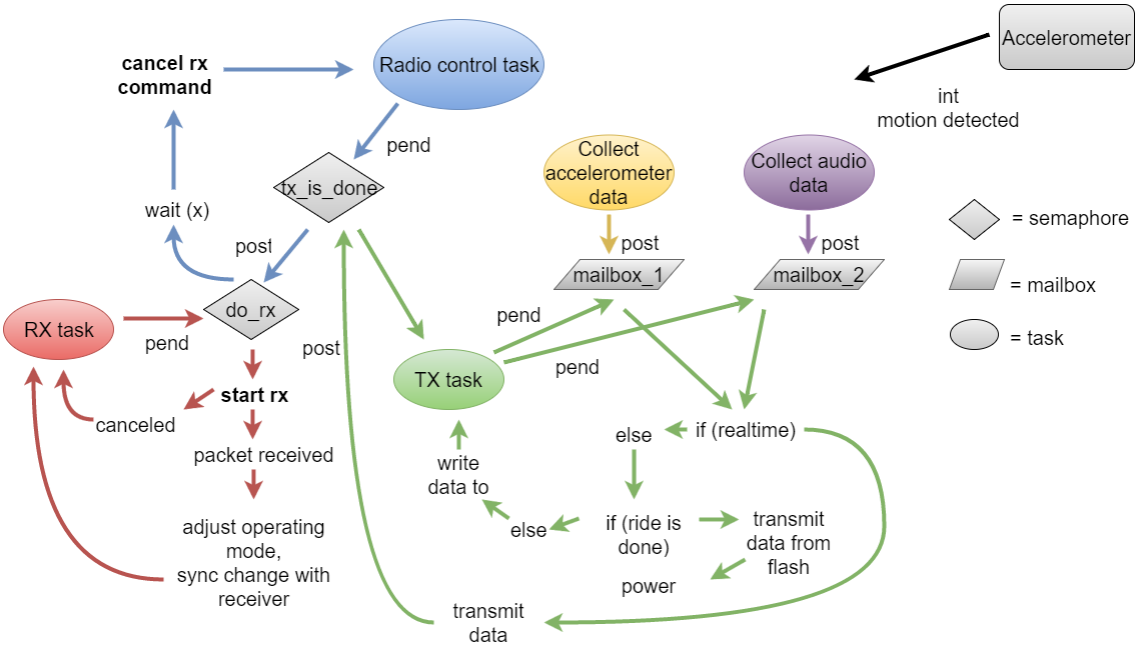

Figure 11: Transmitting node software structure

The structure of the receiving node software is simpler than the transmitter software structure. The receiving node is always powered, and is constantly listening for data from the transmitters. If the receiver node is producing measurement data, the data is gathered from the receiver's own sensors. Four tasks are implemented: `RX task`, `UART task`, and tasks for collecting accelerometer and audio data. Two mailboxes are used for synchronizing measurement data, and a semaphore is used for controlling the use of the radio. An interrupt is implemented for receiving instructions from the UART. Figure 12 presents the software structure of the receiving node. The software operates as follows:

- The semaphore `tx_is_done` is initialized to 1 on wakeup. The `RX task` pends for the semaphore, and then commands the radio to enter listening mode. As the listening command is non-returning, the receiver stays in listening mode forever, listening for packets from the transmitters. If a packet is received, the measurement data from the packet is printed to the UART to be collected by the data processor device.
- If instructions are received from the UART, an interrupt routine is triggered. Other tasks are suspended and the RX command is canceled, and new settings are applied and transferred to the transmitting nodes. As stated in Section 4.1, the receiver stores current settings in order to be able to know the data structure of incoming packets.
- The new settings are synchronized to the transmitting nodes and `tx_is_done` semaphore is posted. If the user has selected that measurement data shall be collected from the receiver node, the `UART task` and data collecting tasks are resumed and `RX task` remains suspended. If a transmitter node is selected as the data producer, `RX task` is resumed and other tasks shall remain suspended.

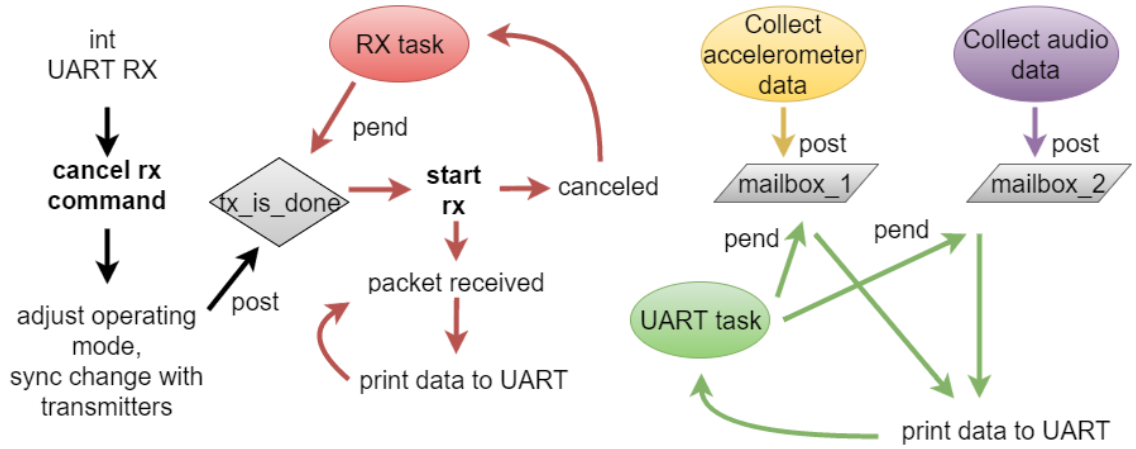

Figure 12: Receiving node software structure

4.3.2 Optimizing wireless data transmission

As explained in Chapter 2, the data rate of the connection affects the receiver sensitivity and thus the range of the wireless link. As the amount of measurement data that the sensor produces may vary, the data rate of the wireless connection can be adjusted to the lowest level that is sufficient for transferring such data. Thus, improved range can be achieved by lowering the data rate of the connection. The range should be maximized especially in real-time operating mode, since connection is required through the shaft and elevator car structures.

On the other hand, decreasing the data rate of the connection will increase the active time of the radio, as it takes longer to transmit the same amount of data. This will increase the average energy consumption of the radio, and decrease battery lifetime. A period of time needs to be reserved for listening for incoming packets, which results in another limit for longest acceptable transmission time. For optimizing energy consumption, data should be transferred as fast as possible, and the radio should be powered down other times.

Clearly both before mentioned targets cannot be met at the same time, and the operation of the radio has to be adjusted according to the specific situation. Adjusting the operation of the radio for both minimum active operation time and a minimum acceptable data rate will be discussed next.

An example scheme for using the radio is presented in Figure 14. The figure represents a situation where only z-axis accelerometer data with the bandwidth of 400 Hz and a resolution of 10 bits is transferred. The accelerometer data is stored in a radio packet that holds 40 measurements, and each measurement is stored as two 8-bit values. Each packet will thus include 100 milliseconds of measurement data, which also results in a packet transmission interval of 100 ms. It is also effectively the delay that the user experiences before receiving information from the transmitter. It is clear that storing 10-bit measurements as two 8-bit values leads to 6 overhead bits for each measurement − an improvement for this issue is presented later.

A larger payload size will increase the delay in transferring information, as it takes longer to fill the entire packet with measurement data. On the other hand, a shorter payload will increase the amount of transmitted packet header overhead. It is therefore necessary to select a suitable payload length according to the amount of measurement

data and the accepted delay in real-time measurements. In order to minimize the ratio of packet overhead compared to actual payload data, as many measurements as possible should be included in each packet. In the case of the selected proprietary sub-GHz technology, each packet includes 0-66 bytes of overhead depending on frame format settings [48, p. 1576], which can significantly lower the efficiency of the data transfers if the payload length is short.

In the example situation shown in Figure 14, a data rate of 50 kb/s is selected for the wireless connection. Each transmitted packet contains 80 bytes of measurement data, and an overhead of 14 bytes. The overhead comprises of a 4-byte preamble, 4-byte synchronization word, a payload length byte, a destination address byte and two CRC bytes. The format of the packet is illustrated in Figure 13.

2 bytes	2 bytes	1 byte	1 byte	80 bytes	2 bytes
Preamble	Sync word	Length field	Address	Payload	CRC

Figure 13: Frame format of the example settings [48, p. 1576]

The resulting total packet size is

$$(80\text{B} + 14\text{B}) * 8 \text{ bits} = 752 \text{ bits}. \tag{22}$$

At the data rate of 50 kb/s, the time it takes to send one packet is

$$\frac{752 \text{ bits}}{50 \text{ kb/s}} = 15.04 \text{ ms}. \tag{23}$$

As the measurement interval is 100 ms, and the transmit time for a packet is 15.04 ms, a period of 84.96 ms is left available for either listening for incoming packets, or powering down the radio for saving power. A 10 ms listening time is selected, which results in approximately 25% active duty cycle for the radio. If the amount of measurement data needs to be increased, such duty cycle leaves much headroom for increasing the rate of transmitted packets. This eliminates the need for increasing the data rate of the connection, which would decrease the range. Naturally when the amount of measurement data increases significantly, the data rate of the connection needs to be increased also.

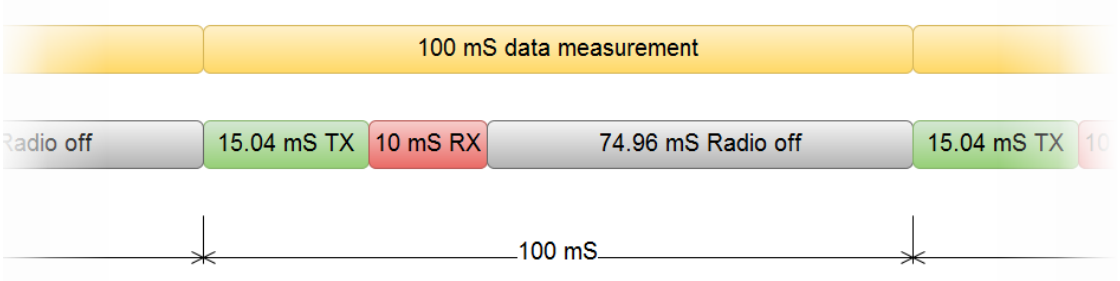

Figure 14: Timing scheme for transmitting node radio

As stated before, it is inefficient to transfer 10-bit measurement data as two 8-bit values, due to increased overhead. The overhead can be easily eliminated, however, by adjusting how accelerometer data is structured in the wireless packet. The radio can

only transfer packets that contain bytes, or 8-bit values. The accelerometer, however, provides measurement resolution of 8, 10 or 12 bits. Transmitting 8-bit measurements is simple, but optimization is required if 10- or 12-bit resolution is used. Transmitting audio data does not require optimization, as the resolution is always 16 bits, and it can be transmitted as two 8-bit values.

Transmitting a 10-bit accelerometer measurement as a two 8-bit values (or two bytes) will result in 6 bits of overhead for each measurement, for example. An optimized structure would combine four 10-bit measurements into 5 bytes, or a sequence of 40 bits, by bit-shift operations. Similarly, two 12-bit measurements can be combined into 3 bytes, by bit shifting the second measurement 4 bits to the left. The method is illustrated in Figure 15. It is clear that 8 overhead bits, or one byte, can be eliminated when combining two 12-bit measurements in such a way. The overhead bits are shown in a dashed line, and the two measurements are separated by the red vertical line.

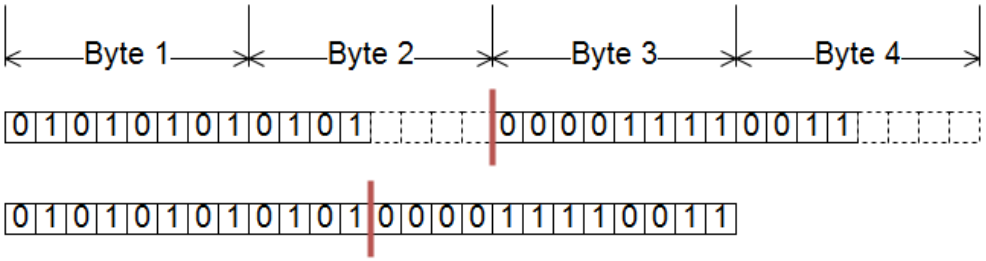

Figure 15: Unoptimized transfer of two 12-bit measurements on top, optimized transfer on bottom

Clearly the payload length of the transferred packets may change when doing operations such as described before. When audio data is included in the same packet, the structure of the packet and the payload will change even more. As stated before, it is thus extremely important that all the units in the whole sensor system know the packet structure in advance, in order to be able to correctly decode the original measurement data from the packets.

4.3.3 Detecting and coping with transmission errors

As suggested by the initial measurements presented in Section 3.3, some transmission errors will always be present in the wireless connection even if the signal is strong. The amount of errors will grow when the distance and the data rate of the connection is increased. This will be especially true in the case of remote troubleshooting, if data needs to be transferred outside of the shaft through car and shaft structures.

Detecting corrupted packets is simple with the selected MCU, as it contains an automatic CRC calculation feature. Packets lost entirely can be detected using a similar incrementing packet ID number as was used in the measurements described in Section 3.3. The problem with CRC calculation and an ID number is the increased overhead in transferred packets. Both the CRC and ID number features will add 1-2 bytes of overhead, resulting in a total overhead increase of 2-4 bytes. However, detecting errors is important, as further processing may require knowledge of missing data.

Depending on the selected measurement settings, one wireless packet may contain measurement data from a period of 10 to 100 ms, for example. If a packet is corrupted or lost entirely, the data of the packet will be lost. In real-time operating mode, functionality for re-sending corrupted data is not implemented, because it would increase overhead and the complexity of the wireless protocol, as discussed in previous

chapters. Furthermore, re-sending data would increase the delay in receiving the information. In the permanent condition monitoring mode, such limitations do not exist, and a protocol for re-sending corrupted packets should be implemented.

In the case of real-time troubleshooting, it is not necessary to always receive completely intact data. If a single packet is missing, its information can be approximated and replaced by the information that was received in the previous packet. This is acceptable as the vibrations, clicks and bangs that are typically of interest in a troubleshooting situation last longer than the duration of measurements in a single packet. Additionally, multiple elevator runs can be made, decreasing the possibility of losing interesting information due to corrupted data. In the event of a lost or corrupted packet, the receiver node shall signal the data processor unit that an error was detected, so that the processor can take appropriate action. The action can be extrapolating the missing data from previously received packets, and indicating the user that some data was lost.

Thus, a packet error rate of a few percent is acceptable in a real-time troubleshooting situation, as long as the errors are sporadic. If multiple consequent packets are lost, the amount of lost information becomes a larger problem. Consequently lost packets lead to a longer break in information, which might result in loss of a valuable event, such as a sudden noise. If the amount of packet losses becomes large, the quality of the wireless link is at its limit and either the distance between the transmitter and the receiver, or the data quality and link speed should be decreased.

4.4 LabVIEW software for PC

National Instruments' LabVIEW is a tool that provides a very fast and intuitive way for interfacing with measurement equipment and visualizing the data they produce. It is especially useful for quick prototyping purposes. The tool includes mathematical operators such as filters for data processing, and interfaces to the host PC's peripherals, such as its USB ports and audio driver. The tool produces Virtual Instruments, which can be exported into executable files and be used on a computer that does not have LabVIEW installed.

A Virtual Instrument was created for reading three axis acceleration data from the USB port of the computer and plotting the data on graphs. The receiver node prints acceleration data to its UART port in the form of x,y,z axis values, which is converted to the USB by the FTDI converter on the receiver. LabVIEW separates the different axis measurements according to the commas, and places the data into an integer array. The three values are then read from the array and displayed on graphs. The data is also saved in CSV files.

Each piece of acceleration data is divided by the value of 16. This operation is required due to the format of the 10-bit measurement data received from the UART port of the sensor. It is not possible to transfer 10-bit data directly via the UART, therefore the data is shifted 6 bits to the left on the sensor, resulting in 16-bit values. In order to obtain the original 10-bit data, the 16-bit data needs to be divided by the value of 64 in the LabVIEW instrument, which is equivalent to bit-shifting 6 digits to the right. However, as the sensitivity of the accelerometer is 4 mG/digit, the divisor of

$$\frac{64}{4\ \mathrm{mG/digit}} = 16 \tag{24}$$

will result in a direct conversion to milli-G's.
The instrument includes the possibility for the user to input a command to the UART for changing the settings on the sensors. The VI will also provide a plot of the RMS value of received audio data, as well as play back the audio through headphones connected to the PC. The audio functionality is not yet implemented as the audio driver is not available for the sensors. The block diagram for the VI is shown in Figure 16.

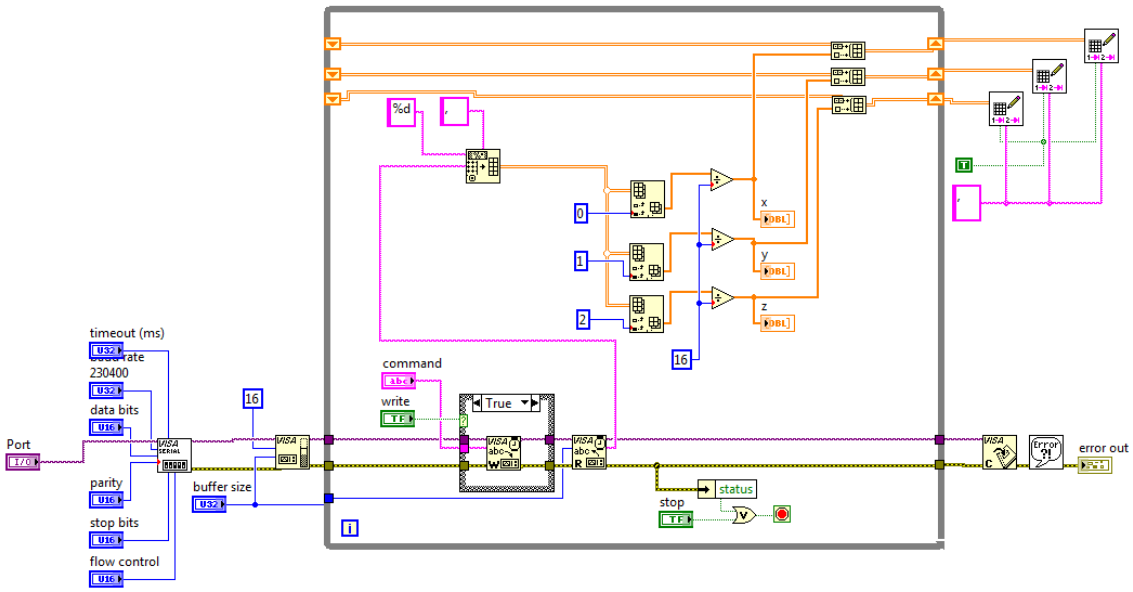

Figure 16: Block diagram of the LabVIEW Virtual Instrument

The Virtual Instrument includes a Graphical User Interface (GUI) for visualizing the accelerometer data to the user. X-axis acceleration is plotted on the top graph, and y- and z-axis accelerations are plotted on the middle and bottom graphs. The graphs show the acceleration in milli-G's. The GUI for the sensor VI is presented in Figure 24 in Section 5.1.4.

4.5 Production of the prototypes

KiCad Electronics Design Automation Suite was used for creating the design documents of the sensor prototype. KiCad is an open-source electronics design tool which includes schematic symbol and component footprint libraries maintained by an active community of users. This minimized the need for creating new symbols from scratch, as the majority of components were found from the libraries. The circuit diagrams and layout design are presented in Appendix B.

A batch of 10 prototype sensors was produced at a local electronics shop in Hyvinkää. The batch consisted of 5 receiver nodes and 5 transmitter nodes. The same circuit board is used for both types of sensors, and sensor type is defined by the components assembled on the PCB.

Manufacturing the prototypes started by applying solder paste on the PCB. The solder paste was spread on the board using a metal stencil with cutouts that ensure that only the solder pads are covered with paste. An automated pick-and-place machine then placed components on the PCB. The machine picks components from a tray or a tube using air suction, optically orients them, and then drops the components on the board according to component locations mapped beforehand. The pick-and-place process could not be used for placing the USB connector, however, which required human

assistance, as seen in Figure 17 on the left. The pick-and-place process is paused on the right in the figure. The machine has placed the audio codec and a few other components on the board, while most of the component footprints are still unpopulated.

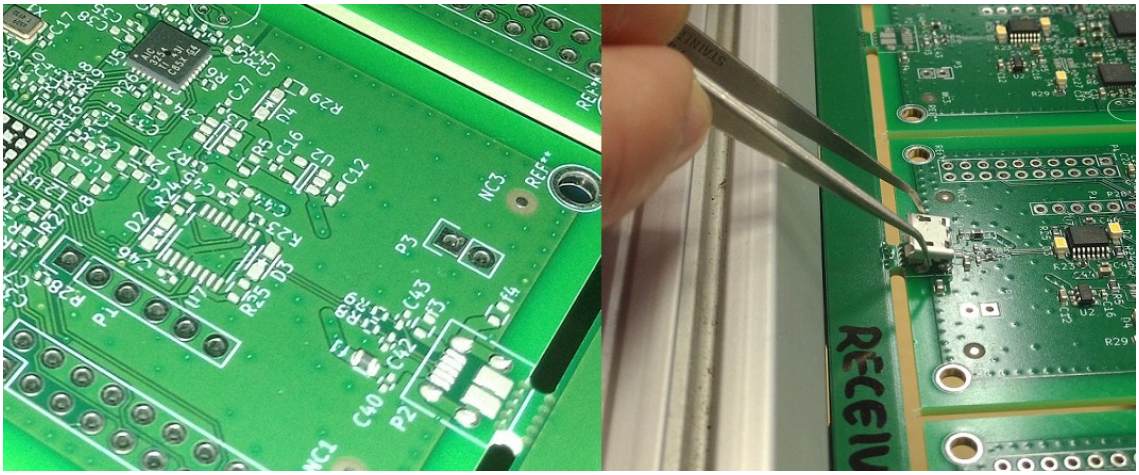

Figure 17: Component placing process

After placing all the components, the board traveled through an infrared oven which subjects the board to varying temperatures, melting the solder paste. The different temperatures inside the oven result in a temperature curve, which changes over time, and is optimized for best soldering results. This process is called reflow soldering. A generic temperature curve was used for the prototypes, but specific components such as large plastic connectors or capacitors may require changes to the temperatures.

After the soldering process was finished, the solder joints on each board were inspected using a microscope. The through-hole connectors, microphone and battery leads were soldered by hand, and the prototypes were ready for functional testing.

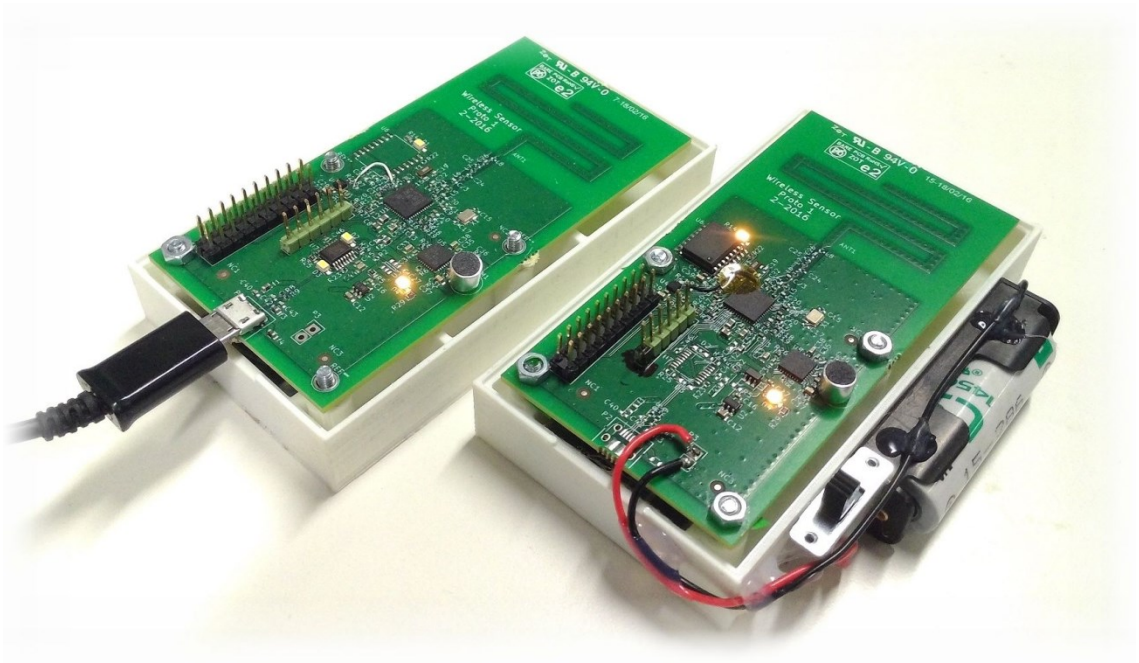

Figure 18: Finished prototypes, receiver on left, transmitter on right

5 Evaluating the prototypes

The requirements for the sensor system specified a wireless range of 100 meters with connection possible through the car metal structures and through the shaft walls. The power consumption of the device should allow an operational lifetime of three years.

The following section explains the tests that were conducted in order to evaluate the performance of the prototype sensors. The range, power consumption and the general functionality of the prototypes were verified. Some issues were observed during the tests, and improvements for asserting the issues are discussed in Section 5.2.

5.1 Validating prototype performance

The following sections aim to verify that the requirements presented in the introduction chapter were fulfilled. First, the range of the prototypes will be evaluated. Although the specified range was achieved, lower than expected signal strength was observed. The reason for this is investigated in Section 5.1.2. The current consumption of the prototypes is evaluated in Section 5.1.3. The overall functionality of the sensor was also verified, which is described in Section 5.1.4.

5.1.1 Range tests at Tytyri

The wireless range of the sensor prototype was evaluated in the KONE test elevator site at Tytyri, using similar methods as described in Section 3.3. The elevators feature a run distance of slightly over 300 meters, in a shaft mined in the base rock in the ground. The machine room is located on top of the shaft, 12 meters above the top landing of the test elevator. There is a sheet metal plate between the machine room and the elevator shaft, with an opening for the elevator ropes to travel through. The structure of the elevator shaft can be viewed in Figure 19.

Six different test cases were measured. Both the sensor prototypes, as well as the Texas Instruments evaluation modules that were used in the preliminary measurements, were tested. The results obtained from the prototypes were compared to the reference evaluation modules, in order to evaluate the performance of the prototype antenna. In each test case, the radio was set to 868 MHz carrier frequency, +14 dBm transmit power, 200 kb/s bit rate and receiver filter bandwidth of 311 kHz. The test cases are summarized in Table 13, and the test setup and different test cases are illustrated in Figure 19. The red rectangles in the figure represent the transmitter and the receiver nodes. The results of the tests are presented in Appendix C.

Table 13: Test cases for wireless range measurements

Test case	Device	Transmitter location	Receiver location	Graph
1	SmartRF06 Evaluation board	Counterweight	Car	Figure C1
2	Sensor prototype	Counterweight	Car	Figure C2
3	SmartRF06 Evaluation board	Counterweight	Machine room	Figure C3
4	Sensor prototype	Counterweight	Machine room	Figure C4
5	Sensor prototype	Car	Machine room	Figure C5
6	Sensor prototype	Car	Machine room, line-of-sight to the shaft	Figure C6

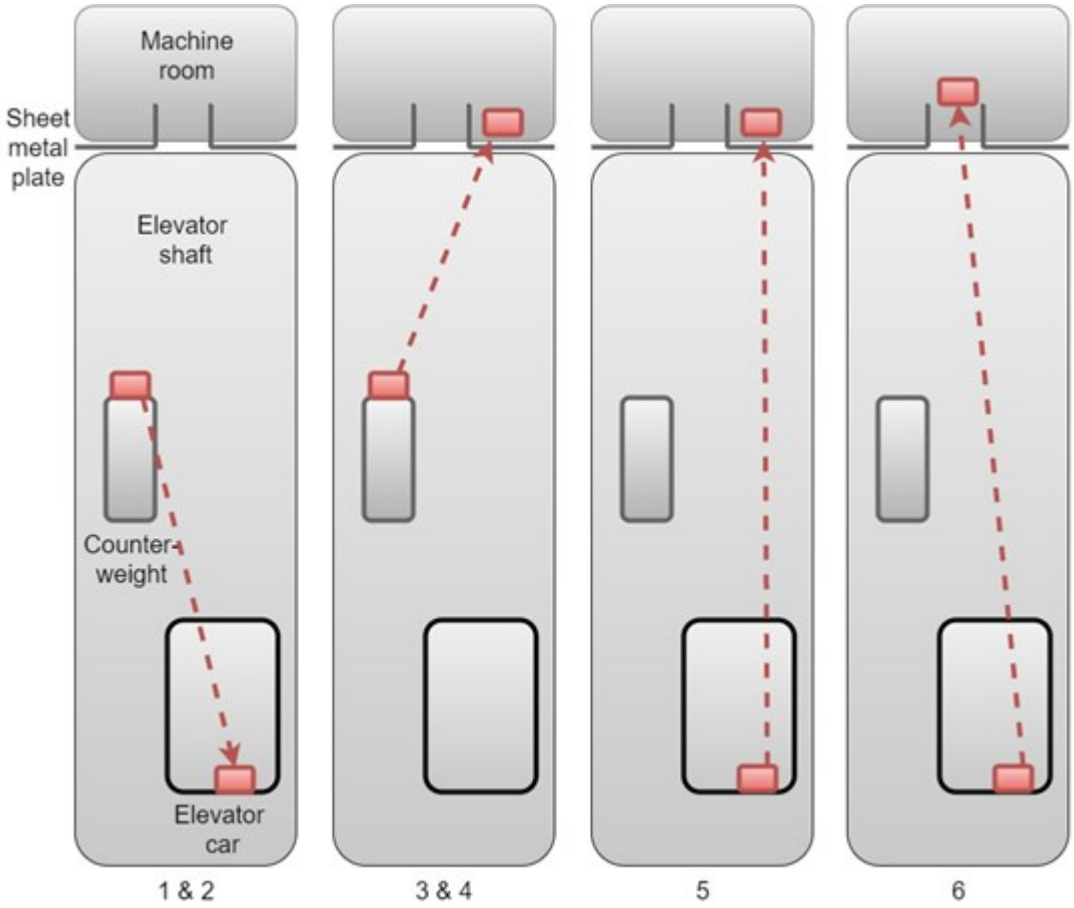

Figure 19: Test setup and different test cases for wireless range measurements

When comparing Figures C1 to C2, and C3 to C4, it is clear that the RSSI levels of the sensor prototype are approximately 10 dB lower than the levels obtained using SmartRF06 evaluation board. There are two likely reasons for the low signal strength: unmatched antenna impedance, and the structure of the prototypes leading to poor positioning of the antenna. These reasons are investigated more closely in Section 5.1.2.

The range achieved in the tests in Tytyri can be calculated from the number of transmitted packets, as the speed and the acceleration of the elevator are known. In test cases 1 and 2, the x-axis of the graphs can be directly used for calculating distance between the transmitter and the receiver. This is because the packet transmission rate of the connection is 20 packets per second, and the speed of the elevator is 10 m/s. As the counterweight and the car move either towards each other or away from each other, the total speed difference is 20 m/s. Thus, between each consecutive packet, the distance between the receiver and the transmitter changes by 1 meter. The wireless range in test cases 1 and 2 can therefore be calculated as

$$d = x_2 - x_1, \tag{25}$$

where x_2 is the x-axis position where the connection is lost, and x_1 is the position where the receiver and the transmitter are closest to each other, or the peak RSSI value in the examined graph. The connection is considered lost when the amount of lost and corrupted packets increases to 5 in a second, or 25 %.

Figure C2 shows the signal quality of the prototype from the counterweight to inside the car. The peak RSSI value is located at x-axis position 168, which is the point where the counterweight and the car are side by side in the shaft. Moving forward on the graph, the first lost packet occurs at position 292, and the connection is completely lost at position 305. Using Eq. (25), the range of the connection from the counterweight to inside the car is

$$305 - 168 = 137\ m. \tag{26}$$

During this time, 6 packets were corrupted according to CRC, and one packet was lost. This results in a CRC error rate of 4.3 %, and lost packet rate of 0.7 %.

In test cases 3-6, the elevator starts from stationary, and its acceleration needs to be taken into account when calculating the range. The acceleration of the elevator is 0.8 m/s^2 and the final speed is 10 m/s, which results in an acceleration time of 12.5 seconds. During the acceleration, 250 packets have been transmitted, and the elevator has moved a distance of 62.5 meters.

After the acceleration phase the elevator moves at a constant speed of 10 m/s. As the receiver is stationary, unlike in test cases 1 and 2, the x-axis of the graphs does not directly indicate the distance change between the receiver and the transmitter. In order to obtain correct distance, the x-axis difference needs to be divided by 2. Additionally, the distance from the machine room to the top floor of the elevator is 12 meters, which is added to all range estimations.

Thus, the range of the connection in test cases 3-6 can be calculated as

$$d = 62.5\ \text{m} + \frac{\text{x}_2 - \text{x}_1 - 250}{2} + \ 12\ \text{m}, \tag{27}$$

where x_1 is the position where the elevator starts moving, and x_2 is the position where the connection is lost. In Figure C4, the counterweight starts moving at x-axis position 261, and the connection is lost at position 690. Using Eq. (27), the resulting range from the counterweight to the machine room is

$$62.5\ \text{m} + \frac{690\ - 261 - 250}{2} + 12\ \text{m} = 164\ \text{m}. \tag{28}$$

The CRC error rate in test case 4 is 1.4 % and the lost packet rate is 2.6 %. The range and packet error rates of all test cases were calculated in a similar manner. The results are presented in Table C1. In all tests, the range of the link surpassed the required specification of 100 meters. As will be explained in the next section, the performance of the antenna on the prototypes can be improved by impedance matching and better positioning. The improved signal strength would allow an even longer range, or decrease the required transmission power and allow longer operational life or a smaller battery.

In test case 6, the receiver is positioned on the edge of the metal plate between the machine room and the elevator shaft. By comparing Figures C5 and C6, it can be seen that the signal strength from the machine room to the shaft can be improved by 10-20 dB by placing the receiver so that direct line-of-sight to the shaft is obtained.

Positioning the receiver in such way resulted in a range of 193 meters from the machine room to the car, an increase of 83 % compared to test case 5, where the metal plate was obstructing the path of the signal.

5.1.2 Investigating antenna performance

As mentioned in the previous section, there are two likely reasons for the 10 dB lower signal strength experienced in Tytyri when comparing the prototypes to the evaluation board. First, the antenna impedance of the prototypes is not matched, which lowers the efficiency of the antenna. The lowered efficiency applies to both the receiving and the transmitting antenna, thus probably accounting for a notable amount of the experienced loss of signal strength. Antenna matching is a process that should always be done when aiming for optimal wireless performance; however, there were no resources and time to match the antenna impedance of the prototypes during the thesis.

Second, the distance of the antenna from conducting materials, such as structures of the counterweight, can greatly affect the characteristics of the antenna. Conducting objects should be kept away particularly from the near-field region of the antenna, as they will alter the antennas radiation pattern and impedance. [2, pp. 62-63] In all tests presented in this thesis, the radio devices were attached to the metal structures of the counterweight using magnets. However, due to the structure of the evaluation board, it was lifted from the surface of the counterweight with 35 mm high plastic poles, whereas the prototype was only 15 mm away from the counterweight due to the structure of its enclosure. Thus, the antenna of the prototypes was close to a metal surface, which lowered its performance, as is verified ahead.

The effect of antenna positioning on the signal strength of the prototypes was investigated further by a test in an elevator shaft. The transmitter was placed onboard the counterweight, and the receiver was positioned inside the elevator car on a wooden desk. Two different antenna setups were tested: in the first measurements, the transmitter was mounted in its enclosure, the same way it was mounted in Tytyri. In the second measurement, the prototype was lifted higher using the 35 mm poles in order to obtain clearance from the counterweight, as shown in Figure 20. The positioning of the transmitter and the receiver was kept otherwise unchanged during the tests. The elevator car traveled from the top of the shaft to the bottom and then back to the top, and the RSSI value of the received signal was recorded. Three measurements were made with each antenna setup in order to obtain better average results.

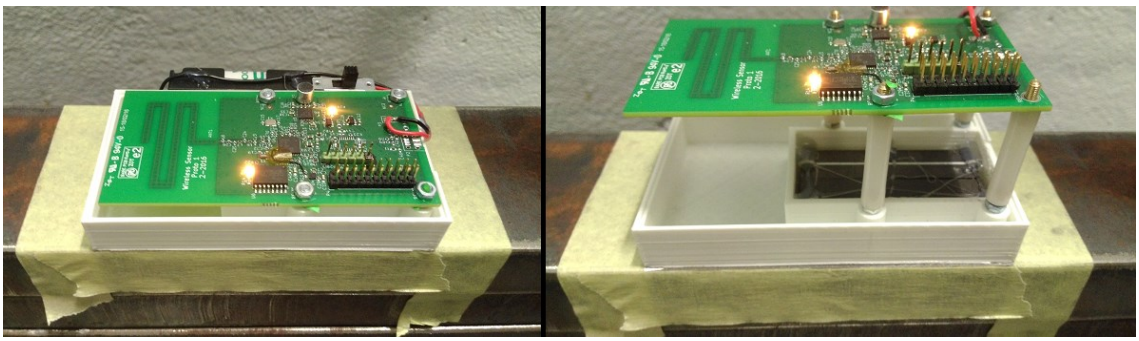

Figure 20: Prototype mounted directly on counterweight on left, prototype lifted off the counterweight on right

From measured RSSI values, it was calculated that lifting the antenna off the counterweight resulted in an average improvement of 5.64 dB to 5.87 dB in signal

strength. Averaged RSSI values of the tests with different antenna setups are plotted in Figure 21. Figure 21 shows that signal strength is improved both when the elevator car is above the counterweight (in the beginning and the end of the graph) and below it (in the middle of the graph). This indicates that the effect is not caused by the counterweight blocking the line of sight from the transmitter to the receiver, but that the counterweight is affecting the performance of the antenna itself. Thus, for future designs, the mounting of the sensor should be redesigned in such way that it provides the antenna more clearance from conducting objects, such as the counterweight structures.

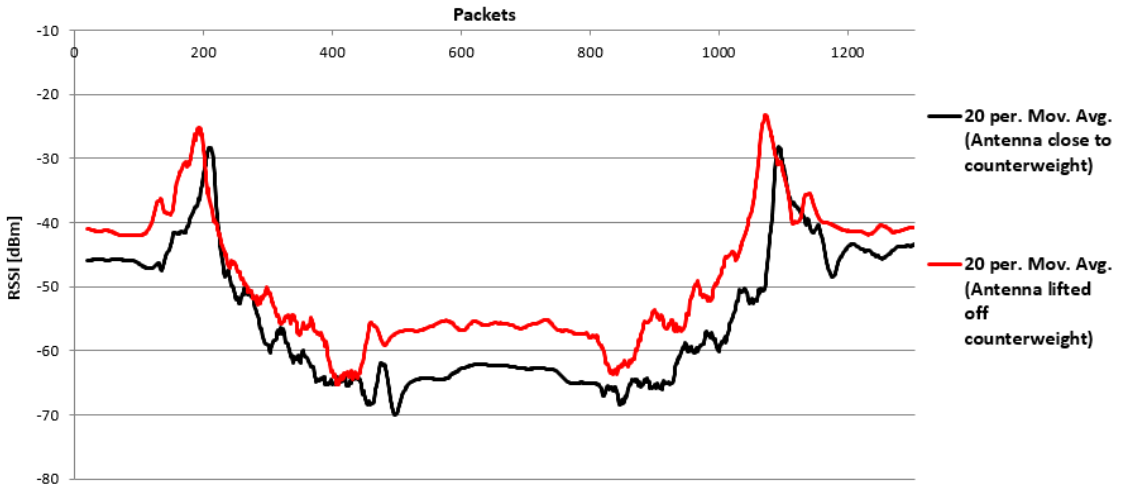

Figure 21: Average RSSI of the test runs with different antenna positioning

5.1.3 Power consumption

The power consumption of the sensor prototypes was measured using a µCurrent current to voltage transducer designed by David L. Jones [58]. The voltage output from the transducer was visualized and analyzed using a PicoScope 5000 series PC oscilloscope. Since the accuracy of the oscilloscope is relatively low, a calibrated Fluke 175 True RMS multimeter, featuring a ± (0.15 % + 2 LSD) accuracy [59], was used in conjunction for validating the accuracy of the test setup.

µCurrent is a current measurement tool aimed for measuring very low currents with great precision and minimal burden voltage. It converts the measured nanoamperes, microamperes or milliamperes directly to millivolts according to the selected range. The voltage can then be measured using a multimeter or an oscilloscope. The accuracy of the GOLD version of µCurrent is specified at ±0.05 % in the nA and µA ranges, and ±0.1 % in the mA range. The device was first published in the Australian Silicon Chip Magazine April 2009 issue [58].

Since the µCurrent is not a calibrated measurement device, the accuracy of the test setup was evaluated before measuring the prototypes. This was done by using 0.1% accuracy resistors and a known voltage source for generating a precise current, and measuring the obtained current using the test setup. The source voltage was verified with the Fluke 175 multimeter. As the error margin of both the source voltage and the resistors is known, the error margin for the resulting current can be calculated using a propagating error formula [60, p. 75]. The current measured by the test setup was compared to the calculated theoretical current. The results of verifying the test setup are presented in Appendix D.

Table D1 shows that the values measured with the multimeter are precisely inside the calculated error margin of the current in all except the first test case. The PicoScope on the other hand shows larger error in measured values. This is especially true when the measured current is close to zero, as the noise of the current transducer, as well as the noise of the measurement devices, becomes a dominant factor. A worst-case error was calculated by comparing the measured values to the furthest possible theoretical value of the current. A worst-case error margin of 1.02 % was obtained for the multimeter. Using the oscilloscope results in an error of several percent at low currents. On the other hand, the oscilloscope is more precise in measuring the quickly current changes that occur in the operation of the prototypes.

Estimates on the power consumption of the device in different operating modes were presented in Section 4.2.5. However, as the Flash-memory and the audio measurement circuit were not implemented for the first prototypes, they are discarded in the following power consumption measurements.

Figure 22 illustrates the current consumption of the transmitter prototype in real-time operating mode. The prototype features the software described in Section 4.3, thus, the measurement rate for the accelerometer is set to 400 Hz, the data transmission time is 15.04 ms and the listening time of the radio is 10 ms. The different states of the radio are clearly seen in Figure 22.

The highest current consumption is triggered at x-axis position 0 ms when the radio starts transmitting, followed by the lower current of the listening mode. After 10 milliseconds of listening, the radio is turned off. The short spikes in current consumption show the accelerometer measurements. It should be noted that a DC offset of −30 mV was added to the measurement, in order to allow increasing the resolution of the oscilloscope without positive clipping of the signal.

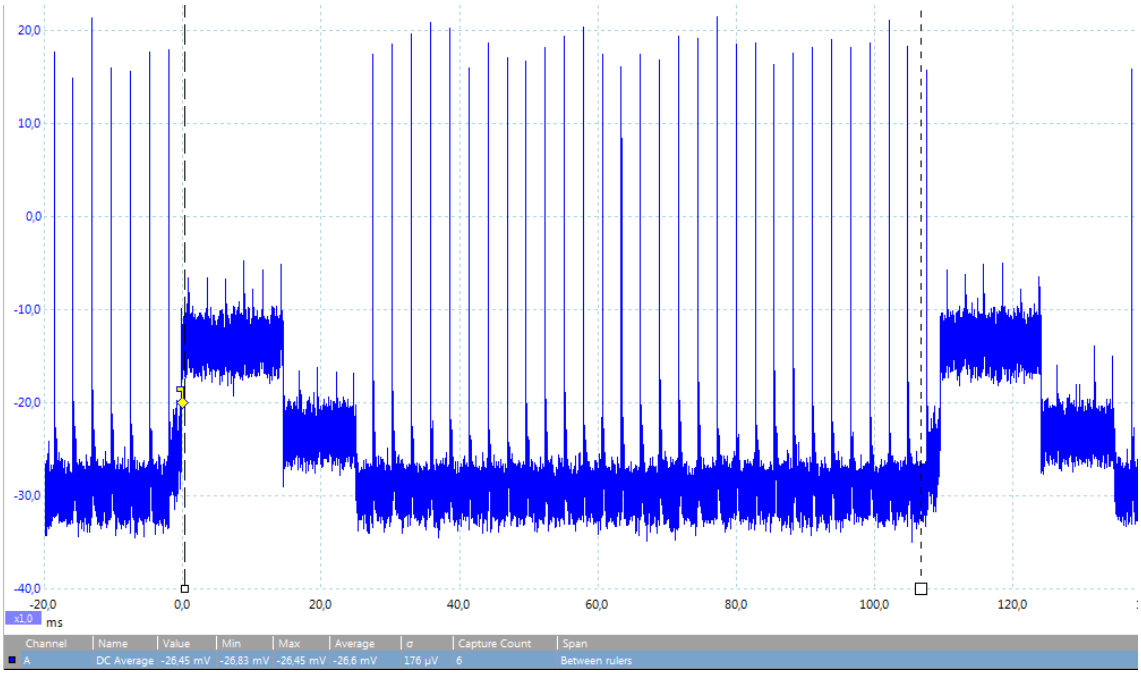

Figure 22: Current consumption of the transmitter node in active mode. Due to offset, input current in mA can be calculated as $I_{in} = V_{measured} + 30$ mV

Figure 22 reveals that the measurement cycle of the device is not 100 ms as it should be according to the software implementation. It can be seen that the transmission interval

of packets is actually 109.5 ms, an almost 10 % longer period than expected. The reason for this issue is discussed in Section 5.2.2.

Due to the rapidly changing current, the multimeter readings were not stable and could not be used for measuring the current of the prototype in active mode. The current consumption in active transmit state should be 15.84 mA according to the estimates in Table 12, excluding the audio measurement and Flash-memory. Using the PicoScope's average measurement, a transmit current of 16.52 mA was measured. The measured current is 4.3 % higher than estimated, which could be explained by the high error margin of the oscilloscope measurements. The current consumption of the different device states was measured in a similar manner. An average value of a single measurement cycle in active mode was also measured. An estimate of the average of one measurement cycle was calculated for comparison reasons.

The results of the measurements are presented in Table 14. It is clear that the current consumption of the device in active real-time mode is lower than estimated, even when taking into account the possible error caused by the oscilloscope. This is mainly due to the significantly lower power consumption of the MCU in radio-off situations than estimated. The estimates assumed that the Cortex M3 core is always active during measurements, which is not the case in real-life operation, as is explained next.

The RTOS on the MCU is designed to achieve lowest possible power consumption at all times. It includes aggressive power policy features, which try to minimize power consumption by entering a low-power state whenever there are no tasks running on the processor. This power cycling is the most likely reason for the lower than estimated power consumption. However, once the audio measurements and Flash-memory operations are implemented in the software, the load on the processor will increase, possibly diminishing the power savings observed in these measurements. Furthermore, the slightly improved MCU current consumption is outweighed by the active operation of the Flash-memory.

The current consumption of the prototype in low-power mode was also measured. In low-power mode, the MCU is in power-down mode and the accelerometer is taking measurements at a rate of 10 Hz. The measured current consumption of the device in low-power mode is shown in Figure 23. A DC offset of −450 mV was added in order to increase the resolution of the oscilloscope measurement.

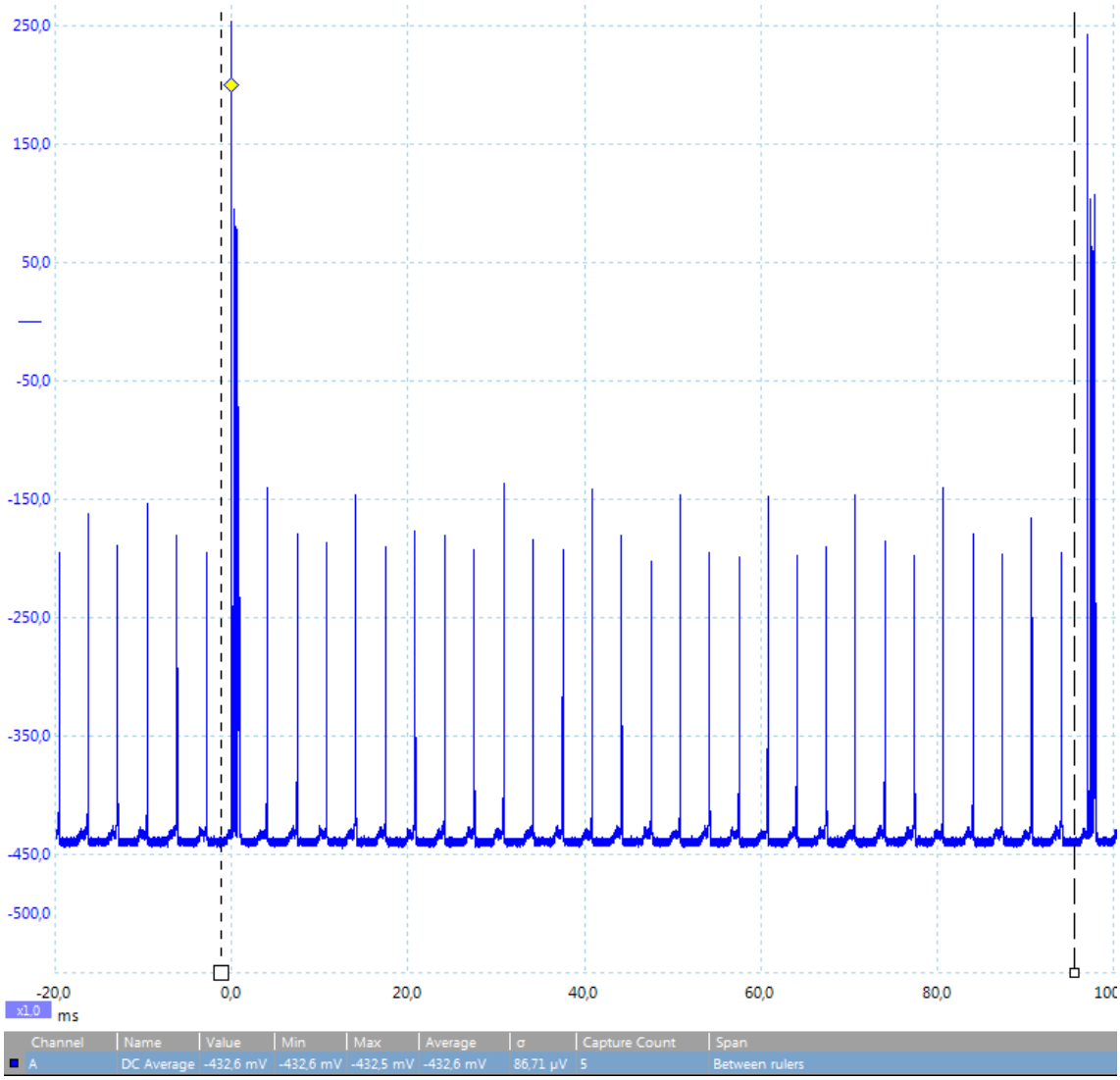

Figure 23: Current consumption of the transmitter in low-power mode. Due to offset, input current in µA can be calculated as $I_{in} = V_{measured} + 450$ mV

The current consumption of the prototype in low-power mode measured 17.4 µA, 10 % higher than estimated. Measuring the components on the prototype separately, the excess current draw was traced to the accelerometer, which draws a current of 4.5 µA instead of the 3 µA presented in the datasheet. This is likely leakage current through the SPI bus between the MCU and the accelerometer. Figure 23 also shows unexplained, higher frequency current spikes in addition to the 10 Hz measurement rate of the accelerometer. The spikes are not present if the supply voltage to either the MCU or the accelerometer is removed, further indicating a leakage between the SPI bus. However, eliminating the current spikes does not affect the average current consumption of the prototype, and thus do not notably contribute to the excess power consumption in low-power mode.

Table 14: Measured current consumption of the prototype compared to estimates

Device state	Estimated	Measured	Difference [%]
Active, transmit +10 dBm	15.84 mA	16.52 mA	+ 4.3
Active, listen	8.44 mA	6.79 mA	− 19.5
Active, radio off	2.94 mA	0.88 mA	− 70.1
Active, 1 cycle average	5.43 mA	3.54 mA	− 34.8
Low-power mode	15.75 µA	17.4 µA	+ 10.5

In summary, although slightly lower than estimated current consumption was observed in active transmit mode, the audio measurement and the Flash-memory will outweigh the slight improvements when implemented. Due to the excessive current consumption in the low-power mode, a more aggressive duty cycle policy than presented in Section 4.2.5 needs to be implemented, in order to achieve the 3 years operational lifetime. However, the power consumption of the device can be reduced by a better component choice, as explained in Section 5.2.1.

5.1.4 Verifying the functionality of the prototypes

The functionality of the real-time operating mode of the sensor prototypes was tested in the office building of KONE. The LabVIEW instrument presented in Section 4.4 was used for visualizing measured data. No automatic error detection methods were implemented for the first prototype; however, an LED indicating received packets was used for monitoring the quality of the connection. The LED changes state every time a packet is received; therefore, as the packet transmission interval of the software is 100 ms, the LED was turning on every 0.2 seconds, or at the rate of 5 Hz. This rate is slow enough to be easily monitored by eye. As the LED was flashing constantly with no breaks, it could be determined that no packets were lost during the tests.

Figure 24 shows the x, y and z-axis accelerations measured from a real elevator moving from the bottom floor to the top floor, and then back to the bottom floor. The measurement rate of the 400 Hz and the resolution of 10 bits was selected. The audio functionality could not be tested, as it is not implemented in software. The transmitting sensor node was placed on the floor inside the elevator car, and the receiver and the host PC were located on the bottom floor. The top and middle graphs present the x- and y-axis accelerations, while z-axis acceleration is displayed in the bottom graph. The graphs in Figure 24 show acceleration in mG.

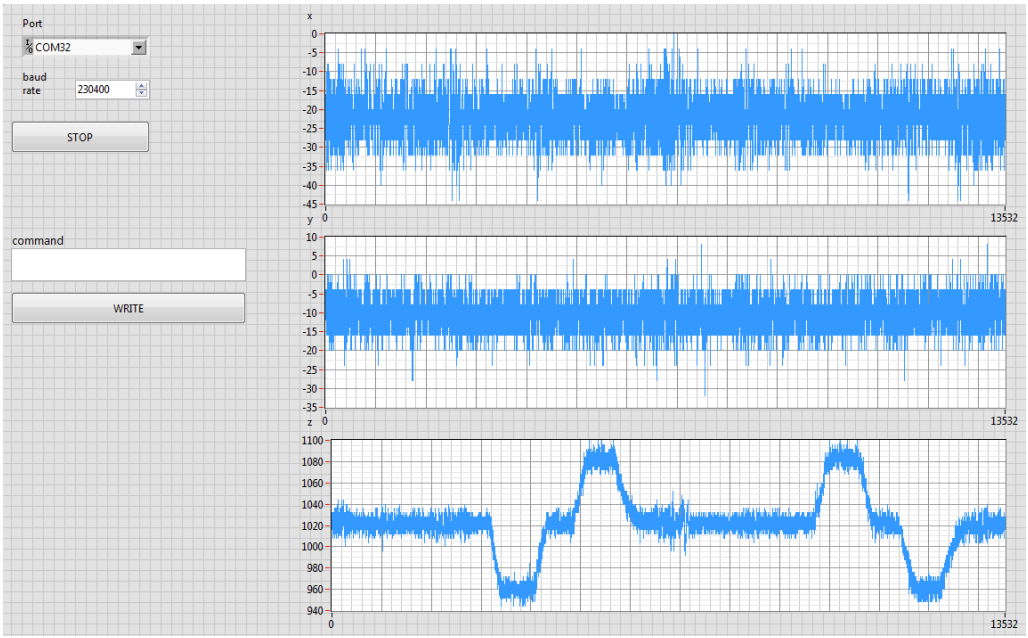

Figure 24: LabVIEW instrument showing the x, y and z-axis acceleration of an elevator in mG

From Figure 24, it can be seen that offset is present in the acceleration measurements. The x- and y-axis measurements show an offset of tens of mG, which is acceptable due to unidealities in manufacturing the accelerometer and the assembly of the accelerometer on the PCB. The z-axis acceleration shows an offset of 1020 mG, or

approximately 1 G, which is equivalent to the gravitational field of the Earth. The accelerometer measures positive acceleration downwards, or towards Earths gravitation, and negative acceleration upwards.

Figure 24 shows that the sensor measures only noise in the x- and y-axis graphs, which is expected. Similar noise is present when the sensor is placed on a stable surface such as a desk. However, the standard deviation of the measured noise is approximately 5 mG for the y- and z-axes, and 9.7 mG for x-axis.

The amount of y- and z-axis noise is relatively normal, as the selected accelerometer is not particularly designed as a low-noise product. For example, many low-noise accelerometers from ST Microelectronics specify a noise of $150\mu G/\sqrt{B}$ [61], which would result in noise of 3 mG at the used 400 Hz bandwidth. No reasonable explanation for the increased noise of the x-axis was discovered, and there is no mention of noise profiles or differences of the axes in the datasheet of the selected accelerometer. On a second sensor node, the standard deviation of noise in x-, y- and z- axes is 7.1, 5.7 and 9.6 mG respectively, indicating that the amount of noise in the axes varies, and might be caused by manufacturing tolerances, for example.

The z-axis graph shows the vertical acceleration of the elevator. The first negative pulse in the graph shows the elevator accelerating from the bottom floor, followed by a positive deceleration at the top floor. After a period of staying stationary, the elevator starts moving and accelerates downwards, followed by a deceleration when stopping at the bottom floor.

The acceleration of the elevator is set to 0.6 m/s^2. From Figure 24, the acceleration measured by the sensor device is

$$1020\ \text{mG} - 960\ \text{mG} = 60\ \text{mG}, \tag{29}$$

which can be translated to m/s^2 as

$$0.060\ \text{G} * 9.81\frac{\text{m}}{\text{s}^2} = 0.59\frac{\text{m}}{\text{s}^2}. \tag{30}$$

The tests verify that the device is capable of constant throughput of measurement data, through multiple floors, the shaft walls and the car structures, at a distance of approximately 15 meters.

5.2 Future improvements

Often in the process of designing electronics, some decisions, as well as issues arisen in testing, leave room for improvement. The sensor prototype is no different, and both the hardware and software design presented in Chapter 4 can be improved for better performance of the device.

The power consumption measurements revealed two issues in the design of the sensor – slightly increased power consumption than estimated, and a delay in gathering measurements from the accelerometer. The following sections introduce solutions for addressing these issues.

5.2.1 Improving power efficiency

The power consumption of the prototypes in low-power mode measured around 10 % higher than estimated. The reason for this is likely leakage current through the SPI bus between the accelerometer and the MCU. Such leakage is difficult to eliminate, as any buffering between the devices will most likely increase the power consumption more than the improvement gained by eliminating the leak. Some leakage is also caused by bypass capacitors in voltage lines, and general non-idealities in all devices and components onboard the prototype.

From Table 12, it is clear that most of the energy consumption of the prototypes in low-power mode is the result of the quiescent current of the linear voltage regulator. In fact, in low-power mode, the LDO is responsible for 69 % of the power consumption of the device. In addition, power dissipated in the LDO is entirely wasted energy, and should therefore be addressed.

A very low quiescent current linear regulator was discovered when revising the power consumption of the device. Texas Instruments TPS783 family linear regulators feature a miniscule quiescent current of 500 nA, which would eliminate the wasted energy of the prototypes almost entirely [62]. Changing the regulator would allow an increased duty cycle, even when taking into account some leakage current on the prototype. The new duty cycle is estimated ahead. As mentioned before, changing to a switching mode regulator is not possible, due to an even larger quiescent current than in linear regulators.

By replacing the LDO and reserving a headroom of 3 µA for leakage currents, a current consumption of 7.25 µA can be estimated for the sensor prototype in the low-power mode. The current consumption in active mode does not change notably, as the quiescent current is insignificant compared to the active components on the sensor. Using Eq. (21) and a 2.6 Ah battery, a duty cycle of

$$\frac{\frac{2.6\ \text{Ah}}{3\ \text{years} * 365\ \text{days} * 24\ \text{h}} - 7.25 * 10^{-6}\ \text{A}}{0.1083\ \text{A} - 7.25 * 10^{-6}\ \text{A}} = 0.000846 \ldots \approx 0.085\ \% \tag{31}$$

can be estimated when the new regulator is used. Such duty cycle allows 73 seconds of active operation daily, during the course of 3 years.

5.2.2 Eliminating software delay

Figure 22 showed significant delay in collecting measurement data and transferring packets. The theoretical sample rate of the device is set to 400 Hz, or a 2.5 ms sampling interval. When investigated using the oscilloscope, the measurement interval is actually 2.75 ms, or 10 % longer than estimated. Furthermore, the observed delay is not stable, as the measurement interval varies from 2.7 to 2.8 milliseconds. As 40 measurements are collected in each packet, this delay leads to the increased packet transmission period of approximately 110 ms.

The measurement interval is implemented in the software using a simple loop, which polls data from the accelerometer with a predefined delay of 2.5 ms between each cycle of the loop. It was verified that the RTOS of the prototypes adds the uncertain delay to the measurement interval, as is explained ahead.

As mentioned before, the RTOS on the device is designed to achieve minimal power consumption. Low power consumption is achieved by actively monitoring the load on the processor, and powering down unused sections of the MCU and even placing the entire device in a low-power state. It was verified that this aggressive power policy adds uncertain delay to the measurements. By removing the power policy, the measurement interval was reduced to 2.63 ms, and more importantly, variation in the delay was no longer observed.

The greatest issue in such uncertainty in receiving information is that further processing of the data may depend on accurate timing of the measurements. Therefore, the delay in the measurements needs to be minimized. Removing the power policy naturally leads to increased power consumption, as some automatic power saving features are disabled. However, a simple solution exists for minimizing the timing errors without the need for sacrificing power efficiency.

An improved implementation of data acquisition takes advantage of the FIFO buffer included in the accelerometer. The accelerometer fills the buffer with measurements at a predefined sampling rate. The accelerometer generates an interrupt when a certain amount of measurements is ready in the buffer, and the MCU then requests the entire buffer from the accelerometer at once. Thus, even though a delay is experienced in obtaining the measurements from the accelerometer, a constant interval between each measured piece of information is achieved. The accuracy of the sampling interval in such situation is defined solely by the accuracy of the sampling rate of the accelerometer. The datasheet of the accelerometer used in the sensor prototypes does not give any indication regarding this timing accuracy.

6 Conclusion

The aim of this thesis was to design a wireless sensor system prototype for monitoring elevator condition. Strict requirements were set for the range, measurement performance and the battery lifetime of the device. The prototype is aimed to meet two very different goals: capability for both medium-quality, real-time measurements as well as permanent monitoring of the health of the elevator, which requires high quality measurement data.

A large part of the thesis focused on researching and selecting a suitable wireless technology for the sensor system. Chapter 2 introduced technical properties that were considered the most important from the perspective of performance requirements of the sensor system. All factors that make up a wireless connection have their advantages and disadvantages.

For example, increased data rates result in reduced signal-to-noise ratio in the wireless system. In order to achieve the most robust and longest range link, the lowest acceptable data rate should be used by selecting the narrowest channel bandwidth and simplest modulation schemes. The range of the wireless signal is inversely proportional to the used carrier wave frequency. It was discovered that a lower carrier wave frequency also results in better propagation through building materials. Additionally, it was determined that the sum of wireless packet frame and protocol overheads, along with methods used for maintaining connection reliability, may result in significantly lowered efficiency in the applicable throughput rate of the connection.

In Chapter 3, different available wireless communication methods were researched in order to determine the most suitable technology for the sensor system. It was realized that many wireless standards had a defining limitation that would lead to sub-par performance of the sensor system. Technologies such as ZigBee and BLE were observed to suffer from very low applicable data throughput rate due to the general operating nature of these low-power standards. In addition, many of the standards operate in the higher carrier wave frequency bands, limiting their range. It was discovered that a few real-time applications had been developed using non-standardized proprietary solutions, which are designed for the applications specifically.

Through the theoretical research and preliminary tests carried out in a real elevator environment, it was determined that due to the range requirements, sub-GHz carrier frequencies would be a viable choice for the system. Unfortunately, 802.11ah – the upcoming sub-GHz WLAN standard that seemed the most suitable for the sensor system – is not yet available and thus could not be selected. The second option of using a proprietary sub-GHz technology was selected for the prototype system. When the 802.11ah standard is more widely available, its feasibility should be reviewed again, as it could be advantageous to select a standardized protocol when developing the sensor system into a finished product. If a proprietary solution is used, functionality such as device authentication in permanent condition monitoring mode remains to be developed.

The design of the prototype sensor system was described in Chapter 4. The hardware of the sensor nodes was based on an MCU including a 32-bit processor, internal memory and an RF front-end capable of communicating in the sub-GHz frequency bands. Selecting a highly integrated solution allowed for fast development and prototyping of the system. The hardware design included a duty cycle scheme for the sensor nodes for

obtaining the required battery lifetime. A batch of sensor node prototypes was manufactured for testing the functionality of the design, and for evaluating whether the requirements set in the beginning of the thesis were fulfilled.

The software of the sensor nodes was designed around an RTOS supplied by the manufacturer of the MCU. All functionality is not yet implemented due to the lack of a specific software driver in the operating system. However, the real-time functionality of the device, excluding audio measurements, was implemented. Some optimization methods for the software and wireless operation were presented, that should be implemented in a finished software. The optimizations will be beneficial when the highest range and lowest power consumption are desired, and the largest amount of measurement data is transferred. A LabVIEW instrument for gathering data from the sensors was also presented.

The functionality and performance of the prototype sensor system was evaluated in Chapter 5. The range achieved in tests in a long elevator shaft surpassed the initially set requirements, however, not by a wide margin. It was determined that mounting the prototypes correctly is crucial for good performance, due to antenna positioning. Even though the recommended antenna design was used for the sensor prototype design, its performance was diminished by low clearance from the conducting counterweight structures. For a future version of the sensor device, the enclosure should be redesigned in a way that results in larger clearance between the antenna and the device that the sensor is mounted on. The improved antenna efficiency could be realized as either longer wireless range, longer battery lifetime or a smaller and lower-priced battery.

The power consumption of the device measured slightly higher than estimated. A timing issue in the operation of the real-time software of the nodes was also discovered. The functionality of the real-time operating mode of the system was verified in an elevator in the office building of KONE. Straightforward improvements for the minor issues observed in testing the sensor prototypes were presented.

To summarize, the selection of the wireless technology proved to fulfill the range requirements set for the system. It was observed that the sub-GHz carrier wave frequency can achieve long range even through multiple obstructive structures. The hardware and software design of the system is sufficient for the required measurement performance, and an operational life of 3 years with a modest-sized battery can be achieved. The prototypes proved to function as expected, while some minor issues remained.

The prototypes show potential to be developed towards a fully functioning product. Remaining future development includes software development for the sensor nodes and the whole sensor system, further developing the wireless protocol or reviewing upcoming standard solutions, and implementing presented design improvements such as redesigning the sensor enclosure and mounting, which would improve antenna performance.

References

[1] L. D. Xu, W. He and S. Li, "Internet of Things in Industries: A Survey," *IEEE Transactions on Industrial Informatics,* vol. 10, no. 4, pp. 2233-2243, 2014.

[2] S. R. Saunders and A. Aragón-Zavala, Antennas and Propagation for Wireless Communication Systems: 2nd Edition, West Sussex, England: John Wiley & Sons ltd., 2007.

[3] Electronic Communications Committee, "Recommendation 70-03," 30 9 2015. [Online]. Available: http://www.erodocdb.dk/docs/doc98/official/pdf/rec7003e.pdf. [Accessed 30 11 2015].

[4] Texas Instruments, "Undestanding and Enhancing Sensitivity in Receivers for Wireless Applications," 05 1999. [Online]. Available: http://www.ti.com/lit/an/swra030/swra030.pdf. [Accessed 25 1 2016].

[5] C. Anderson and T. Rappaport, "In-Building Wideband Partition Loss Measurements at 2.5 and 60 GHz," *IEEE Transactions on Wireless Communications,* vol. 3, no. 3, pp. 922-928, 2004.

[6] S. Shellhammer, "Numerical Spectrum Sensing Requirements," 2006.

[7] B. P. Lathi and Z. Ding, Modern Digital and Analog Communication Systems: 4th edition, New York, The Unites States: Oxford University Press, 2010.

[8] A. Räisänen and A. Lehto, Radiotekniikan Perusteet, 13. painos, Helsinki, Finland: Gaudeamus Helsinki University Press, 2011.

[9] S. Garg and M. Kappes, "An Experimental Study Of Throughput for UDP and VoIP Traffic in IEEE 802.11b Networks," *Wireless Communications and Networking,* vol. 3, pp. 1748-1753, 2003.

[10] W. R. Heinzelman, A. Chandrakasan and H. Balakrishnan, "Energy-Efficient Communication Protocol for Wireless Microsensor Networks," in *33rd Hawaii International Conference on System Sciences*, 2000.

[11] European Telecommunications Standards Institute, "EN 300 220-1 V 2.4.1 European Standard Electromagnetic compatibility and Radio spectrum Matters, Short range Devices, Radio equipment to be used in the 25 MHz to 1 000 MHz frequency range with power levels ranging up to 500 mW," 1 2012. [Online]. Available: http://www.etsi.org/deliver/etsi_en/300200_300299/30022001/02.04.01_40/en_30022001v020401o.pdf. [Accessed 12 1 2016].

[12] Matthew Loy; Raju Karingattil; Louis Williams; Texas Instruments, "ISM-Band and Short Range Device Regulatory Compliance Overview," 5 2005. [Online]. Available: http://www.ti.com/lit/an/swra048/swra048.pdf. [Accessed 9 5 2016].

[13] K. Shuiab, M. Boulmalf, F. Sallabi and A. Lakas, "Co-existence of Zigbee and WLAN, A Performance Study," College of Information Technology, UAE University, Al-Ain, 2006.

[14] D. Brunelli, M. Maggiorotti, L. Beninini and F. Bellifemine, "Analysis of Audio Streaming Capability of Zigbee Networks," University of Bologna, Bologna.

[15] International Telecommunications Union, "Recommendation ITU-R SM.1896: Frequency ranges for global or regional harmonization of short-range devices," 11 2011. [Online]. Available: https://www.itu.int/dms_pubrec/itu-r/rec/sm/R-REC-SM.1896-0-201111-I!!PDF-E.pdf. [Accessed 12 5 2016].

[16] International Telecommunications Union, "Documents of the International Radio Conference - Doc. No. 1-100," 1947. [Online]. Available: http://www.itu.int/dms_pub/itu-s/oth/02/01/S020100002B4813PDFE.pdf. [Accessed 07 12 2015].

[17] N. Golmie and F. Moveaux, "Interference in the 2.4 GHz ISM Band: Impact on the Bluetooth Access Control Performance," *NIST Special Publication,* no. 500-259, pp. 8-13, 2005.

[18] European Comission, "Radio spectrum: harmonised EU rules to foster high-speed wireless internet services and avoid harmful interference," 6 5 2010. [Online]. Available: http://europa.eu/rapid/press-release_IP-10-540_en.pdf. [Accessed 9 5 2016].

[19] V. Nieminen, Evaluation And Experimentation of Sub-GHz Short Range Radio Transreceivers, Espoo: Helsinki University Of Technology, 2009.

[20] N. Baker, "ZigBee and Bluetooth: strengths and weaknesses for industrial applications," *Computing & Control Engineering Journal,* vol. 16, no. 2, pp. 20-25, 2005.

[21] R. Morais, M. A. Fernandes, S. G. Matos and C. Serodio, "A ZigBee multi-powered wireless acquisition device for remote sensing applications in precision viticulture," *Computers and Electronics in Agriculture,* vol. 62, no. 2, pp. 94-106, 2008.

[22] N. Xu, S. Rangwala, K. Chintalapudi, D. Ganesan, A. Broad, R. Govindan and D. Estrin, "A Wireless Sensor Network for Structural Monitoring," University of California, California, 2004.

[23] Bluetoot SIG, Inc., "bluetooth.com, basic rate/enhanced data rate," 2016. [Online]. Available: https://www.bluetooth.com/what-is-bluetooth-technology/bluetooth-technology-basics/br-edr. [Accessed 25 4 2016].

[24] C. Gomez, J. Oller and J. Paradells, "Overview and Evaluation of Bluetooth Low Energy: An Emerging Low-Power Wireless Technology," Universitat Politècnica de Catalunya, 2012.

[25] Steelman Pro, "Bluetooth ChassisEAR," [Online]. Available: http://steelmanpro.com/diagnostics/bluetooth-chassisear.html. [Accessed 7 5 2016].

[26] Intel, "Wireless Networking," 27 10 2014. [Online]. Available: http://www.intel.com/support/wireless/wlan/sb/CS-025321.htm. [Accessed 7 12 2015].

[27] W. Sun, M. Choi and S. Choi, "IEEE 802.11ah: A Long Range 802.11 WLAN at Sub 1 GHz," *Journal of ICT Standardization,* vol. 1, pp. 83-108, 2013.

[28] European Telecommunications Standards Institute, "Digital Enhanced Cordless Telecommunications (DECT); DECT Packet Radio Service (DPRS)," 10 2011. [Online]. Available: http://www.etsi.org/deliver/etsi_en/301600_301699/301649/02.02.00_40/en_301649v020200o.pdf. [Accessed 2 3 2016].

[29] J. P. Carmo and C. Couto, "A 2.4-GHz CMOS Short-Range Wireless-Sensor-Network Interface for Automovite Applicaitions," *IEEE Transactions on Industrial Electronics,* vol. 57, no. 5, pp. 1764-1771, 2010.

[30] M. J. Whelan, M. V. Gangone, K. D. Janoyan and R. Jha, "Real-Time Wireless Vibration Monitoring for Operational Modal Analysis of an Integral Abutment Highway Bridge," *Engineering Structures,* vol. 31, no. 10, p. 2224–2235, 2009.

[31] D. Tsonev, S. Videv and H. Haas, "Light Fidelity (Li-Fi): Towards All-Optical Networking," 2013.

[32] R. Garg, "Li-Fi: Data Onlight Instead of Online," *Anveshanam - a National Journal of Computer Science & Applications,* vol. 1, no. 1, pp. 33-37, 2012.

[33] Ingar Fredriksen; Pal Kastnes; Atmel, "Choosing a MCU for your next design; 8 bit or 32 bit?," 2014. [Online]. Available: http://www.atmel.com/images/45107a-choosing-a-mcu-fredriksen_article_103114.pdf. [Accessed 4 3 2016].

[34] Texas Instruments, "CC1310 SimpleLink Ultralow Power Sub-1GHz Wireless MCU, Datasheet," 10 2015. [Online]. Available: http://www.ti.com/lit/ds/symlink/cc1310.pdf. [Accessed 24 2 2016].

[35] NXP, "MKW01Z128, Highly-integrated, cost-effective single-package solution for sub-1 GHz applications, Datasheet," 3 2014. [Online]. Available: http://cache.nxp.com/files/microcontrollers/doc/data_sheet/MKW01Z128.pdf. [Accessed 14 2 2016].

[36] Silicon Labs, "EZR32LG Wireless MCUs, Datasheet," [Online]. Available: https://www.silabs.com/Support%20Documents/TechnicalDocs/EZR32LG330_DataSheet.pdf. [Accessed 6 2 2016].

[37] Endevco Meggitt Sensing Systems, "Steps to selecting the right accelerometer," [Online]. Available: https://www.endevco.com/news/newsletters/2012_07/tp327.pdf. [Accessed 19 2 2016].

[38] ST Microelectronics, "LIS2DH12 MEMS digital output motion sensor: ultra-low-power high-performance 3-axis "femto" accelerometer, Datasheet," 10 2015. [Online]. Available: http://www.st.com/st-web-ui/static/active/en/resource/technical/document/datasheet/DM00091513.pdf. [Accessed 19 2 2016].

[39] ST Microelectronics, "IIS2DH Ultra-low-power high-performance 3-axis accelerometer with digital output for industrial applications, Datasheet," 4 2015. [Online]. Available: http://www.st.com/st-web-ui/static/active/en/resource/technical/document/datasheet/DM00171283.pdf. [Accessed 23 2 2016].

[40] Bosch, "BMA250 Digital, triaxial acceleration sensor, Datasheet," 31 5 2012. [Online]. Available: http://www.mouser.com/ds/2/783/BST-BMA250-DS002-05-786487.pdf. [Accessed 23 2 2016].

[41] Analog Devices, "ADXL362 Micropower, 3-Axis Digital Output MEMS Accelerometer, Datasheet," 2015. [Online]. Available: http://www.analog.com/media/en/technical-documentation/data-sheets/ADXL362.pdf. [Accessed 23 2 2016].

[42] Measurement Specialities, "Accelerometer ACH-01, Datasheet," 10 07 2008. [Online]. Available: http://www.mouser.com/ds/2/418/ACH_01-736503.pdf. [Accessed 23 2 2016].

[43] Texas Instruments, "TLV320AIC3254 Ultra Low Power Stereo Audio Codec with Embedded miniDSP, Datasheet," 11 2014. [Online]. Available: http://www.ti.com/lit/gpn/tlv320aic3254. [Accessed 19 2 2016].

[44] Texas Instruments, "Design and Configuration Guide for the TLC320AIC3204 and TLC320AIC3254 Audio Codecs," 4 2010. [Online]. Available: http://www.ti.com/lit/pdf/slaa404. [Accessed 19 2 2016].

[45] CUI INC, "CMC-5044PF-A Specifications, Datasheet," 6 2008. [Online].

Available: http://www.cui.com/product/resource/cmc-5044pf-a.pdf. [Accessed 19 2 2016].

[46] Spansion, "S70FL01GS 1 Gbit MirrorBt Flash Non-Volatile Memory, Datasheet," 21 4 2015. [Online]. Available: http://www.spansion.com/Support/Datasheets/S70FL01GS.pdf. [Accessed 2 23 2016].

[47] Toshiba America Electronic Components Inc., "NAND vs. NOR Flash Memory, Technology Overview," 25 4 2006. [Online]. Available: http://aturing.umcs.maine.edu/~meadow/courses/cos335/Toshiba%20NAND_vs_NOR_Flash_Memory_Technology_Overviewt.pdf.

[48] Texas Instruments, "CC13xx, CC26xx SimpleLink Wireless MCU, Technical Reference Manual," 09 2015. [Online]. Available: www.ti.com/lit/pdf/swcu117. [Accessed 23 2 2016].

[49] FTDI Chip, "FT203X USB to Basic UART IC, Datasheet," 2015. [Online]. Available: http://www.ftdichip.com/Support/Documents/DataSheets/ICs/DS_FT230X.pdf. [Accessed 23 2 2016].

[50] K. Furset and P. Hoffman, "High Pulse drain impact on CR2032 coin cell battery capacity," 2011. [Online]. Available: https://www.dmcinfo.com/Portals/0/Blog%20Files/High%20pulse%20drain%20impact%20on%20CR2032%20coin%20cell%20battery%20capacity.pdf. [Accessed 24 2 2016].

[51] Texas Instruments, "LP5907 Ultra Low-Noise, 250-mA Linear Regulator for RF and Analog Circuits, Datasheet," 8 2015. [Online]. Available: http://www.ti.com/lit/ds/symlink/lp5907.pdf. [Accessed 24 2 2016].

[52] Texas Instruments, "Design Note DN019, Powering Low-Power RF Products," 18 9 2009. [Online]. Available: http://www.ti.com/lit/an/swra173b/swra173b.pdf. [Accessed 24 2 2016].

[53] Texas Instruments, "TPS22860 Ultra-Low Leakage Load Switch, Datasheet," 4 2015. [Online]. Available: http://www.ti.com/lit/ds/symlink/tps22860.pdf. [Accessed 24 2 2016].

[54] Saft, "LS 14500 Primary lithium battery, Datasheet," 9 2009. [Online]. Available: www.saftbatteries.com/force_download/LS14500.pdf. [Accessed 24 2 2016].

[55] Texas Instruments, "Application Note AN058: Antenna Selection Guide," 2010. [Online]. Available: http://www.ti.com/lit/an/swra161b/swra161b.pdf. [Accessed 11 5 2016].

[56] "Design Note DN024, Monopole PCB Antenna with Single or Dual Band Option," 2016. [Online]. Available: http://www.ti.com/lit/an/swra227e/swra227e.pdf. [Accessed 11 5 2016].

[57] "Design Note DN031, CC-Antenna-DK and Antenna Measurements Summary," 2010. [Online]. Available: http://www.ti.com/lit/an/swra328/swra328.pdf. [Accessed 11 5 2016].

[58] D. L. Jones, "The μCurrent, A professional precision current adapter for Multimeters," *Silicon Chip Magazine,* vol. April, 2009.

[59] Fluke, "Fluke 175 True RMS Digital Multimeter Specifications," [Online]. Available: http://en-us.fluke.com/products/digital-multimeters/fluke-175-digital-multimeter.html#techspecs. [Accessed 19 4 2016].

[60] J. R. Taylor, An introduction to error analysis: the study of uncertainties in

physical measurements, 2nd edition, University Science Books, 1997.

[61] ST Microelectronics, "MEMS & Sensors Overview," 4 2014. [Online]. Available: http://www.arrow-israel.co.il/_Uploads/dbsAttachedFiles/02_STM_MEMS_Sensors_Overview.pdf. [Accessed 10 5 2016].

[62] Texas Instruments, "TPS783xx 500-nA Iq, 150-mA, Ultralow Quiescent Current Low-Dropout Linear Regulator, Datasheet," 11 2014. [Online]. Available: http://www.ti.com/lit/ds/symlink/tps783.pdf. [Accessed 21 4 2016].

Appendix A: Preliminary comparison of 868 MHz and 2.4 GHz

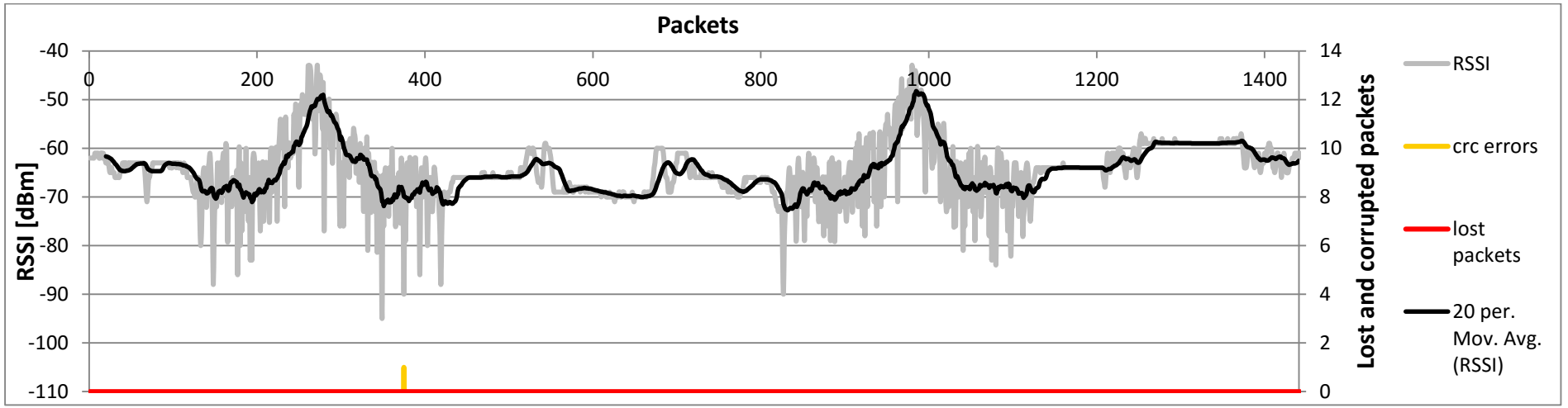

Figure A1: 868 MHz, 200 kbps, +5 dBm

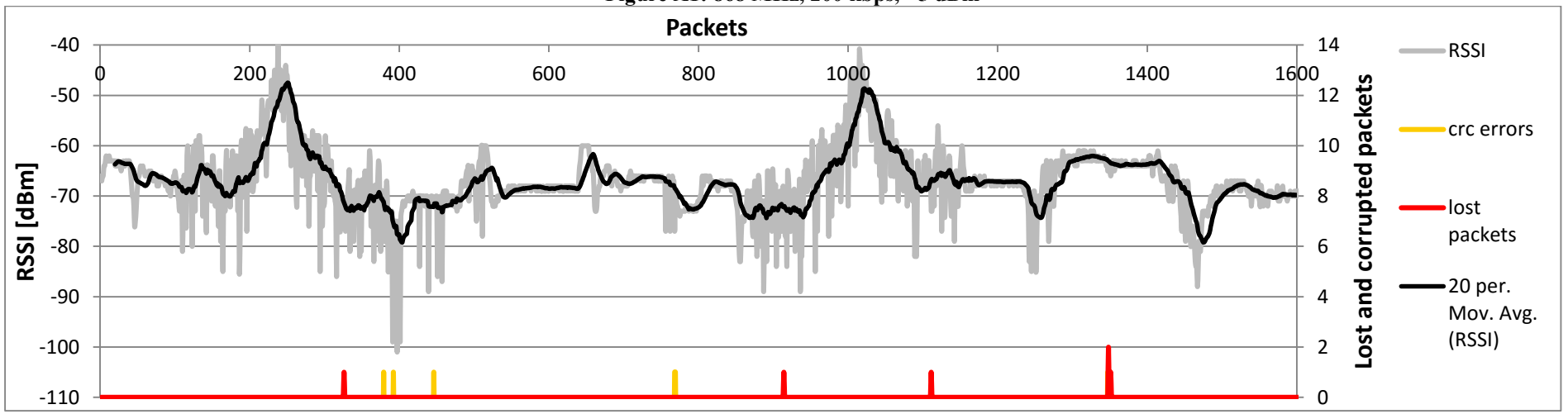

Figure A2: 868 MHz, 400 kbps, +5 dBm

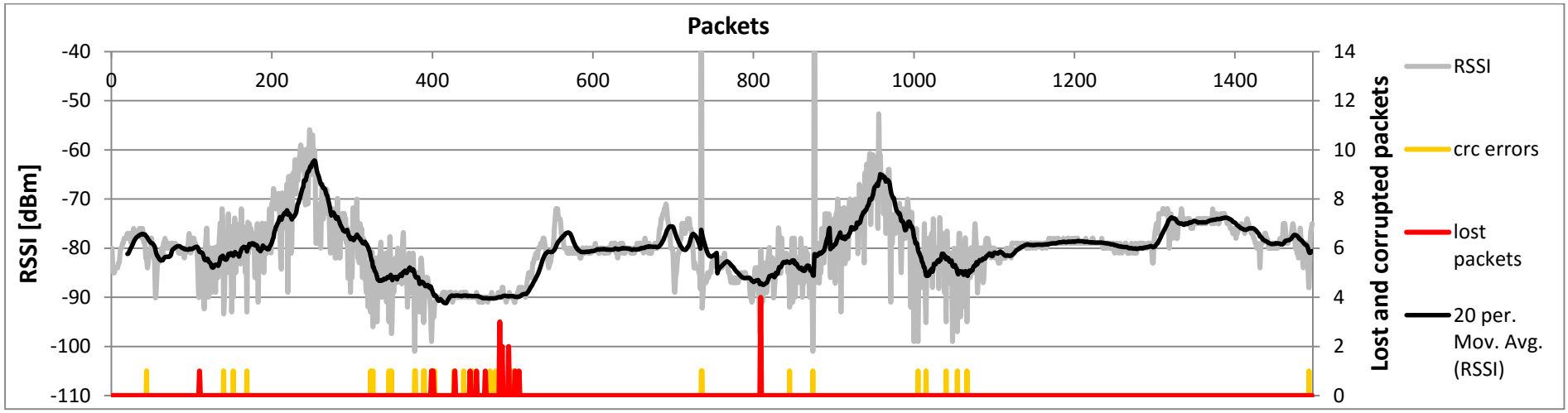

Figure A3: 868 MHz, 400 kbps, -10 dBm

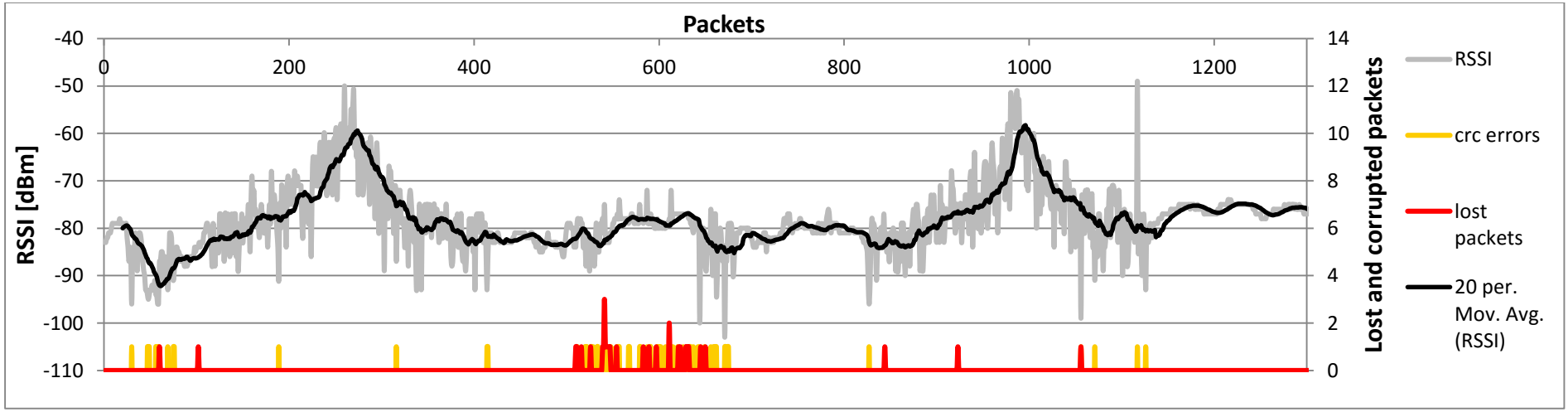

Figure A4: 2.4 GHz ZigBee, +5 dBm

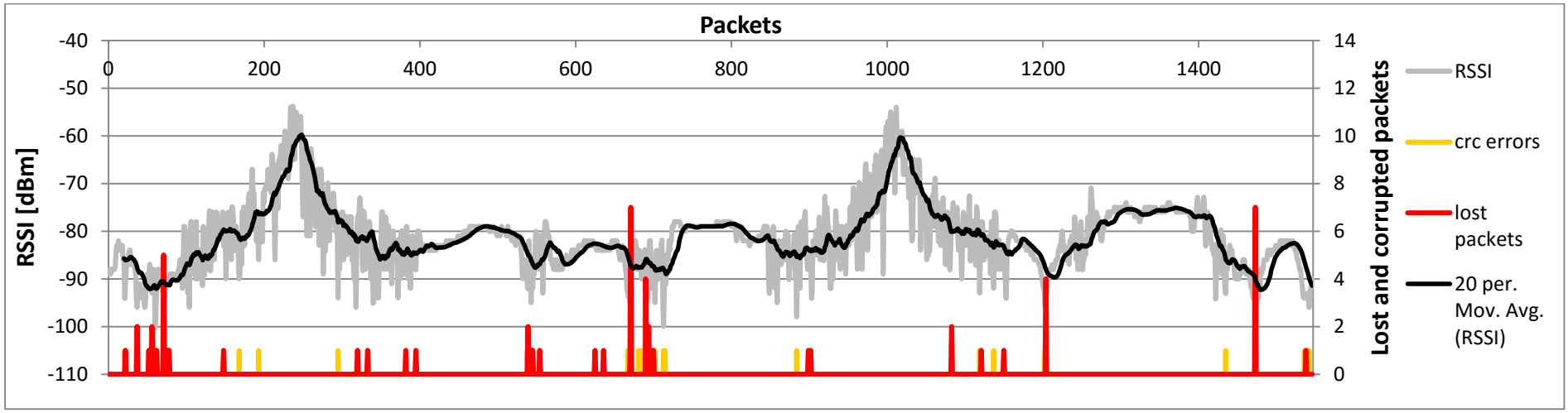

Figure A5: 2.4 GHz BLE, +5 dBm

Table A1: Amount of CRC errors and lost packets using different technologies

Technology	CRC errors [%]	Packets lost [%]
868 MHz proprietary, 200 kbps, +5 dBm	0.07	0.00
868 MHz proprietary, 400 kbps, +5 dBm	0.37	0.37
868 MHz proprietary, 400 kbps, -10 dBm	2.59	2.39
2.4 GHz ZigBee, +5 dBm	4.13	2.22
2.4 GHz BLE, +5 dBm	1.87	3.55

Appendix B: Sensor prototype design documents

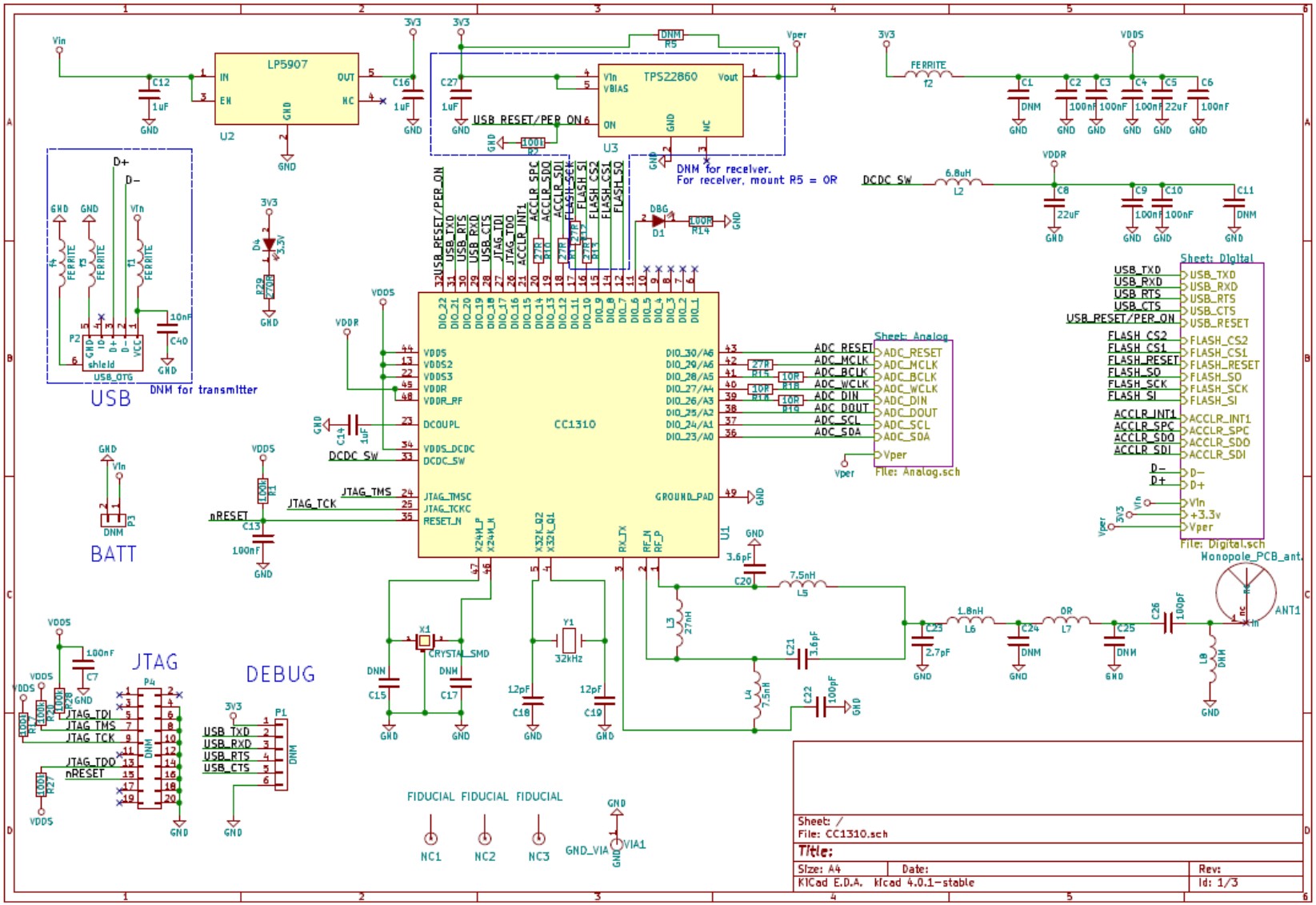

Figure B1: Prototype main circuitry

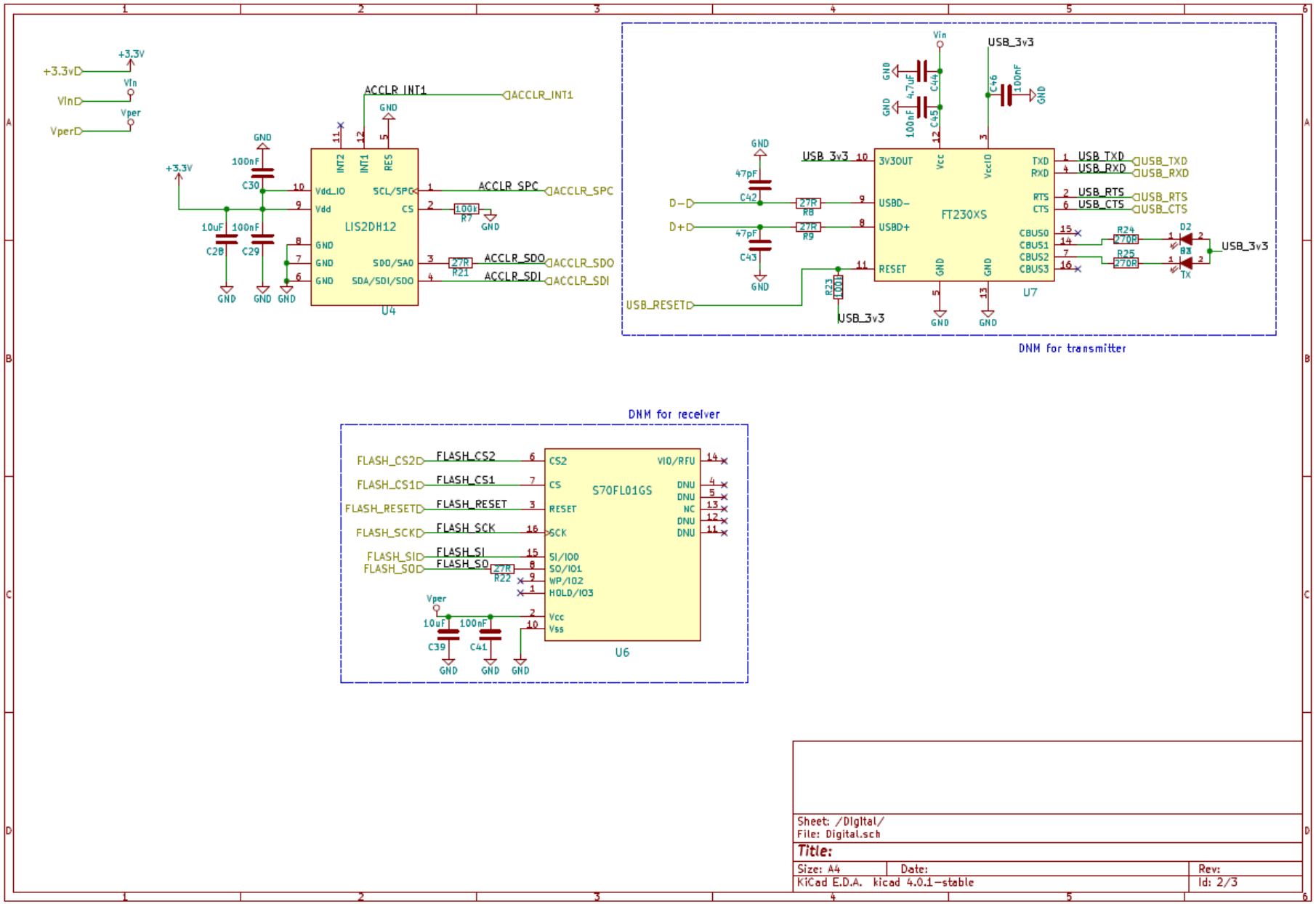

Figure B2: Prototype digial circuits

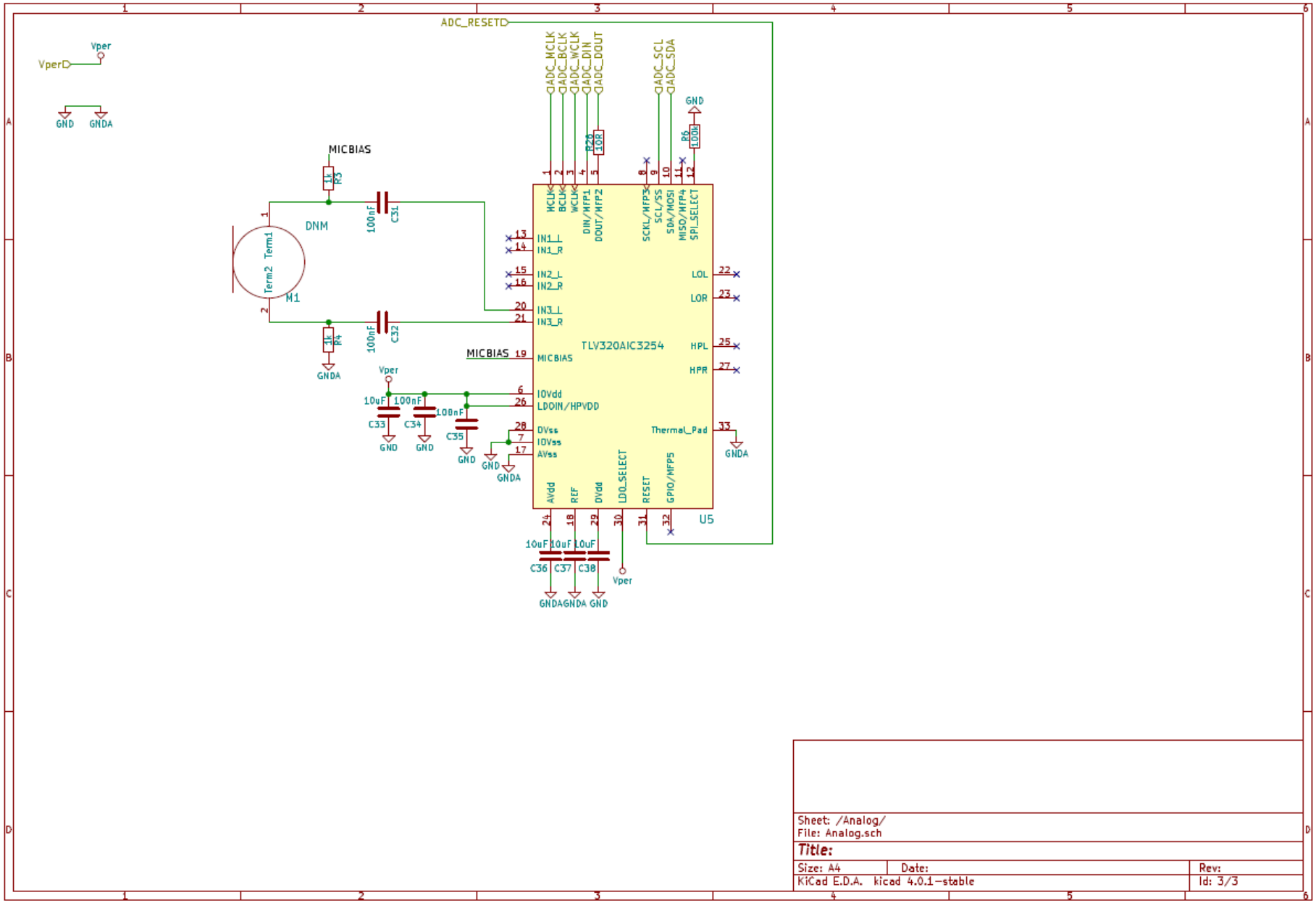

Figure B3: Prototype audio circuit

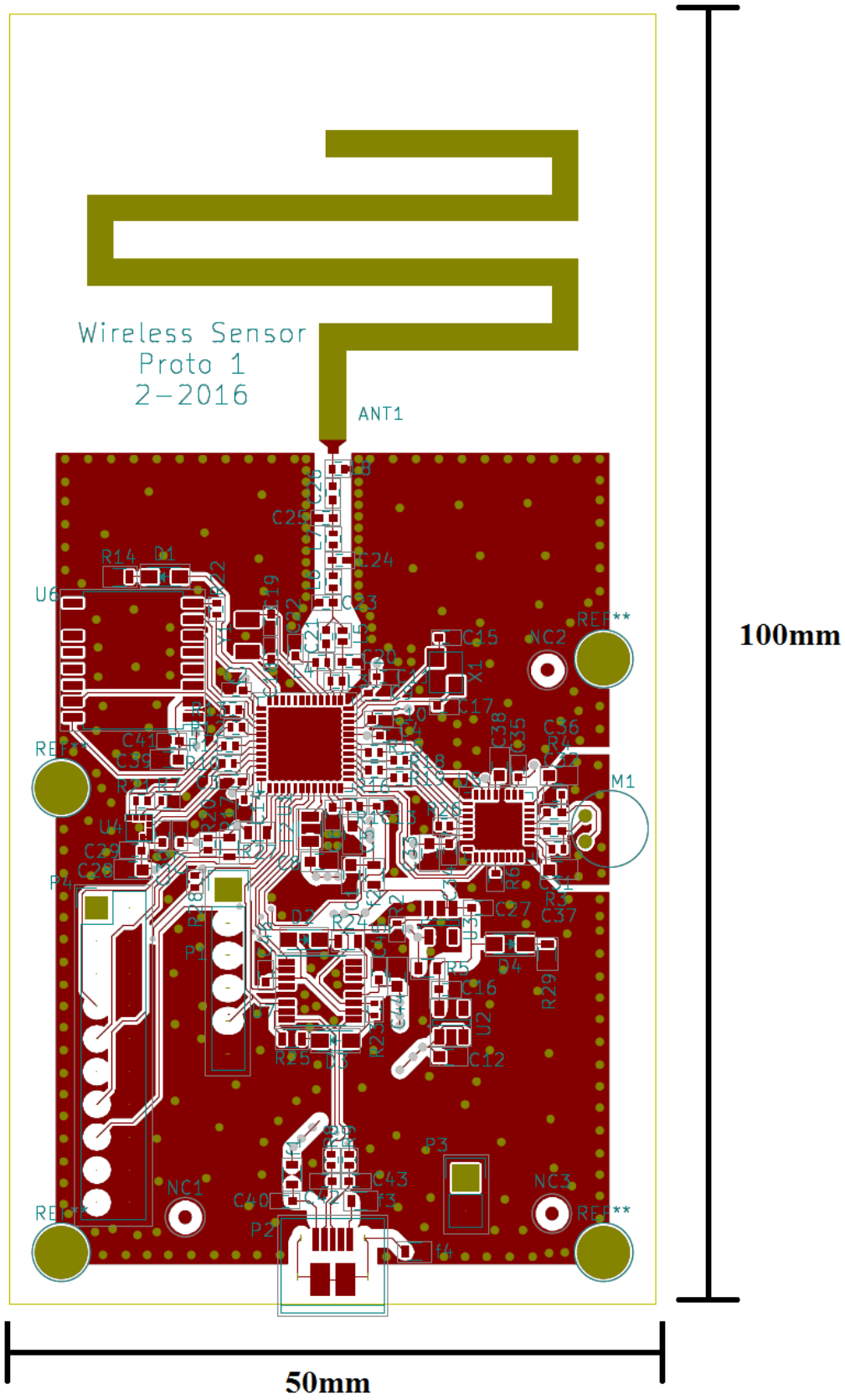

Figure B4: Sensor prototype layout

Appendix C: Prototype range tests at Tytyri

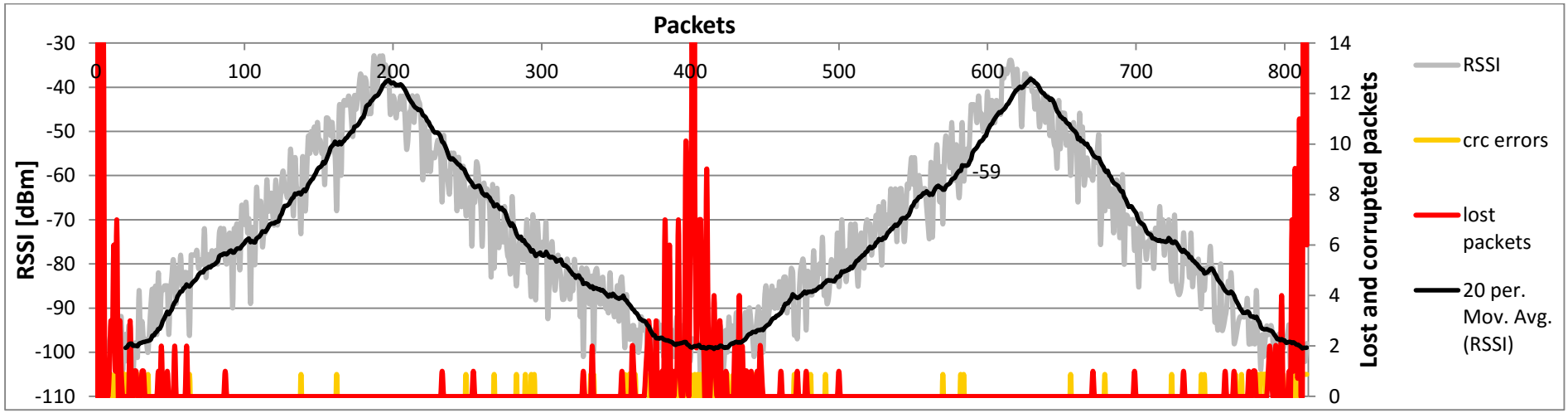

Figure C1: SmartRF06 evaluation board, 868 MHz, 200 kb/s, +14 dBm, from counterweight to car

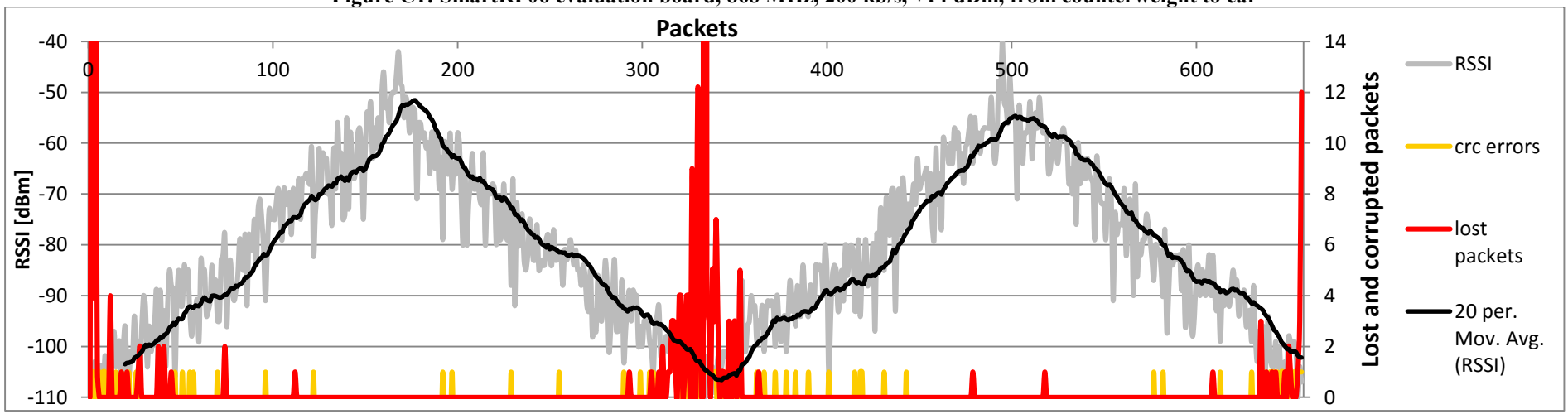

Figure C2: Sensor prototype, 868 MHz, 200 kb/s, +14 dBm, from counterweight to car

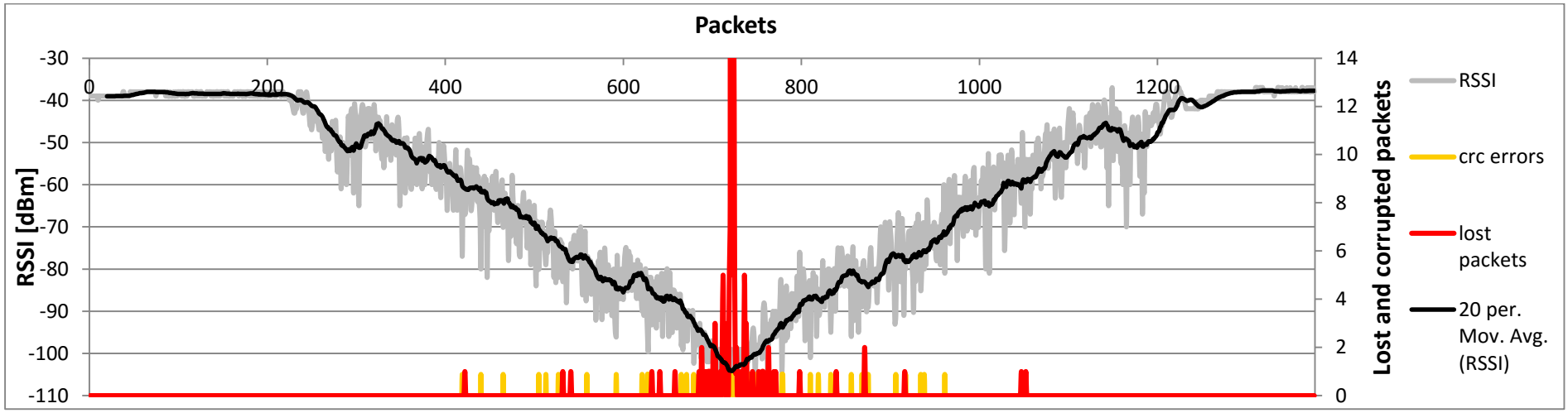

Figure C3: SmartRF06 evaluation board, 868 MHz, 200 kb/s, +14 dBm, from counterweight to machine room

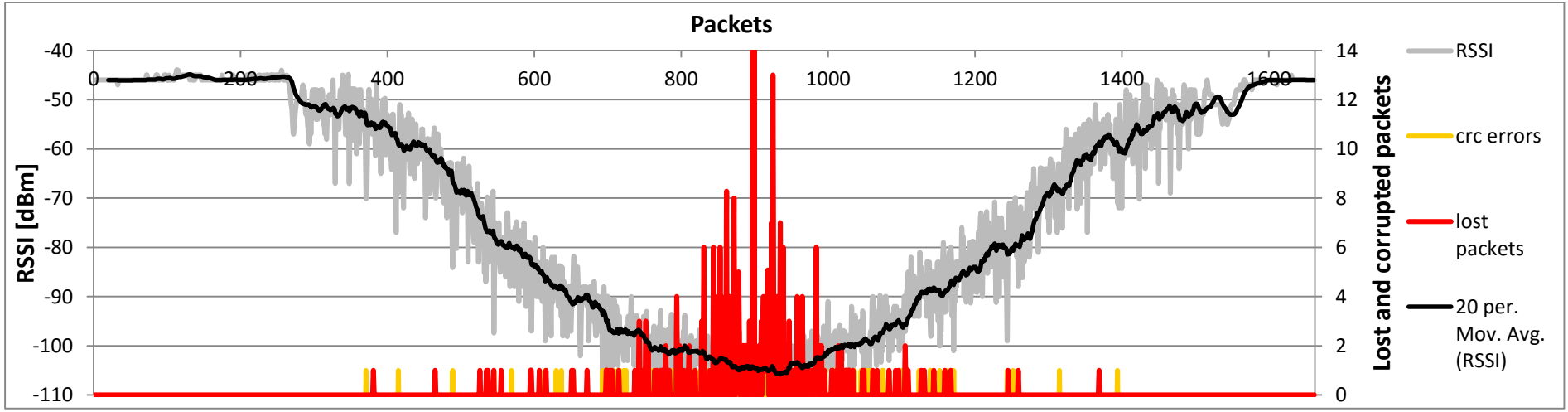

Figure C4: Sensor prototype, 868 MHz, 200 kb/s, +14 dBm, from counterweight to machine room

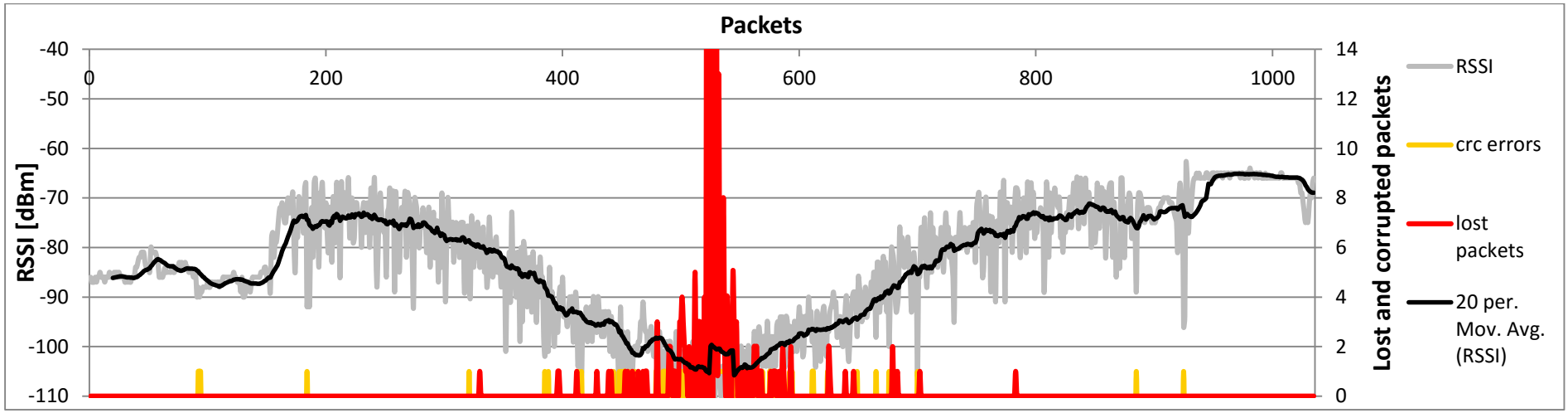

Figure C5: Sensor prototype, 868 MHz, 200 kb/s, +14 dBm, from car to machine room

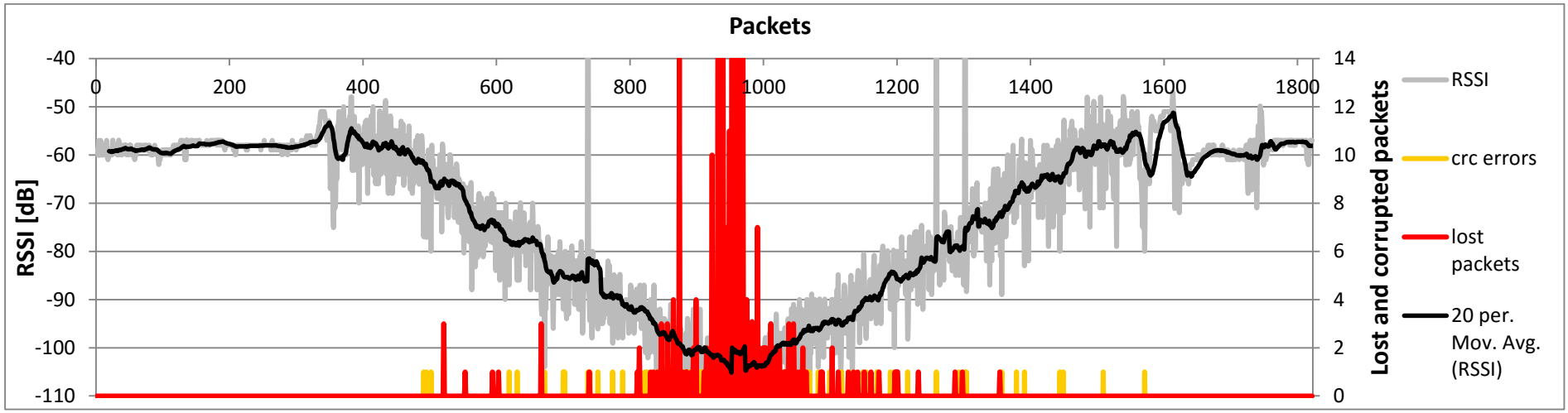

Figure C6: Sensor prototype, 868 MHz, 200 kb/s, +14 dBm, from car to machine room with line-of-sight positioning

Table C1: Range and error rates of the prototype device and evaluation device in different test cases

Test case	Device	Transmitter	Receiver	Range [m]	CRC errors [%]	Packets lost [%]
1	SmartRF06 Evaluation board	Counterweight	Car	164	3.6	3.0
2	Sensor prototype	Counterweight	Car	137	4.3	0.7
3	SmartRF06 Evaluation board	Counterweight	Machine room	191	2.7	1.2
4	Sensor prototype	Counterweight	Machine room	164	1.4	2.6
5	Sensor prototype	Car	Machine room	105.5	1.6	1.9
6	Sensor prototype	Car	Machine room (line-of-sight to shaft)	193	2.2	2.0

Appendix D: Results of validating the current measurement test setup

Table D1: Worst-case error for current measurement test setup

Source voltage ± (0.15 % + 2)	Resistance ± 0.1 %	Theoretical current	PicoScope reading	PicoScope error [%]	Fluke 175 True RMS reading	Fluke error [%]
1.000 ± 0.0035 V	301 kΩ ± 301 Ω	3.32226 µA ± 12.09 nA = 3.310 – 3.334 µA	3.618 µA	9.31	3.3 µA	1.02
2.500 ± 0.00575 V	301 kΩ ± 301 Ω	8.30565 µA ± 20.08 nA = 8.285 – 8.326 µA	8.471 µA	2.25	8.3 µA	0.31
5.000 ± 0.0095 V	301 kΩ ± 301 Ω	16.61130 µA ± 35.67 nA = 16.576 – 16.650 µA	17.4 µA	4.98	16.6 µA	0.39
5.000 ± 0.0095 V	100 kΩ ± 100 Ω	50 ± 0.1074 µA = 49.893 – 50.1074 µA	50.18 µA	0.58	50.0 µA	0.21
15.00 ± 0.0425 V	100 kΩ ± 100 Ω	150 ± 0.4507 µA = 149.549 – 150.451 µA	150.3 µA	0.67	149.9 µA	0.37
15.00 ± 0.0425 V	20 kΩ ± 20 Ω	750 ± 2.2535 µA = 747.747 – 752.253 µA	751.3 µA	0.475	750 µA	0.30
20.00 ± 0.05 V	10 kΩ ± 10 Ω	2 mA ± 5.3852 µA = 1.9946 – 2.0054 mA	2.16 mA	8.29	2.0 mA	0.27
50.00 ± 0.095 V	10 kΩ ± 10 Ω	5 mA ± 10.735 µA = 4.9893 – 5.0107 mA	5.15 mA	3.22	5.0 mA	0.21